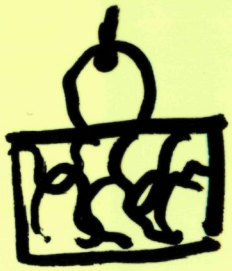

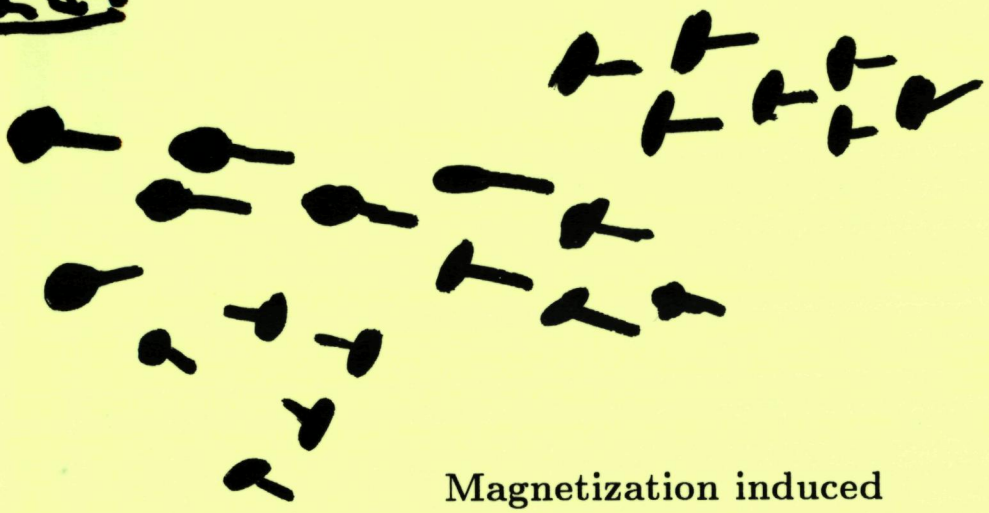

Magnetization induced optical Second-Harmonic Generation on magnetic multilayers

A new probe for interface magnetism

Harald Wierenga

Magnetization induced optical Second-Harmonic Generation on magnetic multilayers

A new probe for interface magnetism

CIP-GEGEVENS KONINKLIJKE BIBLIOTHEEK, DEN HAAG

Wierenga, Harm Albert
Magnetization induced optical Second-Harmonic Generation
on magnetic multilayers: A new probe for interface magnetism/
Harm Albert Wierenga. - [S.l. : s.n.]. - Ill.
Proefschrift Nijmegen. - Met lit. opg. - Met samenvatting in het Nederlands.
ISBN 90-9007762-6
Trefwoorden: magnetisme, multilagen, grenslagen, niet-lineaire optica.
Ontwerp omslag: Layla Rasing

Magnetization induced optical Second-Harmonic Generation on magnetic multilayers

A new probe for interface magnetism

een wetenschappelijke proeve op het gebied van
de Natuurwetenschappen

Proefschrift

ter verkrijging van de graad van doctor aan
de Katholieke Universiteit Nijmegen,
volgens besluit van het College van Decanen
in het openbaar te verdedigen op
vrijdag 10 februari 1995,
des namiddags te 1.30 uur precies

door

Harm Albert Wierenga

geboren op 31 mei 1966
te Coevorden

Promotor : Prof. Dr. H. van Kempen
Co-promotor : Dr. Th. H. M. Rasing

Het werk beschreven in dit proefschrift maakt deel uit van het onderzoeksprogramma van de Stichting voor Fundamenteel Onderzoek der Materie (FOM) en is mede mogelijk gemaakt door financiële steun van de Nederlandse Organisatie voor Wetenschappelijk Onderzoek (NWO).

En God zeide: Er zij licht; en er was licht. En God zag dat het licht goed was...

Genesis 1:3-4

Voor Sandra

Voorwoord

Eén van de eerste teksten die ik las in verband met mijn promotie-onderzoek was de openingszin van het voorwoord bij het proefschrift van Harry Tom: „In the last few hours before submitting this last of 'partial fulfillments', I am sitting before the green screen of the IBM PC with a Cheshire cat grin ... " In de achterliggende vijf jaar heeft dit baken mij steeds toegeschenen als zijnde het einde van de 'reis'. Nu ben ik dan zelf zover. Het groene IBM-scherm is weliswaar inmiddels vervangen door een royale X-terminal, maar het gevoel blijft hetzelfde.

Zoals bij zovelen leek ook mijn promotie in veel opzichten op het moeizame eten door de 'Rijstebrijberg' van technische tegenslagen en onbegrijpelijke resultaten, slechts af en toe leidend tot een kortstondig verblijf in het zo begeerde 'Luilekkerland' van het geslaagde experiment. Afgezien van de bevrediging die ligt in het telkens weer overwinnen van de tegenslagen, zijn het toch vooral deze laatste momenten die het de moeite waard maken.

Alhoewel mijn naam op de omslag vermeld staat is het zeker niet zo dat ik alleen verantwoordelijk ben voor het tot stand komen van dit proefschrift. Ik wil graag van de gelegenheid gebruik maken om deze 'co-auteurs' te noemen en te bedanken. Allereerst mijn begeleiders Herman van Kempen en Theo Rasing. Vooral de laatste vormt met zijn goede fysische aanvoelen en stormende enthousiasme een constante stimulans die niet in woorden uitgelegd kan worden, doch die men eenvoudig moet ondergaan. Daarnaast was er de zeer waardevolle bijdrage van Daniel Abraham, wiens ideeën vaak aan de basis stonden van nieuwe experimenten.

Ik ben blij dat een groot aantal studenten geïnteresseerd was in ons onderzoek en bereid was hieraan een afstudeerstage te wijden. Marcel Verheijen, Geert Spierings, George Malliaras en Vasilis Koutsos hielpen niet alleen met de noodzakelijke opbouw van het laboratorium, maar leverden ook bruikbaar onderzoek af. Een deel van hun werk is in dit proefschrift verwerkt.

De noodzakelijke technische ondersteuning en onderricht werden gegeven door Albert van Etteger, Jan Hermsen, Jan Gerritsen, Adriaan van 't Hof, Willy Vollenberg, Kees Beers en Henk Neyenhuisen. Met Ferry Derksen en Wim Schut wil ik alle mensen van de instrumentmakerij bedanken. Hun werk was van vitaal belang bij de voortgang van het onderzoek.

De kontakten met de leden van de EVSF 2 groep waren altijd zeer prettig en een constante bron van ontspanning, waarbij ik toch niet kan nalaten Riki Gommers nog eens extra te bedanken voor het beschikbaar stellen van een pot drop, twee gewillige oren en een privé-collectie van anti-frustratie speeltjes.

De samenwerking met collega's uit binnen- en buitenland leidde steeds tot goede resultaten. Door de discussies met Maziar Nekovee (K.U. Nijmegen) en Wolfgang Hübner (K.F.A. Jülich) verbeterde mijn begrip van Tweede-Harmonische Generatie aan gemagnetiseerde systemen. Menno Prins (K.U. Nijmegen) wil ik niet alleen bedanken voor de preparatie van de cobalt/goud samples, maar ook voor de prettige samenwerking die leidde tot een zeer bruikbaar stuk theorie. Ik ben blij dat Bert Koopmans in de korte tijd dat hij in Nijmegen werkzaam was een aantal zaken die in

dit proefschrift zijn beschreven heeft geverifieerd en waar nodig nog wat puntjes op kale i's heeft gezet.

Ook de korte maar intense samenwerking met Wim de Jong (K.U. Nijmegen) en Rudiger Vollmer, Andre Kirilyuk, Hartmut Schwabe en J. Kirschner (Max-Planck-Institut, Halle/Saale) was bijzonder vruchtbaar. De laatstgenoemde bedank ik tevens voor het beschikbaar stellen van het ijzer kristal en de vele persoonlijke adviezen tijdens mijn (ijdele) pogingen om een schoon Fe(110) oppervlak te realiseren. Verder ben ik Ron Shen (U.C. Berkeley) zeer erkentelijk voor het feit dat ik drie maanden in zijn groep mocht meedraaien. Het was leerzaam om samen met Diethelm Johansmann te werken aan vloeibare kristallen, voor mij tot dan totaal onbekende systemen. Al met al was dit één van de interessantste periodes uit mijn leven.

Wim de Jong en Monique Wittebrood waren gelukkig bereid om de eerste versies van mijn proefschrift door te lezen, waardoor ik de gelegenheid kreeg een aantal zaken te verbeteren. Verder ben ik dankbaar dat de heer Migchelsen het hoofdstuk 'Voor niet-natuurkundigen' op het Nederlands heeft gecontroleerd. Ik hoop dat dit deel door veel mensen die niet bekend zijn met de natuurkunde gelezen zal worden, waardoor zij wellicht enig idee krijgen van de inhoud en de achtergronden van dit proefschrift.

Ik bedank John Inglesfield (K.U. Nijmegen) en Reinder Coehoorn (Philips Research, Eindhoven) voor het feit dat ze een deel van hun tijd beschikbaar hebben willen stellen voor het beoordelen van dit proefschrift.

Mijn familie dank ik voor hun nimmer aflatende belangstelling voor mijn werk en Layla Rasing voor de prachtige tekening op de omslag.

Over mijn meest naaste collega en 'bloedbroeder in de fysica' Kees van Hasselt zou ik een lang verhaal kunnen schrijven. We hebben vijf jaar lang samen onze dagen gesleten in hetzelfde laboratorium en de hoogte- en dieptepunten gedeeld. Ik zal me echter beperken tot twee regels: bedankt voor alle plezier, hulp, discussie en het feit dat je me hebt willen verdragen. Ik wens je vanaf deze plaats veel succes met jouw 'laatste loodjes'.

En dan als laatste is er nog degene die samen met mij het meest blij is met de voltooiing van dit proefschrift: Sandra, bedankt voor alle steun en Liefde. Het is me een grote vreugde dit proefschrift aan jou op te dragen.

Harald Wierenga
27 november 1994

Contents

Chapter 1

Introduction

The magnetic properties of thin films and multilayers containing ferromagnetic material provide a fascinating field of research, and are a subject of great current interest. Interfaces are a major influence on the magnetic characteristics of these systems. Therefore, a study of their properties is desirable, yet difficult. As buried interfaces in thin film systems are accessible by light an optical technique might lead the way. Second-Harmonic Generation is a well established optical probe, that derives its sensitivity to (buried) interfaces from symmetry breaking at boundaries between centrosymmetric media. On theoretical grounds it has been shown that magnetic effects should be detectable with SHG, and first experimental proof of Magnetization induced Second-Harmonic Generation (MSHG) was given by Reif *et al.* for the clean Fe(110) surface. In this thesis the influence of the magnetization on the second-harmonic signal from Co/Au and Co/Cu multilayers is discussed, and it is demonstrated that MSHG is sensitive to the magnetic properties of buried interfaces.

1.1 Magnetic multilayers and interfaces

Known for ages, and examined by both experienced scientists and curious children, magnetism has become an indispensable element in our every day life. Magnetism shuts the doors of cupboards and refrigerators, navigates the boy scouts, puts 'Oprah' on the videotape, and saves the love letter on the harddisc, for future use.

Due to the continuous need to miniaturize e.g. videocameras and computers, and at the same time enlarge their image quality and speed, artificial materials like thin films and multilayers have become of utmost importance,

as they allow both high data densities and increased storage and retrieval speeds [1]. Besides their technological significance, a number of extraordinary phenomena are observed in these systems, such as the change of the magnetization from in plane to normal for thin iron films [2-4], and in particular, the observed oscillatory exchange coupling through non-magnetic spacers, which has stimulated both experimental and theoretical research [5-18].

Interfaces have a major influence on the magnetic characteristics of multilayers [1, 5, 7, 19, 20]. Furthermore, the spin behavior at clean surfaces is quite different from the bulk [1,21-26], and from a general point of view interface magnetism is likely to differ from bulk behavior [19, 21, 23, 27]. Therefore, a study of buried interfaces in magnetic multilayers is both desirable and interesting.

There exist several electronic techniques, e.g. Spin Polarized Photoemission Spectroscopy [28], Spin Polarized Low Energy Electron Diffraction (SPLEED) [29], and Spin Polarized Electron Energy Loss Spectroscopy (SPEELS) [30], to study the magnetic properties of clean surfaces. Unfortunately (polarized) electrons are difficult to use for studying buried interfaces due to their short mean free path.

Polarized Neutron Reflectrometry (PNR) [31-33] is capable of probing the depth dependence of the magnetization in thin magnetic films, or at the surface of bulk magnetic systems [1]. Although PNR is sensitive to ultrathin magnetic films [34], the technique still lacks true interface sensitivity, as to the best of our knowledge, the depth resolution is limited to typically 2nm [1, 35]. PNR experiments require grazing incidence, and even with the present available neutron fluxes, flat sample areas of the order of $10cm^2$ are required [1,36-38]. Needless to say that sample preparation is quite demanding for such experiments.

Mössbauer Spectroscopy is a well established tool for the hyperfine structure of magnetic atoms [1]. After absorption of a γ photon, the Mössbauer nucleus (usually ^{57}Fe) de-excites by re-emitting γ rays, x-rays, or Auger electrons [39]. Although originally developed as a bulk probe, (buried) interface sensitivity is obtained after positioning the isotope at the interface, while the rest of the ferromagnetic film has the standard (natural) nucleus [40].

Since interfaces between thin metallic films are easily accessible to light, an optical technique has appealing possibilities. Second-Harmonic Generation is a well established interface sensitive optical probe, that is in principle sensitive to the magnetization of the interface. The advantages of this technique are manifold: (1) Small sample areas are sufficient, (2) no special materials/isotopes are required, (3) the technique can be used both in-situ and

ex-situ, (4) spectroscopy allows resolution of the electronic structure at the interface, (5) high spatial resolution, and (6) high temporal resolution.

1.2 Optical Second-Harmonic Generation (SHG)

Optical Harmonic Generation, as many other fields in physics, was initiated by the development of the laser [41, 42]. The process is in principle simple: Due to the nonlinear response of a medium, wave mixing of the incoming laser field induces a polarization containing harmonics:[1]

$$P = P(0) + P(\omega) + P(2\omega) + P(3\omega) + ... \tag{1.1}$$

where the subsequent terms describe Optical Rectification, linear reflection and refraction, Second-Harmonic Generation (SHG), and Third-Harmonic Generation (THG).[2] These polarizations act as the source of radiation at the corresponding frequency. Within this group SHG is particularly interesting due to its interface sensitive character.[3]

Although conversion rates up to 95 % are possible under optimum conditions [43], Second-Harmonic Generation is in general a very inefficient process. SHG was first demonstrated by Franken *et al*, after focussing a ruby laser beam into a crystalline quartz crystal [44]. One year later Terhune *et al.* showed that optical harmonic generation is not limited to crystals lacking a center of inversion. Both Second-Harmonic and Third-Harmonic Generation were observed in centrosymmetric calcite [45].

Bloembergen and Pershan gave the first thorough theoretical analysis of transmitted and reflected SHG from a semi-infinite nonlinear medium (i.e. the medium lacks inversion symmetry) and of a nonlinear slab positioned in between two semi-infinite linear media [46]. In the limit that the slab thickness goes to zero, their analysis describes SHG from interfaces. This started SHG experiments in a reflection geometry; Ducuing and Bloembergen showed SHG from GaAs [47, 48], and Brown *et al.* from a centrosymmetric silver mirror [49]. Whereas SHG in the first system is of the electric dipole type, such radiation is symmetry forbidden in the bulk of centrosymmetric media. Here SHG originates from electric quadrupole sources [45, 49, 50]. The latter

[1] Comparable to the generation of higher harmonics in an anharmonic oscillator [60].

[2] Mixing two laser fields with different frequencies leads to so called Sum and Difference Frequency Generation (SFG and DFG): $P = P(\omega_1) + P(\omega_2) + P(\omega_1 - \omega_2) + P(\omega_1 + \omega_2) + ...$

[3] Every even harmonic has in principle the same interface senstive character. However, fourth and higher even harmonics are less efficiently generated than the second-harmonic, and usually much more difficult to detect due to the poor transmission of optical components at high frequencies.

contributions were related to the gradient of the fundamental electric field at the interface, and gave an acceptable explanation of all known experimental results [50, 51].

However, in the early 1980's, the Shen group in Berkeley published several experimental results that showed that this description cannot be complete [51]. SHG from a silver surface was strongly enhanced by surface roughness [52]. The technique proved to be sensitive to monolayers, and even capable of determining the orientation of molecules adsorbed on a substrate [53-55], and Tom *et al.* showed that SHG is sensitive to the crystal structure of silicon [56]. These results proved that second-harmonic generation from centrosymmetric media could not be exclusively determined by the field gradient at the interface, and that a second source must exist. This second source is of the electric dipole type, and it is caused by the fact that the centrosymmetry is broken at the interface. This started strong activity to apply SHG as a truly interface sensitive probe [51, 57].

The modern theoretical description of SHG from centrosymmetric media was introduced by Guyost-Sionnest *et al.* [51, 58]. All second-harmonic sources up to first order in the spatial derivative are included in an effective second-harmonic polarization:[4]

$$\mathbf{P}^{(2)}_{eff}(2\omega) = \mathbf{P}^{(2)}(2\omega) - \nabla\cdot \overleftrightarrow{Q}^{(2)}(2\omega) + \frac{c}{i2\omega}\nabla \times \mathbf{M}^{(2)}(2\omega) \qquad (1.2)$$

The subsequent terms describe the electric dipole, electric quadrupole and magnetic dipole contributions. Considering for the moment only non-magnetic materials, the magnetic dipole contributions equal zero [58]. Substituting expressions for $\mathbf{P}^{(2)}(2\omega)$ and $\overleftrightarrow{Q}^{(2)}(2\omega)$ in terms of the fundamental electric field and the nonlinear susceptibilities gives [58, 59]:

$$\mathbf{P}^{(2)}_{eff}(2\omega) = \overleftrightarrow{\chi}^{(D)} : \mathbf{EE} + \overleftrightarrow{\chi}^{(Q)}_{FG} : \mathbf{E}\nabla\mathbf{E} - (\nabla\cdot \overleftrightarrow{\chi}^{(Q)}_{SG}) : \mathbf{EE} \qquad (1.3)$$

The first term describes a source of electric dipole radiation. Symmetry considerations show that these contributions are zero in a centrosymmetric medium, i.e. $\overleftrightarrow{\chi}^{(D)}$ describes the real interface contributions [60]. The second and third term in the equation are related to the field gradient and the structural gradient at the interface, respectively, and have an electric quadrupolar character. These latter contributions are the bulk contributions to SHG from centrosymmetric media.

[4] See also Ref. [59] for further reading.

The major problem in SHG is that the three terms in equation 1.3 are not only principally inseparable, as they can all be written as effective interface contributions [58], but can also be of the same order of magnitude, if the large volume difference between interface and bulk is taken into account [51].

Avoiding elaborate discussion of the magnetic dipole contributions, that will be present in the magnetic systems that are the subject of this thesis, we make a worst case approach by assuming that these contributions are also principally inseparable from the (magnetic) interface dipole radiation. Therefore, sensitivity to magnetic interfaces must be, and will be, verified for all systems, by explicit modification of the interface contributions.

1.3 Magnetization induced SHG (MSHG)

The Magneto-Optical Kerr Effect (MOKE) is a well known and frequently used linear optical technique to study the changes in the linear susceptibility as a function of the applied magnetic field. Though very sensitive and even applicable to monolayers, MOKE is not interface specific [1].

It has been shown, theoretically, that magnetization induced effects from interfaces should be detectable with SHG [61-63]. functions of the system are altered by a combination of spin-orbit coupling and exchange interaction. Changes of the wave functions have the largest influence on the optical susceptibility, and causes detectable effects [61-63].

Phenomenologically, the origin of Magnetization induced Second-Harmonic Generation (MSHG) can be understood from a symmetry analysis of magnetized systems. As a result we may distinguish two sets of tensor elements: odd and even in the magnetization, respectively [61]. The SH-intensity from the electric dipole sources at a single magnetic interface may be written as:

$$I(2\omega) = \left|\alpha_{even}\chi^{(D)}_{even}(\mathbf{M}) + \alpha_{odd}\chi^{(D)}_{odd}(\mathbf{M})\right|^2 I^2(\omega) \qquad (1.4)$$

where $\chi^{(D)}_{even}(\mathbf{M})$ and $\chi^{(D)}_{odd}(\mathbf{M})$ are linear combinations of even and odd tensor elements, respectively, α_{even} and α_{odd} are constants including the Fresnel coefficients, and $I(\omega)$ is the intensity of the fundamental beam. Changing the sign of $\mathbf{M}$ causes[5] a phase change of 180° between the two contributions in equation 1.4, and leads to a different SH-intensity. Equation 1.4 shows that the SH-intensity changes, upon inversion of the magnetization, are only observed if both even and odd elements are contributing to the SH-signal.

[5]This corresponds to e.g. switching from positive to negative magnetic saturation.

First experimental proof of Magnetization induced SHG was given by Reif *et al.* on the Fe(110) surface [64]. At present MSHG has already been observed in a variety of systems: PtMnSb(111) [65], polycrystalline nickel [66], $Mn_{0.6}Zn_{0.35}Fe_{2.05}O_4$ [67], polycrystalline Co/Au multilayers [68, 69, 70] (chapter 5), epitaxially grown fcc Co/Cu(001) [71] (chapter 6) and bcc Fe/Cu(001) (chapter 7).

1.4 Scope of this thesis

The main goal of this thesis is to prove that Magnetization induced Second-Harmonic Generation is sensitive to magnetic interfaces in a multilayer. Chapter 2 gives the phenomenological theory of MSHG, and in chapter 3 a multiple reflection model for SHG from interfaces in a multilayers is discussed. Together they form the theoretical basis for the analysis of the experiments. Chapter 4 describes the experimental systems. In chapter 5 we discuss MSHG from Co/Au-multilayers. It is shown that the results are in good agreement with the phenomenological theory of chapter 2. An analyses with the multiple reflection model of chapter 3 gives indirect proof of interface sensitivity. In chapter 6 the layer thickness dependence of MOKE and MSHG on epitaxially grown Co/Cu multilayers is discussed, as well as the influence of gas adsorption. The experiments give direct experimental proof of interface sensitivity in these well defined systems. We speculate on the possible relation between oscillations in the relative magnetic effect in MSHG and quantum well states in copper and cobalt. Chapter 7 briefly describes the results of our experiments on Ni(110) and Fe(110), where magnetization induced effects in the SH-intensity were not observed. Appendix A gives the derivation of the boundary conditions for an infinitesimal nonlinear sheet, and appendix B describes the elementary quantum mechanical theory of MSHG, as an introduction to its final goal: Magnetization induced Second-Harmonic Generation as an external macroscopic probe for the microscopic structural, electronical and magnetic properties of buried interfaces.

References

[1] L.M. Falicov *et al.*, J. Mater. Res. **5**, 1299 (1990).

[2] A. Vaterlaus, M. Stampanoni, M. Aeschlimann, and F. Meier, J. Appl. Phys. **64**, 5331 (1988).

[3] M. Stampanoni, A. Vaterlaus, M. Aeschlimann, F. Meier, and D. Pescia, J. Appl. Phys. **64**, 5321 (1988).

[4] Dongqi Li, M. Freitag, J. Pearson, Z.Q. Qiu, and S.D. Bader, Phys. Rev. Lett. **72**, 3112 (1994).

[5] M.T. Johnson, S.T. Purcell, N.W.E. McGee, R. Coehoorn, J. aan de Stegge, and W. Hoving, Phys. Rev. Lett. **68**, 2688 (1992).

[6] P. Grünberg, R. Schreiber, Y. Pang, M.B. Brodsky, and H. Sowers, Phys. Rev. Lett. **57**, 2442 (1986).

[7] Y. Wang, P.M. Levy, and J.L. Fry, Phys. Rev. Lett. **65**, 2732 (1990).

[8] D. Mauri, D. Scholl, H.C. Siegmann, and E. Kay, Phys. Rev. Lett. **62**, 1900 (1989).

[9] A. Cebollada, R. Miranda, C.M. Schneider, P. Schuster, and J. Kirschner, J. Magn. Magn. Mat. **102**, 25 (1991).

[10] S.S.P. Parkin, N. More and K.P. Roche, Phys. Rev. Lett. **64**, 2304 (1990)

[11] S.S.P. Parkin, Phys. Rev. Lett. **67**, 3598 (1991).

[12] S.S.P. Parkin, A. Mansour, and G.P. Felcher, Appl. Phys. Lett. **58**, 1473 (1991).

[13] P. Bruno and C. Chappert, Phys. Rev. Lett. **67**, 1602 (1991).

[14] P. Bruno and C. Chappert, Phys. Rev. B. **46**, 261 (1992).

[15] V. Grolier, D. Renard, B. Bartenlian, P. Beauvillain, C. Chappert, C. Dupas, J. Ferré, M. Galtier, E. Kolb, M. Mulloy, J.P. Renard, and P. Veillet, Phys. Rev. Lett. **71**, 3023 (1993).

[16] R. Coehoorn, Phys. Rev. B. **44**, 9331 (1991).

[17] J.E. Ortega, F.J. Himpsel, Phys. Rev. Lett. **69**, 844 (1992).

[18] J.E. Ortega, F.J. Himpsel, G.J. Mankey, and R.F. Willis, Phys. Rev. B **47**, 1540 (1993).

[19] N.B. Brookes, Y. Chang and P.D. Johnson, Phys. Rev. Lett. **67**, 354 (1991).

[20] R. Schad, C.D. Potter, P. Beliën, G. Verbanck, V.V. Moshchalkov, and Y. Bruynseraede, Appl. Phys. Lett. **64**, 3500 (1994).

[21] C.L. Fu, A.J. Freeman, and T. Oguchi, Phys. Rev. Lett. **54**, 2700 (1985).

[22] D. Weller, S.F. Alvarado, and M. Campagna, Physica B&C **130**, 72 (1985).

[23] A.J. Freeman, and C.L. Fu, J. Appl. Phys. **61**, 3356 (1987).

[24] T. Kaneyoshi, J. Phys.: Condens. Matter. **3**, 4497 (1991).

[25] D.P. Landau, and K. Binder, J. Appl. Phys. **63**, 3077 (1988).

[26] J. Bansmann, M. Getzlaff, C. Westphal, and G. Schönhense, J. Magn. Magn .Mat. **117**, 38 (1992).

[27] O.Paul, S. Toscano, K. Totland, and M. Landolt, Surf. Sci. **251/252**, 27 (1991).

[28] M. Campagna, D.T. Pierce, F. Meier, K. Sattler, and H.C. Siegmann, Adv. Electr. and Electr. Phys. **41**, 113 (1976).

[29] see for example: *Polarized Electrons in Surface Physics*, edited by R. Feder (World Scientific, Singapore, 1985).

[30] D.L. Abraham and H. Hopster, Phys. Rev. Lett. **62**, 1157 (1989).

[31] G.P Felcher, Phys. Rev. B **24**, 1595 (1981).

[32] G.P Felcher, R.O. Hilleke, R.K. Crawford, J. Haumann, R. Kleb, and G. Ostrowski, Rev. Sci. Instrum. **58**, 609 (1987).

[33] C.F. Majkrzak, Physica B **173**, 75 (1991).

[34] S.S.P. Parkin, A. Mansour, and G.P. Felcher, Appl. Phys. Lett. **58**, 1473 (1991).

[35] M. Mâaza, J. Magn. Magn. Mat. **121**, 112 (1993).

[36] M.P. Nutley, A.T. Broothroyd, C.R. Staddon, D.M^{c}K. Paul, and J. Penfold, Phys. Rev. B **49**, 15789 (1994).

[37] M. Loewenhaupt, W. Hahn, Y.Y. Huang, G.P. Felcher, and S.S.P. Parkin, J. Magn. Magn. Mat. **121**, 173 (1993).

[38] J.F. Anker, C.F. Majkrzak, D.A. Neumann, A. Matheny, and C.P. Flynn, Physica B **173**, 89 (1991).

[39] H.R. Borsje *Experimental investigations of surface magnetism* (Thesis, Katholieke Universiteit Nijmegen, Nijmegen, The Netherlands, 1991).

[40] J. Korecki, and U. Gradmann, Phys. Rev. Lett. **55**, 2491 (1985).

[41] T.H. Maiman, Nature **187**, 493 (1960).

[42] R.J. Collins, D.F. Nelson, A.L. Schawlow, W. Bond, C.G.B. Garrett, and W. Kaiser, Phys. Rev. Lett. **5**, 303 (1960).

[43] D. Eimerl, IEEE J. Quant. El. **23**, 1361 (1987).

[44] P.A. Franken, A.E. Hill, C.W. Peters, and G. Weinreich, Phys. Rev. Lett. **7**, 118 (1961).

[45] R.W. Terhune, P.D. Maker, and C.M. Savage, Phys. Rev. Lett. **8**, 404 (1962).

[46] N. Bloembergen, and P.S. Pershan, Phys. Rev. **128**, 606 (1962).

[47] J. Ducuing, and N. Bloembergen, Phys. Rev. Lett. **10**, 474 (1963).

[48] R.K. Chang, and N. Bloembergen, Phys. Rev. **144**, 775 (1966).

[49] F. Brown, R.E. Parks, and A.M. Sleeper, Phys. Rev. Lett. **14**, 1029 (1965).

[50] N. Bloembergen, R.K. Chang, S.S. Jha, and C.H. Lee, Phys. Rev. **174**, 813 (1968).

[51] P. Guyot-Sionnest, W. Chen, and Y.R. Shen, Phys. Rev. B **33**, 8254 (1986).

[52] C.K. Chen, A.R.B. de Castro, and Y.R. Shen, Phys. Rev. Lett. **46**, 145 (1981).

[53] C.K. Chen, T.F. Heinz, D. Ricard, and Y.R. Shen, Phys. Rev. Lett. **46**, 1010 (1981).

[54] T.F. Heinz, C.K. Chen, D. Ricard, and Y.R. Shen, Phys. Rev. Lett. **48**, 478 (1982).

[55] D.V. Murphy, K.U. von Raben, T.T. Chen, J.F. Owen, and R.K. Chang, Surf. Sci. **124**, 529 (1983).

[56] H.W.K. Tom, T.F. Heinz, and Y.R. Shen, Phys. Rev. Lett. **51**, 1983 (1983).

[57] Y.R. Shen, J. Vac. Sci. Technol. B **3**, 1464 (1985).

[58] P. Guyot-Sionnest, and Y.R. Shen, Phys. Rev. B **38**, 7985 (1988).

[59] B. Koopmans, *Interface and bulk contributions in optical second-harmonic generation* (Thesis, Rijksuniversiteit Groningen, Groningen, The Netherlands, 1993).

[60] Y.R. Shen, *The principles of nonlinear optics* (Wiley, New York, 1984).

[61] Ru-Pin Pan, H.D. Wei, and Y.R. Shen, Phys. Rev. B **39**, 1229 (1989).

[62] W. Hübner, Phys. Rev. B **42**, 11553 (1990).

[63] U. Pustogowa, W. Hübner, and K.H. Bennemann, Phys. Rev. B **48**, 8607 (1993).

[64] J. Reif, J.C. Zink, C.M. Schneider, and J. Kirschner, Phys. Rev. Lett. **67**, 2878 (1991).

[65] J. Reif, C. Rau, and E. Matthias, Phys. Rev. Lett. **71**, 1931 (1993).

[66] K. Böhmer, J. Hohlfeld, and E. Matthias, to appear in Appl. Phys. A.

[67] Th. Rasing, and H.A. Wierenga, accepted for publication in Ferroelectrics.

[68] G. Spierings, V. Koutsos, H.A. Wierenga, M.W.J. Prins, D. Abraham, and Th. Rasing, Surf.Sci. **287-288**, 747 (1993).

[69] G. Spierings, V. Koutsos, H.A. Wierenga, M.W.J. Prins, D. Abraham, and Th. Rasing, J. Magn. Magn. Mat. **121**, 109 (1993).

[70] H.A. Wierenga, M.W.J. Prins, D.L. Abraham, and Th. Rasing, Phys. Rev. B **50**, 1282 (1994).

[71] H.A. Wierenga, W. de Jong, M.W.J. Prins, Th. Rasing, R. Vollmer, R. Kirilyuk, H. Schwabe, and J. Kirschner, submitted.

Chapter 2

Phenomenological theory

A phenomenological approach to Magnetization induced Second-Harmonic Generation (MSHG) shall be discussed. This symmetry based analysis has been introduced by Ru-Pin Pan *et al.* [1]. It gives the complete set of nonzero tensor elements in the presence of a magnetization, and offers a good qualitative description of the experimental results, as shall be shown in chapter 5. The properties of the tensor elements under time-inversion shall be discussed. Finally, the relations between tensor elements of two comparable, but mirrored interfaces are determined.

2.1 Tensor elements of magnetized materials

In this section we present the symmetry-analysis that gives all the nonzero tensor elements of any magnetized system once its unmagnetized (crystallographical) symmetry is known. For practical reasons we limit ourselves to a detailed analysis of two systems: **(a)** cubic(001), and **(b)** isotropic.[1] However, the tensor elements of other systems can be derived along similar lines.

Figure 2.1 shows a simple reflection geometry for SHG on the (001) plane of a cubic sample in vacuum. The surface is parallel to the **x**,**y**-plane. The **x**-axis is lying in the plane of incidence, and the **z**-axis is normal to the interface and pointing inwards. **x**, **y** and **z** are also the crystal axes. The general formula describing SHG is given by:

$$P_j(2\omega) = \chi^{(D)}_{jkl} E_k(\omega) E_l(\omega) + \chi^{(Q)}_{jklm} E_k(\omega) \nabla_l E_m(\omega) + \ldots \quad \text{with } j,k,l,m = x,y,z \tag{2.1}$$

[1] We shall see that these systems are virtually identical.

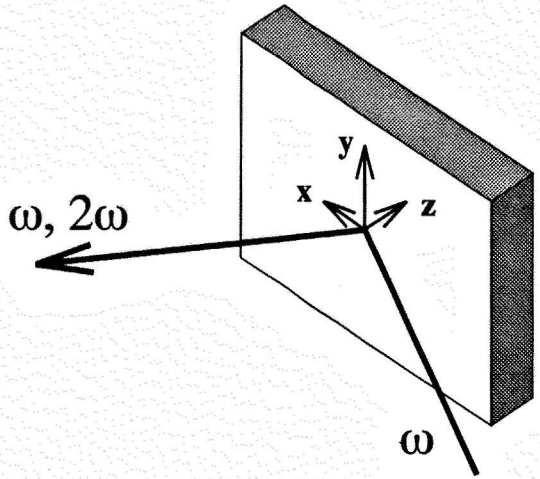

Figure 2.1: *Simple reflection geometry for SHG.*

The expression is limited to electric dipole contributions by the surface, and field gradient related electric quadrupole contributions by the bulk (see equation 1.3), as we are merely interested in showing that both surface and bulk contributions are influenced by the magnetization, thereby emphasizing the necessity of explicit experimental proof of interface sensitivity (see chapter 1).

According to Neumann's principle $\chi^{(D)}$ and $\chi^{(Q)}$ must reflect the symmetry of the system [2]. Therefore, the nonzero elements are easily derived from the invariance of $\chi^{(D)}$ and $\chi^{(Q)}$ under symmetry operations:

$$\chi^{(D)}_{jkl} = T_{jj'}T_{kk'}T_{ll'}\chi^{(D)}_{j'k'l'} \quad \text{and} \quad \chi^{(Q)}_{jklm} = T_{jj'}T_{kk'}T_{ll'}T_{mm'}\chi^{(Q)}_{j'k'l'm'} \tag{2.2}$$

where T is the transformation matrix for a symmetry operation and autosummation is implied. Because of the equivalence of the fundamental fields $E_k(\omega)$ and $E_l(\omega)$ in the first term of eq. 2.1, we always find: $\chi^{(D)}_{jkl} = \chi^{(D)}_{jlk}$.[2]

We shall follow the analysis of Ru-Pin Pan *et al.* [1] and include the magnetic properties of the material by introducing magnetization dependent nonlinear susceptibility tensors: $\chi^{(D)}(\mathbf{M})$ and $\chi^{(Q)}(\mathbf{M})$. It is important to realize that the inversion symmetry of the bulk is not broken by the magnetization.

[2]The relation $\chi^{(Q)}_{jklm} = \chi^{(Q)}_{jmlk}$ does not hold in general, as $E_k(\omega)\nabla_l E_m(\omega)$ is not a priori equal to $E_m(\omega)\nabla_l E_k(\omega)$.

Since $\mathbf{M}$ is an axial vector its orientation is conserved under inversion.[3] This means that magnetizing the material does not induce electric dipole contributions from the bulk, and the basic argument for potential interface sensitivity of MSHG remains valid. However, the magnetization does lower the symmetry of the surface, which introduces extra nonzero tensor elements. Let us first consider the electric dipole contributions: $\chi^{(D)}_{jkl}(\mathbf{M})$, from the cubic(001) surface for a magnetization $\mathbf{M} = M\mathbf{y}$, i.e. the magnetization is lying in the plane of the sample and is oriented perpendicular to the plane of incidence. The magnetization reduces the original $4mm$ symmetry of the surface to $1m$-like, i.e. it would be $1m$ if the magnetization did not have an axial character. This $1m$-like system has only two operations that leave the system invariant:

(1) In the absence of a magnetization, $\mathcal{M}_{\mathbf{x}}$ (the mirror operation in the $\mathbf{y}$,$\mathbf{z}$-plane) would be a perfect symmetry operation. With magnetization, however, the operation is accompanied by the transformation $M\mathbf{y} \rightarrow -M\mathbf{y}$, due to the axial character of $\mathbf{M}$.[4] So the real symmetry operation of the complete magnetized system must also involve a correction of this inversion of $\mathbf{M}$, and we obtain:

$$\mathcal{M}^{-}_{\mathbf{x}} \circ \chi^{(D)}_{jkl}(M\mathbf{y}) = \chi^{(D)}_{jkl}(M\mathbf{y}) \tag{2.3}$$

where the superscript minus of $\mathcal{M}^{-}_{\mathbf{x}}$ refers to the inversion of $\mathbf{M}$. Let us consider two examples:

$$\mathcal{M}^{-}_{\mathbf{x}} \circ \chi^{(D)}_{zxx}(M\mathbf{y}) = \chi^{(D)}_{zxx}(M\mathbf{y}) \tag{2.4}$$

$$\Leftrightarrow \quad \chi^{(D)}_{zxx}(-M\mathbf{y}) = \chi^{(D)}_{zxx}(M\mathbf{y}) \tag{2.5}$$

and

$$\mathcal{M}^{-}_{\mathbf{x}} \circ \chi^{(D)}_{xxx}(M\mathbf{y}) = \chi^{(D)}_{xxx}(M\mathbf{y}) \tag{2.6}$$

$$\Leftrightarrow \quad -\chi^{(D)}_{xxx}(-M\mathbf{y}) = \chi^{(D)}_{xxx}(M\mathbf{y}) \tag{2.7}$$

(2) $\mathcal{M}_{\mathbf{y}}$ (the mirror operation in the $\mathbf{x}$,$\mathbf{z}$-plane) is also a crystallographic

[3] Inversion is equivalent to mirroring in three mutually perpendicular planes. Take one of the mirror planes normal to $\mathbf{M}$ and imagine $\mathbf{M}$ being the result of a circular current. Verify that mirroring in the plane normal to $\mathbf{M}$ leaves $\mathbf{M}$ invariant, while the orientation of $\mathbf{M}$ is inverted under the other two mirror operations. The total result of these three operations is that $\mathbf{M}$ is conserved.

[4] Imagine $\mathbf{M}$ being the result of a circular current, and verify that mirroring in the $\mathbf{y}$,$\mathbf{z}$-plane inverts the direction of the current.

symmetry operation, but this operation does not affect the orientation of $\mathbf{M}$, so we find:

$$\mathcal{M}_{\mathbf{y}}^{+} \circ \chi_{jkl}^{(D)}(M\mathbf{y}) = \chi_{jkl}^{(D)}(M\mathbf{y}) \tag{2.8}$$

As a result, we can distinguish two sets of tensor elements: one set is even, and the other set is odd in the magnetization. Because the distinction is found for any orientation of the magnetization and also for $\chi^{(Q)}(\mathbf{M})$, we can generalize that in magnetized materials $\chi^{(D)}(\mathbf{M})$ and $\chi^{(Q)}(\mathbf{M})$ have two sets of elements:

$$\chi^{(D/Q),even}(-\mathbf{M}) = \chi^{(D/Q),even}(\mathbf{M}) \tag{2.9}$$

$$\chi^{(D/Q),odd}(-\mathbf{M}) = -\chi^{(D/Q),odd}(\mathbf{M}) \tag{2.10}$$

In the remainder of this thesis we may describe tensor elements as being even or odd, where we implicitly refer to their dependence on $\mathbf{M}$.

The cubic(001) and the isotropic surface have the same symmetry group ($4mm$), so both systems have a similar set of tensor elements, also if magnetized. Because there is also only a minimal difference between the quadrupole-like tensors $\chi^{(Q)}(\mathbf{M})$ for magnetized cubic and magnetized isotropic bulk, we shall refer to both systems as being isotropic. The slight difference in $\chi^{(Q)}(\mathbf{M})$ shall be mentioned explicitly, later in this section.

Table 2.1 shows the complete set of nonzero tensor elements of the isotropic surface, with $\mathbf{M} = M\mathbf{y}$. For comparison table 2.2 gives the tensor elements of this system if it is not magnetized (see for example Ref. [3]). It is interesting to realize that this set is nearly identical to the set of even tensor elements of the magnetized system. So breaking the symmetry by magnetizing induces new tensor elements that are all odd.

The nonzero elements of $\chi^{(D)}(\mathbf{M})$ for a magnetization in the plane of the film and parallel to the plane of incidence ($\mathbf{M} = M\mathbf{x}$) are of course easily obtained from the previous results by exchanging x and y in table 2.1 . For isotropic systems with a magnetization normal to the surface ($\mathbf{M} = M\mathbf{z}$) we derive the nonzero elements of $\chi^{(D)}(\mathbf{M})$ from the symmetry operations:

$$\mathcal{M}_{\mathbf{x}}^{-} \circ \chi_{jkl}^{(D)}(M\mathbf{z}) = \chi_{jkl}^{(D)}(M\mathbf{z}) \tag{2.11}$$

$$\mathcal{M}_{\mathbf{y}}^{-} \circ \chi_{jkl}^{(D)}(M\mathbf{z}) = \chi_{jkl}^{(D)}(M\mathbf{z}) \tag{2.12}$$

$$\mathcal{R}_{\mathbf{z},\alpha}^{+} \circ \chi_{jkl}^{(D)}(M\mathbf{z}) = \chi_{jkl}^{(D)}(M\mathbf{z}) \tag{2.13}$$

Even in $\mathbf{M}$	$\chi_{xxz}(M\mathbf{y}) = \chi_{xzx}(M\mathbf{y})$, $\chi_{yyz}(M\mathbf{y}) = \chi_{yzy}(M\mathbf{y})$, $\chi_{zxx}(M\mathbf{y})$, $\chi_{zyy}(M\mathbf{y})$, $\chi_{zzz}(M\mathbf{y})$
Odd in $\mathbf{M}$	$\chi_{xxx}(M\mathbf{y})$, $\chi_{xyy}(M\mathbf{y})$, $\chi_{xzz}(M\mathbf{y})$ $\chi_{yxy}(M\mathbf{y}) = \chi_{yyx}(M\mathbf{y})$, $\chi_{zxz}(M\mathbf{y}) = \chi_{zzx}(M\mathbf{y})$,

Table 2.1: *Nonzero tensor elements of the nonlinear susceptibility tensor $\chi^{(D)}(\mathbf{M})$ for the magnetized isotropic surface. The magnetization $\mathbf{M}$ is parallel to the $\mathbf{y}$-axis, $\mathbf{z}$ is parallel to the surface normal, and $\mathbf{x}$ is in the plane of incidence.*

Non-magnetized	$\chi_{xxz} = \chi_{xzx} = \chi_{yyz} = \chi_{yzy}$, $\chi_{zxx} = \chi_{zyy}$, χ_{zzz}

Table 2.2: *Nonzero tensor elements of the nonlinear susceptibility tensor $\chi^{(D)}$ for the non-magnetized isotropic surface.*

Here $\mathcal{R}^{+}_{\mathbf{z},\alpha}$ represents a rotation around the $\mathbf{z}$-axis over an arbitrary angle α. It is convenient to start the analysis from the consideration that combining the symmetry operations in eq. 2.11 and 2.12 leads to:

$$\mathcal{M}^{-}_{\mathbf{x}} \circ \mathcal{M}^{-}_{\mathbf{y}} \circ \chi^{(D)}_{jkl}(M\mathbf{z}) = \chi^{(D)}_{jkl}(M\mathbf{z}) \tag{2.14}$$

Table 2.3 shows the resulting nonzero elements of $\chi^{(D)}(M\mathbf{z})$. The set is slightly different from the one obtained in Ref. [1].[5] Although all sets of tensor elements in tables 2.1 through 2.3 were obtained for a surface in vacuum, brief

[5]Probably because the authors overlooked the minus signs that occur after applying equation 2.13.

Even in $\mathbf{M}$	$\chi_{xxz}(M\mathbf{z}) = \chi_{xzx}(M\mathbf{z}) = \chi_{yyz}(M\mathbf{z}) = \chi_{yzy}(M\mathbf{z})$, $\chi_{zxx}(M\mathbf{z}) = \chi_{zyy}(M\mathbf{z})$, $\chi_{zzz}(M\mathbf{z})$
Odd in $\mathbf{M}$	$\chi_{xyz}(M\mathbf{z}) = \chi_{xzy}(M\mathbf{z}) = -\chi_{yxz}(M\mathbf{z}) = -\chi_{yzx}(M\mathbf{z})$,

Table 2.3: *Nonzero tensor elements of the nonlinear susceptibility tensor $\chi^{(D)}(\mathbf{M})$ for a magnetized isotropic surface. The magnetization $\mathbf{M}$ is parallel to the $\mathbf{z}$-axis, $\mathbf{z}$ is parallel to the surface normal, and $\mathbf{x}$ is in the plane of incidence.*

consideration learns that identical results are found for a buried cubic(001) or isotropic interface, as it has the same symmetry.

The elements of $\chi^{(Q)}$ for the bulk cubic system with $\mathbf{M} = M\mathbf{y}$ (remember that $\mathbf{y}$ is a crystal axis) are enlisted in table 2.4. They are derived from the symmetry operations:

$$\mathcal{M}^{-}_{\mathbf{x}} \circ \chi^{(Q)}_{jklm}(M\mathbf{y}) = \chi^{(Q)}_{jklm}(M\mathbf{y}) \quad (2.15)$$

$$\mathcal{M}^{+}_{\mathbf{y}} \circ \chi^{(Q)}_{jklm}(M\mathbf{y}) = \chi^{(Q)}_{jklm}(M\mathbf{y}) \quad (2.16)$$

$$\mathcal{M}^{-}_{\mathbf{z}} \circ \chi^{(Q)}_{jklm}(M\mathbf{y}) = \chi^{(Q)}_{jklm}(M\mathbf{y}) \quad (2.17)$$

$$\mathcal{R}^{+}_{\mathbf{y},90^\circ} \circ \chi^{(Q)}_{jklm}(M\mathbf{y}) = \chi^{(Q)}_{jklm}(M\mathbf{y}) \quad (2.18)$$

For the isotropic system with $\mathbf{M} = M\mathbf{y}$ we have an identical set of symmetry operations, with one exception: $\mathcal{R}^{+}_{\mathbf{y},\alpha} \circ \chi^{(Q)}_{jklm}(M\mathbf{y}) = \chi^{(Q)}_{jklm}(M\mathbf{y})$ is a symmetry operation for all α. This leads to one extra relation between the even tensor elements, that is also found for the $\chi^{(Q)}$ of a non-magnetized isotropic material [4, 5]:

$$\chi^{(Q)}_{xxxx}(M\mathbf{y}) = \chi^{(Q)}_{xxzz}(M\mathbf{y}) + \chi^{(Q)}_{xzzx}(M\mathbf{y}) + \chi^{(Q)}_{xzxz}(M\mathbf{y}) \quad (2.19)$$

We also obtain one extra relation between the odd tensor elements:[6]

[6]These relations can of course be obtained in a full analysis of the influence of a rotation

even in $\mathbf{M}$	$\chi_{xxxx}(M\mathbf{y}) = \chi_{zzzz}(M\mathbf{y})$, $\chi_{xxyy}(M\mathbf{y}) = \chi_{zzyy}(M\mathbf{y})$, $\chi_{xyyx}(M\mathbf{y}) = \chi_{zyyz}(M\mathbf{y})$, $\chi_{xxzz}(M\mathbf{y}) = \chi_{zzxx}(M\mathbf{y})$, $\chi_{xzzx}(M\mathbf{y}) = \chi_{zxxz}(M\mathbf{y})$, $\chi_{xyxy}(M\mathbf{y}) = \chi_{zyzy}(M\mathbf{y})$, $\chi_{xzxz}(M\mathbf{y}) = \chi_{zxz\hat{x}}(M\mathbf{y})$, $\chi_{yxxy}(M\mathbf{y}) = \chi_{yzzy}(M\mathbf{y})$, $\chi_{yyxx}(M\mathbf{y}) = \chi_{yyzz}(M\mathbf{y})$, $\chi_{yxyx}(M\mathbf{y}) = \chi_{yzyz}(M\mathbf{y})$, $\chi_{yyyy}(M\mathbf{y})$
odd in $\mathbf{M}$	$\chi_{xxxz}(M\mathbf{y}) = -\chi_{zzzx}(M\mathbf{y})$, $\chi_{xxzx}(M\mathbf{y}) = -\chi_{zzxz}(M\mathbf{y})$, $\chi_{xzzz}(M\mathbf{y}) = -\chi_{zxxx}(M\mathbf{y})$, $\chi_{yxzy}(M\mathbf{y}) = -\chi_{yzxy}(M\mathbf{y})$, $\chi_{yyzx}(M\mathbf{y}) = -\chi_{yyxz}(M\mathbf{y})$, $\chi_{xyzy}(M\mathbf{y}) = -\chi_{zyxy}(M\mathbf{y})$, $\chi_{xyyz}(M\mathbf{y}) = -\chi_{zyyx}(M\mathbf{y})$, $\chi_{xzyy}(M\mathbf{y}) = -\chi_{zxyy}(M\mathbf{y})$, $\chi_{yxyz}(M\mathbf{y}) = -\chi_{yzyx}(M\mathbf{y})$, $\chi_{xzxx}(M\mathbf{y}) = -\chi_{zxzz}(M\mathbf{y})$,

Table 2.4: *Nonzero tensor elements of the nonlinear susceptibility tensor* $\chi^{(Q)}(\mathbf{M})$ *for magnetized cubic bulk. The magnetization* $\mathbf{M}$ *is parallel to the* $\mathbf{y}$*-axis.*

$$\chi^{(Q)}_{xzzz}(M\mathbf{y}) = \chi^{(Q)}_{xxxz}(M\mathbf{y}) + \chi^{(Q)}_{xzxx}(M\mathbf{y}) + \chi^{(Q)}_{xxzx}(M\mathbf{y}) \tag{2.20}$$

The elements of $\chi^{(Q)}(M\mathbf{x})$ are obtained by exchanging y and x in table 2.4 and the elements of $\chi^{(Q)}(M\mathbf{z})$ are obtained by exchanging y and z in the same table.

2.2 Time-inversion properties of χ

Interesting aspects of the elements of $\chi^{(D)}(\mathbf{M})$ and $\chi^{(Q)}(\mathbf{M})$ are found in an analysis of the time-inversion properties of the system. Let us reconsider the general formula describing SHG:

$$P_{2\omega,j}(\mathbf{r},t) = \chi^{(D)}_{jkl} E_{\omega,k}(\mathbf{r},t) E_{\omega,l}(\mathbf{r},t) + \chi^{(Q)}_{jklm} E_{\omega,k}(\mathbf{r},t) \nabla_l E_{\omega,m}(\mathbf{r},t) + \ldots \tag{2.21}$$

over an arbitrary angle α. However it is more convenient to do a first order of magnitude analysis after rotating over an infinitesimal angle δ.

The explicit time- and position-dependence of the fields and the polarization will be discussed in the next chapter (see eq. 3.2 and further). Here we simply state that time-inversion implies: $t \rightarrow -t$, $\mathbf{k} \rightarrow -\mathbf{k}$, and $\phi \rightarrow -\phi$, where $\mathbf{k}$ represents the wave vector and ϕ the phase. If we neglect losses due to dissipation, this leads to:

$$P_{2\omega,j}(\mathbf{r},t) \rightarrow P^*_{2\omega,j}(\mathbf{r},t) \quad \text{and} \quad E_{\omega,k}(\mathbf{r},t) \rightarrow E^*_{\omega,k}(\mathbf{r},t) \tag{2.22}$$

However, for a magnetized system, due to the axial character of $\mathbf{M}$, time-inversion leads to: $\mathbf{M} \rightarrow -\mathbf{M}$. We have shown in the previous section that one can distinguish odd and even tensor elements, and it is useful to write this down explicitly:

$$P_{2\omega,j}(\mathbf{r},t) = \left[\chi^{(D),even}_{jkl}(\mathbf{M}) + \chi^{(D),odd}_{jkl}(\mathbf{M}) \right] E_{\omega,k}(\mathbf{r},t) E_{\omega,l}(\mathbf{r},t) \tag{2.23}$$

where we have limited ourselves for the moment to the electric dipole sources. Using eq. 2.22, 2.9, and 2.10 we find that time-inversion leads to:

$$P^*_{2\omega,j}(\mathbf{r},t) = \left[\chi^{(D),even}_{jkl}(\mathbf{M}) - \chi^{(D),odd}_{jkl}(\mathbf{M}) \right] E^*_{\omega,k}(\mathbf{r},t) E^*_{\omega,l}(\mathbf{r},t) \tag{2.24}$$

Adding eq. 2.23 and 2.24 gives:

$$\begin{aligned} P_{2\omega,j}(\mathbf{r},t) + \text{c.c.} \;=\; & \chi^{(D),even}_{jkl}(\mathbf{M}) \left[E_{\omega,k}(\mathbf{r},t) E_{\omega,l}(\mathbf{r},t) + \text{c.c.} \right] \\ & + \chi^{(D),odd}_{jkl}(\mathbf{M}) \left[E_{\omega,k}(\mathbf{r},t) E_{\omega,l}(\mathbf{r},t) - \text{c.c.} \right] \end{aligned} \tag{2.25}$$

The left hand side of this equation is real. Because the equation must hold for all $\mathbf{r}$ and t, we obtain that both terms in the right hand side of eq. 2.25 must be real, and we conclude that the $\chi^{(D),even}_{jkl}(\mathbf{M})$ are pure real, while the $\chi^{(D),odd}_{jkl}(\mathbf{M})$ are pure imaginary:

$$\chi^{(D),even}_{jkl}(\mathbf{M}) \in \Re \quad \text{and} \quad i\chi^{(D),odd}_{jkl}(\mathbf{M}) \in \Re \tag{2.26}$$

The same result is found for $\chi^{(Q)}(\mathbf{M})$. These are extremely powerful relations. However, they only hold if dissipation is negligible, which implies that the dielectric constant of the material should be real, both at the fundamental and the second-harmonic frequency. One could also say that eq. 2.26 holds only at frequencies far from the resonance frequencies of the system. At frequencies where dissipation is not negligible, the phase difference between $\chi^{(D/Q),even}_{jkl}(\mathbf{M})$ and $\chi^{(D/Q),odd}_{jkl}(\mathbf{M})$ is no longer a priori determined by simple arguments. At these frequencies the dielectric constant has a complex value.

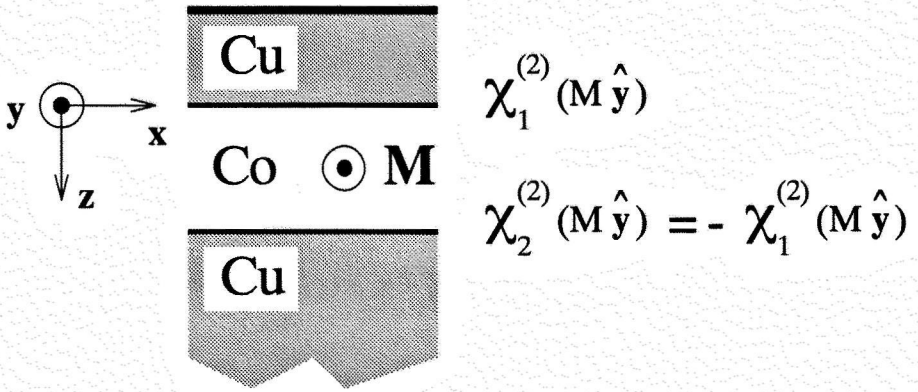

Figure 2.2: *A trilayer of cobalt and copper. The system has two identical, but mirrored magnetic Co/Cu interfaces. The tensor elements of these two interfaces have opposite phases.*

2.3 Mirrored interfaces

Many relevant multilayered systems contain alternating layers of two materials [6-10]. Such a multilayer has only two types of interfaces. As an example figure 2.2 shows a simple trilayer system of copper and magnetized cobalt. The system contains one non-magnetic interface between copper and the ambient medium and two identical, but mirrored magnetic interfaces between cobalt and copper. The relations between the tensor elements of these Co/Cu interfaces can be derived from considering the influence of mirroring in the **x**,**y**-plane:

$$\mathcal{M}_{\mathbf{z}}^{-} \circ \chi_{jkl,1}^{(D)}(M\mathbf{y}) = \chi_{jkl,2}^{(D)}(M\mathbf{y}) \tag{2.27}$$

where $\chi_{jkl,1}^{(D)}(M\mathbf{y})$ and $\chi_{jkl,2}^{(D)}(M\mathbf{y})$ are the nonlinear susceptibility tensor elements of interface 1 and interface 2 respectively (see figure 2.2). The relation expresses the fact that mirroring interface 1 in the **x**,**y**-plane gives the morphology of interface 2, but that it is accompanied by the inversion: $M\mathbf{y} \rightarrow -M\mathbf{y}$. Let us consider the relation between $\chi_{zxx,1}^{(D)}(M\mathbf{y})$ and $\chi_{zxx,2}^{(D)}(M\mathbf{y})$ in detail. Eq. 2.27 implies:

$$\mathcal{M}_{\mathbf{z}}^{-} \circ \chi_{zxx,1}^{(D)}(M\mathbf{y}) = -\chi_{zxx,1}^{(D)}(-M\mathbf{y}) = -\chi_{zxx,1}^{(D)}(M\mathbf{y}) = \chi_{zxx,2}^{(D)}(M\mathbf{y}) \tag{2.28}$$

where we have used the fact that $\chi^{(D)}_{xxx,n}(M\mathbf{y})$ is even. We find a phase difference of 180° between the elements. For the tensor elements $\chi^{(D)}_{xxx,n}(M\mathbf{y})$ we find:

$$\mathcal{M}^-_{\mathbf{z}} \circ \chi^{(D)}_{xxx,1}(M\mathbf{y}) = \chi^{(D)}_{xxx,1}(-M\mathbf{y}) = -\chi^{(D)}_{xxx,1}(M\mathbf{y}) = \chi^{(D)}_{xxx,2}(M\mathbf{y}) \quad (2.29)$$

where we have used the fact that $\chi^{(D)}_{xxx,n}(M\mathbf{y})$ is odd. Again we find a phase difference of 180° between the elements. A brief look at table 2.1 tells us that all elements of $\chi^{(D)}(M\mathbf{y})$ with an odd number of indices equal to z are even in $\mathbf{M}$, while all elements with an even number of indices equal to z are odd in $\mathbf{M}$. So we find:

$$\mathcal{M}^-_{\mathbf{z}} \circ \chi^{(D),even}_1(M\mathbf{y}) = -\chi^{(D),even}_1(-M\mathbf{y}) = -\chi^{(D),even}_1(M\mathbf{y}) = \chi^{(D),even}_2(M\mathbf{y}) \quad (2.30)$$

and

$$\mathcal{M}^-_{\mathbf{z}} \circ \chi^{(D),odd}_1(M\mathbf{y}) = \chi^{(D),odd}_1(-M\mathbf{y}) = -\chi^{(D),odd}_1(M\mathbf{y}) = \chi^{(D),odd}_2(M\mathbf{y}) \quad (2.31)$$

Giving the general equation:

$$\chi^{(D)}_1(M\mathbf{y}) = -\chi^{(D)}_2(M\mathbf{y}) \quad (2.32)$$

Of course we find a similar relation for $\mathbf{M} = M\mathbf{x}$, and also for $\mathbf{M} = M\mathbf{z}$ we find the phase difference of 180° between the elements of $\chi^{(D)}_1(M\mathbf{z})$ and $\chi^{(D)}_2(M\mathbf{z})$, because:

$$\mathcal{M}^+_{\mathbf{z}} \circ \chi^{(D)}_{jkl,1}(M\mathbf{z}) = \chi^{(D)}_{jkl,2}(M\mathbf{z}) \quad (2.33)$$

and both even and odd tensor elements in table 2.3 have an odd number of indices equal to z.

These relations are very important because they drastically reduce the number of free parameters in the systems we shall discuss in this thesis, and in fact in many systems of fundamental or technological interest.

References

[1] Ru-Pin Pan, H.D. Wei, and Y.R. Shen, Phys. Rev. B **39**, 1229 (1989).

[2] J.F. Nye, *Physical properties of crystals* (Oxford University Press, Oxford, 1957).

[3] P. Guyot-Sionnest, W. Chen, and Y.R. Shen, Phys. Rev. B **33**, 8254 (1986).

[4] P. Guyot-Sionnest, and Y.R. Shen, Phys. Rev. B **38**, 7985 (1988).

[5] B. Koopmans, *Interface and bulk contributions in optical second-harmonic generation* (Thesis, Rijksuniversiteit Groningen, Groningen, The Netherlands, 1993).

[6] M.T. Johnson, S.T. Purcell, N.W.E. McGee, R. Coehoorn, J. aan de Stegge, and W. Hoving, Phys. Rev. Lett. **68**, 2688 (1992).

[7] S.S.P Parkin, N. More, and K.P. Roche, Phys. Rev. Lett. **64**, 2304 (1990).

[8] V. Grolier, D. Renard, B. Bartenlian, P. Beauvillain, C. Chappert, C. Dupas, J. Ferré, M. Galtier, E. Kolb, M. Mulloy, J.P. Renard, and P. Veillet, Phys. Rev. Lett. **71**, 3023 (1993).

[9] A. Cebollada, R. Miranda, C.M. Schneider, P. Schuster, and J. Kirschner, J. Magn. Magn. Mat. **102**, 25 (1991).

[10] R. Schad, C.D. Potter, P. Beliën, G. Verbanck, V.V. Moshchalkov, and Y. Bruynseraede, Appl. Phys. Lett. **64**, 3500 (1994).

Chapter 3

SHG from multilayers

A quantitative analysis of Second-Harmonic Generation on multilayers requires a model that accounts for the multiple reflections of the light.[1] A convenient and flexible description is obtained after extending standard matrix theory for light propagation in multilayers. The analysis considers only electric dipole sources of second-harmonic radiation at the interfaces, and describes the propagation of the light along classical lines, i.e. in terms of forward and backward travelling waves.[2] The general observation is that such an approach leads to good results, even for layer thicknesses much smaller than the wavelength [1-4]. We shall see that our theory leads to a rather good description of the experiments and is probably a good starting point for further analysis. This model has been developed in close cooperation with M.W.J. Prins.[3]

3.1 Historical background

Although Optical Harmonic Generation (OHG) from two semi-infinite media separated by a single interface has attracted a lot of attention, both theoretically and experimentally, there exist only few studies of multilayered systems. The full theoretical analysis of such systems must necessarily describe the generation of second-harmonic light from the fundamental beam, and treat the multiple reflections of both waves.

[1] Since we are studying systems of thin metallic films with thicknesses that lead to small intensity reductions (the $1/e$-thickness is typically of the order of 100Å), we need to take into account the multiple reflections of both fundamental and generated second-harmonic light.

[2] A summary of this chapter will appear in Physica B.

[3] Research Institute for Materials, Toernooiveld 1, Nijmegen, The Netherlands.

Early experiments on a simple multilayer were done by Dick *et al.* [5]. They studied Sum Frequency Generation (SFG) and Difference Frequency Generation (DFG) from a nonlinear layer of rhodamine-6G in between two semi-infinite linear media. They described both reflected and transmitted OHG in the limit that the thickness of the nonlinear layer is much smaller than the wavelength. Yeganeh *et al.* have studied a two layer system of ZnSe on top of GaAs [4]. As the system lacks a center of inversion their paper discusses SHG from the bulk of the material. They neglected the reflections of the fundamental beam from the buried interface, but included the multiple reflections of the second-harmonic in their analysis. Both authors come to a proper description of the results after simultaneously solving the boundary conditions at the two interfaces, both for the fundamental and the harmonic frequency, as was already suggested by Bloembergen and Pershan [6]. Recently Koopmans *et al.* have given a full description of SHG in a two layer system, including interface and bulk contributions and describing the multiple reflections of both the fundamental and the second-harmonic beams in terms of reflection and transmission coefficients [1, 2]. Although complete, that approach cannot be easily extended to systems that contain more than two layers.

A well known concept in optics is to treat the boundary conditions at an interface, and the propagation of light through a homogeneous slab in terms of matrices that relate the field components on both sides of the interface and the layer respectively. Describing the full multilayer is thus reduced to a simple matrix multiplication [7-10]. Although this approach is equivalent to simultaneously solving the boundary conditions at all interfaces, it is much more flexible when it comes to describing stratified media with an arbitrary number of layers.

An extensive theoretical study of Third Harmonic Generation in the bulk of both optically isotropic and optically anisotropic laminar structures has been given by Bethune [11, 12]. He described these structures in terms of matrices on a basis of Berreman vectors, and the analysis involves a full description of an arbitrary multilayer, and treats generation and emission, including all multiple reflections.

The model that we describe in this chapter also describes the multilayer in terms of matrices, but only considers electric dipole sources of second-harmonic radiation at the interfaces. It is in fact closely related to work by Sipe [13]. He developed a Green-function formalism for calculating fields generated by sources in the presence of a multilayer geometry. We use the nonlinear boundary conditions as derived by Heinz [14], giving the discontinuity of the second-harmonic fields at the nonlinear interface (i.e. at the source). Our

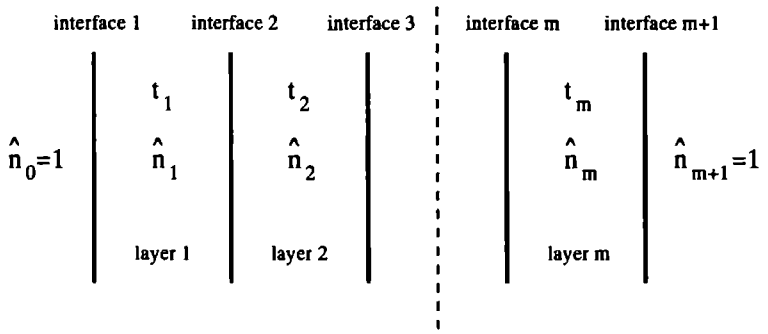

Figure 3.1: *Schematic representation of a multilayer in vacuum; $\hat{n}_j$ - refractive index of layer j; t_j - thickness of layer j.*

treatment of the emitted fields is similar to his approach. However, we come to an equivalent description of both the propagation of the fundamental and the second-harmonic after introducing infinitesimal vacuum sheets between the layers, which is extremely convenient for converting the model into a computer program. Furthermore, we have calculated the excitation of sources in a nonlinear sheet at the interface by the incident fundamental field. This introduction of a nonlinear sheet within the vacuum sheet provides an elegant equivalent treatment of mirrored interfaces.

3.2 Multiple reflection theory for one wavelength

Figure 3.1 shows a schematic representation of a system consisting of m layers with arbitrary thicknesses and indices of refraction.[4] The multilayer is situated in a vacuum environment ($n_0 = n_{m+1} = 1$).

To obtain the amplitudes of the electric fields at the interfaces we divide the system into abrupt interfaces and homogeneous layers, similar to the multiple reflection theory described by for example Palik [7]. The influence of the layers on the electromagnetic field can be expressed in terms of transfer-matrices, of which the elements contain the wave vectors, layer thicknesses and complex refractive indices. Finally the complete multilayer system can be described as a matrix multiplication:

[4]Even for the very thin films of only a few atomic layers as studied in chapter 6, we shall use the macroscopic concept of an index of refraction. Due to the strong screening in metals, such an approach appears to be justified.

$$C_{total} = M_{0,1} \otimes C_1 \otimes M_{1,2} \otimes \ldots \otimes C_m \otimes M_{m,m+1} \tag{3.1}$$

where $M_{j,j'}$ is the matrix describing the abrupt interface between the layers j and j', and C_j the matrix describing the homogeneous layer j.

Let us first derive the relations between the electric fields at interface j in the multilayer in figure 3.1. We choose the plane of the interface parallel to the **x**,**y**-plane situated at $z = z_j$. We separate forward and backward waves, i.e. waves that travel in the positive and negative **z**-direction respectively. The total field at any point within layer j is given by:

$$\mathbf{E}_{\omega,j}(\mathbf{r},t) = Re(\mathbf{E}_{\omega,j}(\mathbf{r})e^{-i\omega t}) \tag{3.2}$$

with

$$\mathbf{E}_{\omega,j}(\mathbf{r}) = \mathbf{E}^{+}_{\omega,j}e^{i\mathbf{k}^{+}_{j}(\omega)\cdot\mathbf{r}} + \mathbf{E}^{-}_{\omega,j}e^{i\mathbf{k}^{-}_{j}(\omega)\cdot\mathbf{r}} \quad \text{while} \quad z_j < z < z_j + t_j \tag{3.3}$$

and

$$\mathbf{k}^{+}_{j}(\omega) = \hat{k}_{j,x}(\omega)\mathbf{x} + \hat{k}_{j,y}(\omega)\mathbf{y} + \hat{k}_{j,z}(\omega)\mathbf{z} \tag{3.4}$$

$$\mathbf{k}^{-}_{j}(\omega) = \hat{k}_{j,x}(\omega)\mathbf{x} + \hat{k}_{j,y}(\omega)\mathbf{y} - \hat{k}_{j,z}(\omega)\mathbf{z} \tag{3.5}$$

In these equations $\mathbf{k}^{+}_{j}(\omega)$ and $\mathbf{k}^{-}_{j}(\omega)$ represent the forward and backward wave vectors in medium j respectively. $\mathbf{E}_{\omega,j}(\mathbf{r})$ is the total electric field at position **r**. $\mathbf{E}^{+}_{\omega,j}$ and $\mathbf{E}^{-}_{\omega,j}$ are respectively the forward (i.e. corresponding to $\mathbf{k}^{+}_{j}$) and backward (i.e. corresponding to $\mathbf{k}^{-}_{j}$) fields at $x = y = 0, z = z_j$. Notice that due to the translation symmetry parallel to the interface the choice of x and y is not critical, as it merely results in an unimportant overall phase shift. Every layer has a unique $\mathbf{k}^{+}_{j}(\omega)$ and $\mathbf{k}^{-}_{j}(\omega)$, given by the refractive index and the propagation direction. $\mathbf{E}^{+}_{\omega,j}$ and $\mathbf{E}^{-}_{\omega,j}$ have complex amplitudes.

The waves are in general not simple plane waves since the refractive index is complex. Therefore, the planes of constant amplitude and the planes of constant phase do not coincide. This also implies that in general the angle of propagation is complex, and that there is no propagation direction of the electric fields in the classical sense (where $\theta \in \Re$). Before we start analysing the boundary conditions we first introduce, in analogy with the classical picture, a 'complex angle of propagation': $\hat{\theta}$, that is determined by the angle between the complex wave vector and the boundary normal. Within this analogy the waves remain transversal, because we still have (in CGS units) [15]:

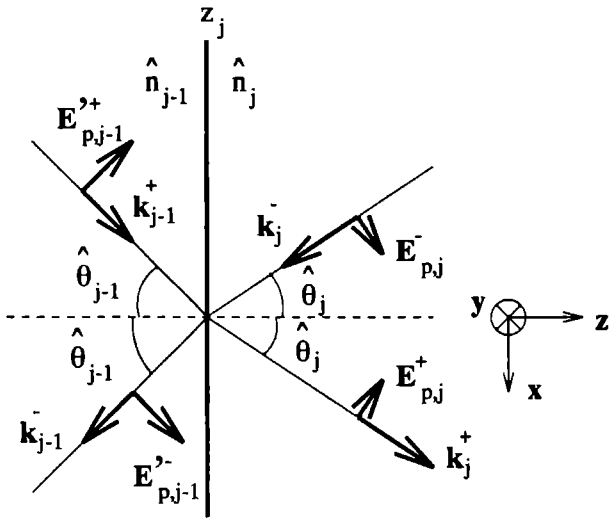

Figure 3.2: *Schematic representation of the fields of frequency ω at interface j, between layers $j-1$ and j. $\mathbf{E}'^{+}_{p,j-1}$ and $\mathbf{E}'^{-}_{p,j-1}$ represent the forward respectively backward electric fields in medium $j-1$ at the position $z_j^- = z_j - \delta$, $\mathbf{E}^{+}_{p,j}$ and $\mathbf{E}^{-}_{p,j}$ represent the forward respectively backward electric fields in medium j at the position $z_j^+ = z_j + \delta$, $\hat{\theta}_{\omega,j}$ is the 'complex angle of propagation' in layer j, $\mathbf{k}_j^+(\omega)$ and $\mathbf{k}_j^-(\omega)$ represent the forward respectively backward complex wave vector in layer j. The label ω has been omitted in the picture for clarity.*

$$\nabla \cdot \mathbf{E} = \frac{4\pi\rho_f}{\hat{\epsilon}(\omega)} = 0 \quad \text{and} \quad \nabla \times \mathbf{H} = -\frac{i\omega\hat{\epsilon}(\omega)}{c}\mathbf{E} \tag{3.6}$$

as there is no free charge and no free current within the system. This leads to:

$$\mathbf{k}^{\pm} \cdot \mathbf{E}^{\pm} = 0 \quad \text{and} \quad \mathbf{k}^{\pm} \times \mathbf{H}^{\pm} = -\frac{i\omega\hat{\epsilon}(\omega)}{c}\mathbf{E}^{\pm} \tag{3.7}$$

Notice that since $\mathbf{k}^{\pm}$ is complex, this is not a situation that can be visualized in a 3D-picture.

We now choose the **x**,**z**-plane as the plane of incidence.[5] Figure 3.2 shows

[5] $\hat{k}_y(\omega) = 0$ throughout the system.

the p-polarized (polarization in the plane of incidence) fields of frequency ω at interface j. $E'^{+}_{\omega,p,j-1}$ and $E'^{-}_{\omega,p,j-1}$ (notice the accents) represent the complex amplitudes of the forward respectively backward electric field in medium $j-1$ at the position $z_j^- = z_j - \delta$ ('just left of the interface'). $E^{+}_{\omega,p,j}$ and $E^{-}_{\omega,p,j}$ represent the complex amplitudes of the forward respectively backward electric field in medium j at the position $z_j^+ = z_j + \delta$ ('just right of the interface'). The relations between these fields are easily derived from three boundary conditions:

A: $k_{\|}$ is conserved:

$$\begin{aligned} \hat{k}_{j-1,x}(\omega) &= \hat{k}_{j,x}(\omega) && (3.8)\\ \Leftrightarrow \hat{k}_{j-1}(\omega)\sin\hat{\theta}_{\omega,j-1} &= \hat{k}_j(\omega)\sin\hat{\theta}_{\omega,j} && (3.9)\\ \Leftrightarrow \hat{n}_{j-1}(\omega)\sin\hat{\theta}_{\omega,j-1} &= \hat{n}_j(\omega)\sin\hat{\theta}_{\omega,j} && (3.10) \end{aligned}$$

where we used

$$\hat{k}(\omega) = \hat{n}(\omega)\omega/c, \quad \text{with} \quad \hat{n}(\omega) = n(\omega) + ik(\omega) \tag{3.11}$$

Notice that this is the general expression of Snell's law. We shall only consider systems in vacuum, so $n_0 = n_{m+1} = 1$. This leads to:

$$\hat{n}_j(\omega)\sin\hat{\theta}_{\omega,j} = \sin\theta_{\omega,0} \quad \text{for all } j \tag{3.12}$$

Because $\theta_{\omega,0}$ is the real angle of incidence in vacuum, we find:[6]

$$\hat{n}_j(\omega)\sin\hat{\theta}_{\omega,j} \in \Re \quad \text{and} \quad \hat{k}_{j,x}(\omega) \in \Re \tag{3.13}$$

B: $E_{\|}$ is continuous:

If we define the directions of the electric fields indicated in figure 3.2 as positive, we obtain:

$$[-E'^{+}_{\omega,p,j-1} + E'^{-}_{\omega,p,j-1}]\cos\hat{\theta}_{\omega,j-1} = [-E^{+}_{\omega,p,j} + E^{-}_{\omega,p,j}]\cos\hat{\theta}_{\omega,j} \tag{3.14}$$

[6] This shows that it is not necessary to introduce a complex sine-function, since $\widehat{(\sin\theta_{\omega,j})} = \sin\theta_{\omega,0}/\hat{n}_j(\omega)$ can be introduced as a new variable. Similarly we could introduce: $\widehat{(\cos\theta_{\omega,j})} = \sqrt{1-[\sin\theta_{\omega,0}/\hat{n}_j(\omega)]^2}$.

C: $H_{\|}$ is continuous:

The continuity of $H_{\|}$ implies that $\frac{c}{\omega}(\mathbf{k}\times\mathbf{E})_{\|}$ is continuous [15]. Again defining the directions of the electric fields indicated in figure 3.2 as positive, we obtain for p-polarized fields:

$$\begin{aligned} H_y &= \frac{c}{\omega}[\hat{k}^+_{j,z}(\omega)E^+_{\omega,x,j} - \hat{k}^+_{j,x}(\omega)E^+_{\omega,z,j} + \hat{k}^-_{j,z}(\omega)E^-_{\omega,x,j} - \hat{k}^-_{j,x}(\omega)E^-_{\omega,z,j}] \\ &= -\frac{c}{\omega}\hat{k}_j(\omega)[E^+_{\omega,p,j} + E^-_{\omega,p,j}] \end{aligned} \tag{3.15}$$

is continuous. Using eq. 3.11 we obtain:

$$\hat{n}_{j-1}(\omega)[E'^+_{\omega,p,j-1} + E'^-_{\omega,p,j-1}] = \hat{n}_j(\omega)[E^+_{\omega,p,j} + E^-_{\omega,p,j}] \tag{3.16}$$

The same equation is obtained from the continuity of $D_{\perp}$, and it expresses the fact that there is no net charge at the interface ($\nabla\cdot\mathbf{D}=0$)

After combining eq. 3.14 and 3.16 we derive that the changes of the p-polarized field at an abrupt interface between layers $j-1$ and j can be written as:

$$\begin{pmatrix} E'^+_{\omega,p,j-1} \\ E'^-_{\omega,p,j-1} \end{pmatrix} = M^{\omega,p}_{j-1,j} \begin{pmatrix} E^+_{\omega,p,j} \\ E^-_{\omega,p,j} \end{pmatrix} \tag{3.17}$$

with

$$M^{\omega,p}_{j-1,j} = \frac{1}{f^{\omega,+}_{j-1,j-1}} \begin{pmatrix} f^{\omega,+}_{j-1,j} & -f^{\omega,-}_{j-1,j} \\ -f^{\omega,-}_{j-1,j} & f^{\omega,+}_{j-1,j} \end{pmatrix} \tag{3.18}$$

and

$$f^{\omega,\pm}_{j',j} \equiv \hat{n}_{j'}(\omega)\cos\hat{\theta}_{\omega,j} \pm \hat{n}_j(\omega)\cos\hat{\theta}_{\omega,j'} \tag{3.19}$$

$M^{\omega,p}_{j-1,j}$ expresses the relation between the p-polarized fields of frequency ω on both sides of interface j. Notice that $M^{\omega,p}_{j-1,j}$ involves a basis transformation from medium j to medium $j-1$.

The changes of the electric field due to a homogeneous layer j (see figure 3.3) are easily expressed in a matrix formalism after realizing that:

$$\begin{aligned} E^{\pm}_{\omega,p}(z) &= E^{\pm}_{\omega,p}(z_j)e^{\pm i\hat{k}_{j,z}(\omega)(z-z_j)} = E^{\pm}_{\omega,p,j}e^{\pm i\hat{k}_{j,z}(\omega)(z-z_j)} \\ &\quad \text{with } z_j < z < z_j + t_j \end{aligned} \tag{3.20}$$

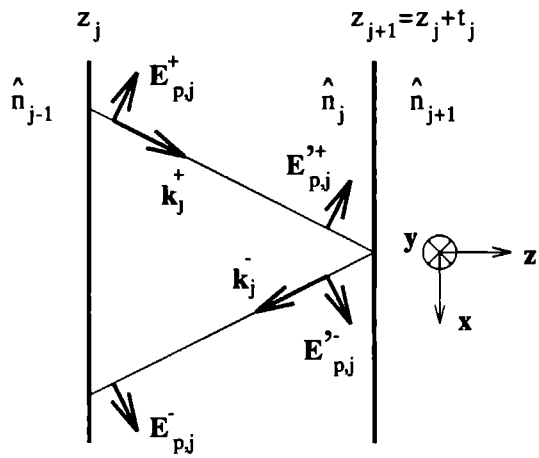

Figure 3.3: *Schematic representation of the fields of frequency ω in layer j near the interfaces j (at $z = z_j$) and $j+1$ (at $z = z_j + t_j = z_{j+1}$). $\mathbf{E}^+_{p,j}$ and $\mathbf{E}^-_{p,j}$ represent the forward respectively backward electric fields in medium j at the position $z_j^+ = z_j + \delta$. $\mathbf{E}'^+_{p,j}$ and $\mathbf{E}'^-_{p,j}$ represent the forward respectively backward electric fields in medium j at the position $z_{j+1}^- = z_{j+1} - \delta$. The label ω has been omited in the picture for clarity.*

This leads to:

$$E'^{\pm}_{\omega,p,j} = E^{\pm}_{\omega,p}(z_j + t_j) = E^{\pm}_{\omega,p,j} e^{\pm i \hat{k}_{j,z}(\omega) t_j} \tag{3.21}$$

The influence of the layer can now be expressed as:

$$\begin{pmatrix} E^+_{\omega,p,j} \\ E^-_{\omega,p,j} \end{pmatrix} = C^{\omega}_j \begin{pmatrix} E'^+_{\omega,p,j} \\ E'^-_{\omega,p,j} \end{pmatrix} \tag{3.22}$$

with

$$C^{\omega}_j = \begin{pmatrix} e^{-i\hat{k}_{j,z}(\omega)t_j} & 0 \\ 0 & e^{i\hat{k}_{j,z}(\omega)t_j} \end{pmatrix} \tag{3.23}$$

and

$$\hat{k}_{j,z}(\omega) = \frac{\hat{n}_j(\omega)\omega}{c} \cos\hat{\theta}_{\omega,j} \tag{3.24}$$

C^{ω}_j expresses the changes of the electric field of frequency ω due to layer j.

Along similar lines we can derive the matrices for s-polarized light, i.e. a polarization perpendicular to the plane of incidence. Using $k_{\|}$ conservation, and the continuity of $E_{\|}$ and $H_{\|}$ we find[7]:

$$\begin{pmatrix} E'^{+}_{\omega,s,j-1} \\ E'^{-}_{\omega,s,j-1} \end{pmatrix} = M^{\omega,s}_{j-1,j} \begin{pmatrix} E^{+}_{\omega,s,j} \\ E^{-}_{\omega,s,j} \end{pmatrix} \tag{3.25}$$

with

$$M^{\omega,s}_{j-1,j} = \frac{1}{g^{\omega,+}_{j-1,j-1}} \begin{pmatrix} g^{\omega,+}_{j-1,j} & g^{\omega,-}_{j-1,j} \\ g^{\omega,-}_{j-1,j} & g^{\omega,+}_{j-1,j} \end{pmatrix} \tag{3.26}$$

and

$$g^{\omega,\pm}_{j',j} \equiv \hat{n}_{j'}(\omega)\cos\hat{\theta}_{\omega,j'} \pm \hat{n}_{j}(\omega)\cos\hat{\theta}_{\omega,j} \tag{3.27}$$

$M^{\omega,s}_{j-1,j}$ expresses the relation between the s-polarized fields of frequency ω on both sides of interface j. Of course the homogeneous layer has the same effect on s and p-polarized light, as there is no distinction between the two inside the layer.

A very elegant treatment of the multilayer in figure 3.1 is obtained after introducing infinitesimal vacuum sheets in between all layers. They have no influence on the characteristics of the system, as $k_{\|}$, $E_{\|}$, $H_{\|}$, and $D_{\perp}$ are continuous across the sheets. The advantage is that this description is more symmetric, since every single layer is now embedded in vacuum. The influence of a layer can be treated by going from one vacuum sheet across the layer to the next vacuum sheet, thus avoiding the inherent basis changes that were involved in the matrix transformations.[8]

Since any polarization can be written as a vector sum of s and p components, it can be treated with the above formulas. It is therefore convenient to introduce a new matrix that combines our previous results for s and p polarized fields and serves as a complete description of the changes of a field due to layer j embedded in vacuum sheets:

[7]The continuity of $H_{\|}$ implies continuity of $H_x = -\hat{k}_{j,z}(\omega)(E^{+}_{\omega,s,j} - E^{-}_{\omega,s,j})$ across the interface. Notice that the continuity of $D_{\perp}$ does not give any extra information, since $E_z = 0$ for s-polarized electric fields.

[8]See for example eq. 3.25 and realize that $E'^{\pm}_{\omega,s,j-1}$ and $E^{\pm}_{\omega,s,j}$ are expressed on respectively the bases $\mathbf{k}^{\pm}_{j-1}(\omega)$ and $\mathbf{k}^{\pm}_{j}(\omega)$.

$$\begin{pmatrix} E^+_{\omega,p,j} \\ E^-_{\omega,p,j} \\ E^+_{\omega,s,j} \\ E^-_{\omega,s,j} \end{pmatrix} = \begin{pmatrix} T^{\omega,p}_j & \ominus \\ \ominus & T^{\omega,s}_j \end{pmatrix} \begin{pmatrix} E^+_{\omega,p,j+1} \\ E^-_{\omega,p,j+1} \\ E^+_{\omega,s,j+1} \\ E^-_{\omega,s,j+1} \end{pmatrix} \tag{3.28}$$

with:

$$T^{\omega,p}_j = M^{\omega,p}_{0,j} \otimes C^{\omega}_j \otimes M^{\omega,p}_{j,0} \quad \text{and} \quad T^{\omega,s}_j = M^{\omega,s}_{0,j} \otimes C^{\omega}_j \otimes M^{\omega,s}_{j,0} \tag{3.29}$$

$T^{\omega,p}_j$ and $T^{\omega,s}_j$ express the relation between respectively the p and s-polarized fields of frequency ω in the vacuum sheets on both sides of layer j. $M^{\omega,p}_{j,j'}$, $M^{\omega,s}_{j,j'}$ and C^{ω}_j are the 2×2 matrices given in eq. 3.17, 3.22 and 3.25 respectively. The index 0 stands for medium 0 (vacuum). The vector $(E^+_{p,j}, E^-_{p,j}, E^+_{s,j}, E^-_{s,j})$ represents the electric field at interface j. It is expressed on the vacuum basis $(\mathbf{e}^+_p, \mathbf{e}^-_p, \mathbf{e}^+_s, \mathbf{e}^-_s)$, that is determined by the orientation of the incoming electric field:

$$\mathbf{e}^{\pm}_p = \mp \cos\theta_{\omega,0}\mathbf{x} + \sin\theta_{\omega,0}\mathbf{z} \tag{3.30}$$

$$\mathbf{e}^{\pm}_s = \mathbf{y} \tag{3.31}$$

Using eq. 3.28 we can easily derive the amplitudes of the electric fields at all the interfaces, relative to an incoming field from the left in figure 3.1. We start from the consideration that there is no backward field in medium $m+1$ (no incoming field from the right):

$$\begin{pmatrix} E^+_{\omega,p,m+1} \\ E^-_{\omega,p,m+1} \\ E^+_{\omega,s,m+1} \\ E^-_{\omega,s,m+1} \end{pmatrix} = \begin{pmatrix} E^+_{\omega,p,out} \\ 0 \\ E^+_{\omega,s,out} \\ 0 \end{pmatrix} \tag{3.32}$$

From this boundary condition we calculate the fields inside the vacuum sheet between layers $m-1$ and m relative to $E^+_{\omega,p,out}$ and $E^+_{\omega,s,out}$. Then we proceed to the sheet between layers $m-2$ and $m-1$ etc. The total effect of the whole multilayer can be written as:

$$\begin{pmatrix} E^+_{\omega,p,in} \\ E^-_{\omega,p,in} \\ E^+_{\omega,s,in} \\ E^-_{\omega,s,in} \end{pmatrix} = T^{\omega}_{total} \begin{pmatrix} E^+_{\omega,p,out} \\ 0 \\ E^+_{\omega,s,out} \\ 0 \end{pmatrix} \tag{3.33}$$

with

$$T^{\omega}_{total} = \prod_{j=1}^{m} \begin{pmatrix} T^{\omega,p}_{j} & \ominus \\ \ominus & T^{\omega,s}_{j} \end{pmatrix} \tag{3.34}$$

Because we can now derive the ratios $E^{+}_{\omega,p,out}/E^{+}_{\omega,p,in}$ and $E^{+}_{\omega,s,out}/E^{+}_{\omega,s,in}$, we are able to give expressions for the values of the fields at all the interfaces relative to the incoming field.

3.3 Multiple reflected SHG from interfaces

In the previous section we have developed a complete matrix description of the propagation of electric fields in a multilayer. We have accounted for the multiple reflections, and to obtain a more symmetric description we have introduced infinitesimal vacuum sheets at every interface. From the formulas we can derive the amplitudes and phases of the electric fields at all the interfaces in the multilayer relative to the incoming field. In the following pages we will introduce the nonlinear sources that are situated at the interfaces and deduce the emitted second-harmonic fields.

We assume that the system contains only electric dipole sources of second-harmonic at the interfaces and that all other sources (magnetic dipole and electric quadrupole, i.e. the bulk contributions) are negligible. Using the ideas of Bloembergen and Pershan [6] we situate these sources in an infinitesimal nonlinear sheet of thickness $2\delta_2$, inside the infinitesimal vacuum sheet (thickness $2\delta_1$), which we had already introduced in the previous section (see fig 3.4). This sheet has a refractive index $\hat{n}^{i}_{j}$, the refractive index of the interface. Its value is not known. However, it can be shown that $\hat{n}^{i}_{j}$ works as a scaling factor for the tensor elements (see Ref. [2] for more detailed information). The precise value of $\hat{n}^{i}_{j}$ is therefore of no vital importance. If we take the $\mathbf{x}$,$\mathbf{z}$-plane as the plane of incidence ($k_y = 0$, $y = 0$), we find that the fundamental fields induce a 2ω-polarization in the sheet:

$$P^{sh}_{2\omega,k}(\mathbf{r}_j, t) = P^{sh}_{2\omega,k,j} e^{i(2k_x(\omega)x - 2\omega t)} \tag{3.35}$$

where $\mathbf{r}_j$ is lying in the plane of interface j and:

$$P^{sh}_{2\omega,k,j} = \chi^{(D)}_{klm,j}(2\omega)\mathcal{E}_{\omega,l,j}\mathcal{E}_{\omega,m,j} \quad \text{with} \quad k,l,m = x,y,z \tag{3.36}$$

where $\chi^{(D)}_{klm,j}(2\omega)$ represents the nonlinear susceptibility tensor elements of interface j. $\mathcal{E}_{\omega,j}$ is the total fundamental field in the nonlinear sheet and

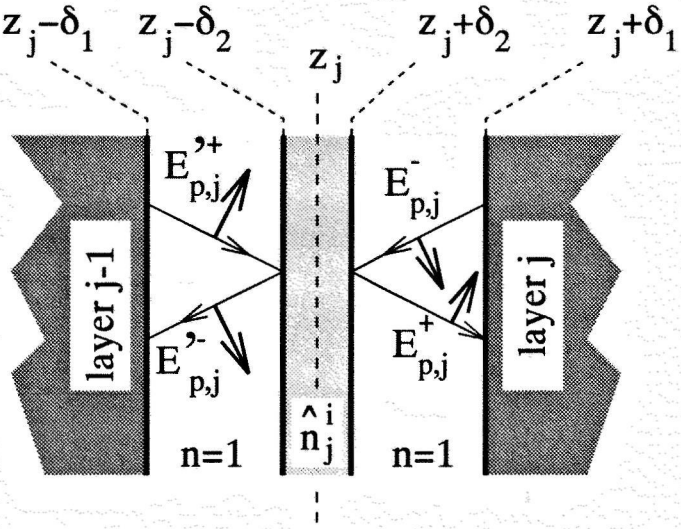

Figure 3.4: *Infinitesimal nonlinear sheet of thickness $2\delta_2$ inside infinitesimal vacuum sheet of thickness $2\delta_1$, at interface j at $z = z_j$. $\mathbf{E}'^{\pm}_{p,j}$ represents the p-polarized second harmonic field in the vacuum sheet with: $z_j - \delta_1 < z < z_j - \delta_2$ ('just left of the nonlinear sheet') and $\mathbf{E}^{\pm}_{p,j}$ the p-polarized second-harmonic field in the vacuum sheet with: $z_j + \delta_2 < z < z_j + \delta_1$ ('just right of the nonlinear sheet'), $\hat{n}^i_j$ is the refractive index of the interface. The label 2ω has been omitted for clarity.*

autosummation is implied. The total fundamental field in the nonlinear sheet is in general a sum of forward and backward fields, that are derived from the fields in the vacuum sheet:

$$\begin{pmatrix} \mathcal{E}^{+}_{\omega,p,j} \\ \mathcal{E}^{-}_{\omega,p,j} \\ \mathcal{E}^{+}_{\omega,s,j} \\ \mathcal{E}^{-}_{\omega,s,j} \end{pmatrix} = \begin{pmatrix} L^{\omega,p}_j & \ominus \\ \ominus & L^{\omega,s}_j \end{pmatrix} \begin{pmatrix} E^{+}_{\omega,p,j} \\ E^{-}_{\omega,p,j} \\ E^{+}_{\omega,s,j} \\ E^{-}_{\omega,s,j} \end{pmatrix} \tag{3.37}$$

with

$$L^{\omega,p}_j = \frac{1}{u^{\omega,+}_j} \begin{pmatrix} u^{\omega,+}_j & -u^{\omega,-}_j \\ -u^{\omega,-}_j & u^{\omega,+}_j \end{pmatrix} \; ; \; L^{\omega,s}_j = \frac{1}{v^{\omega,+}_j} \begin{pmatrix} v^{\omega,+}_j & v^{\omega,-}_j \\ v^{\omega,-}_j & v^{\omega,+}_j \end{pmatrix} \tag{3.38}$$

and

$$u_j^{\omega,\pm} \equiv \hat{n}_j^i(\omega)\cos\theta_{\omega,0} \pm \cos\hat{\theta}_{\omega,j}^i \tag{3.39}$$

$$v_j^{\omega,\pm} \equiv \hat{n}_j^i(\omega)\cos\hat{\theta}_{\omega,j}^i \pm \cos\theta_{\omega,0} \tag{3.40}$$

The matrix $L_j^{\omega,p}$ expresses the relation between $\mathbf{E}_{\omega,p,j}^{\pm}$, the fields in the vacuum sheet at interface j, and $\mathcal{E}_{\omega,p,j}^{\pm}$, the fields in the nonlinear sheet at interface j. $L_j^{\omega,s}$ gives this relation for the s-polarized fields. $\hat{\theta}_{\omega,j}^i$ is the complex angle of propagation in the nonlinear sheet. The expressions are completely analogous to $M_{j-1,j}^{\omega,p}$ and $M_{j-1,j}^{\omega,s}$ in eq. 3.17 and 3.25 respectively, that describe the changes of the electric fields across an interface. The total fundamental field in the nonlinear sheet j follows from the equations:

$$\mathcal{E}_{\omega,x,j} = (-\mathcal{E}_{\omega,p,j}^{+} + \mathcal{E}_{\omega,p,j}^{-})\cos\hat{\theta}_{\omega,j}^i \tag{3.41}$$

$$\mathcal{E}_{\omega,y,j} = \mathcal{E}_{\omega,s,j}^{+} + \mathcal{E}_{\omega,s,j}^{-} \tag{3.42}$$

$$\mathcal{E}_{\omega,z,j} = (\mathcal{E}_{\omega,p,j}^{+} + \mathcal{E}_{\omega,p,j}^{-})\sin\hat{\theta}_{\omega,j}^i \tag{3.43}$$

Substituting these equations into eq. 3.36 gives the total polarization of the sheet.

The final steps in our analysis involve the derivation of the fields of frequency 2ω that are generated by this polarization, and the transmission of these fields through the multilayer, again accounting for multiple reflections.

The presence of the source $\mathbf{P}_{2\omega,j}^{sh}$ causes a discontinuity of the second-harmonic fields at interface j. This discontinuity is derived from the boundary conditions, accounting for the presence of a (nonlinear) source polarization [14, 16] (an extended derivation of these boundary conditions is given in appendix A):

$$\Delta E_{2\omega,x,j} = -\frac{ik_x(2\omega)}{[\hat{n}_j^i(2\omega)]^2}4\pi P_{2\omega,z,j}^{sh} \tag{3.44}$$

$$\Delta H_{2\omega,y,j} = \frac{i2\omega}{c}4\pi P_{2\omega,x,j}^{sh} \tag{3.45}$$

$$\Delta E_{2\omega,y,j} = 0 \tag{3.46}$$

$$\Delta H_{2\omega,x,j} = -\frac{i2\omega}{c}4\pi P_{2\omega,y,j}^{sh} \tag{3.47}$$

where the equations express the difference between the complex amplitudes of the field components in the vacuum sheets on both sides of nonlinear

sheet j (see figure 3.4). With these boundary conditions we derive the second-harmonic fields generated by the interface along similar lines as presented in the previous section. For the p-polarization we use:

$$\Delta E_{2\omega,x,j} = E_{2\omega,x,j} - E'_{2\omega,x,j} \tag{3.48}$$

$$\Delta H_{2\omega,y,j} = H_{2\omega,y,j} - H'_{2\omega,y,j} \tag{3.49}$$

where $\mathbf{E}'_{2\omega,j}$ and $\mathbf{H}'_{2\omega,j}$ are the electric respectively magnetic field components in the vacuum sheet with: $z_j - \delta_1 < z < z_j - \delta_2$ (see figure 3.4), and where $\mathbf{E}_{2\omega,j}$ and $\mathbf{H}_{2\omega,j}$ are the fields in the vacuum sheet with: $z_j + \delta_2 < z < z_j + \delta_1$ (see figure 3.4). Separating forward and backward field components gives:

$$\Delta E_{2\omega,x,j} = -\cos\theta_{\omega,0}(E^+_{2\omega,p,j} - E^-_{2\omega,p,j}) + \cos\theta_{\omega,0}(E'^+_{2\omega,p,j} - E'^-_{2\omega,p,j}) \tag{3.50}$$

$$\Delta H_{2\omega,y,j} = -(E^+_{2\omega,p,j} + E^-_{2\omega,p,j}) + (E'^+_{2\omega,p,j} + E'^-_{2\omega,p,j}) \tag{3.51}$$

Here we have used the nonlinear equivalent of Snell's law (see Ref. [16], or appendix A). Because there is no dispersion in vacuum, we have found:

$$\theta_{2\omega,0} = \theta_{\omega,0} \tag{3.52}$$

After introducing:

$$\kappa'_{2\omega,p,j} \equiv \frac{E'^+_{2\omega,p,j} - E'^-_{2\omega,p,j}}{E'^+_{2\omega,p,j} + E'^-_{2\omega,p,j}} \quad ; \quad \kappa_{2\omega,p,j} \equiv \frac{E^+_{2\omega,p,j} - E^-_{2\omega,p,j}}{E^+_{2\omega,p,j} + E^-_{2\omega,p,j}} \tag{3.53}$$

we derive,

$$E'^+_{2\omega,p,j} + E'^-_{2\omega,p,j} = \frac{\Delta E_{2\omega,x,j} - \kappa_{2\omega,p,j}\cos\theta_{\omega,0}\cdot\Delta H_{2\omega,y,j}}{(\kappa'_{2\omega,p,j} - \kappa_{2\omega,p,j})\cos\theta_{\omega,0}} \tag{3.54}$$

A similar expression can be derived for the s-polarized second-harmonic fields, using:

$$\Delta E_{2\omega,y,j} = E_{2\omega,y,j} - E'_{2\omega,y,j} = 0 \tag{3.55}$$

$$\Delta H_{2\omega,x,j} = H_{2\omega,x,j} - H'_{2\omega,x,j} \tag{3.56}$$

We derive

$$E'^{+}_{2\omega,s,j} + E'^{-}_{2\omega,s,j} = \frac{\Delta H_{2\omega,x,j}}{\cos\theta_{\omega,0}(\kappa'_{2\omega,s,j} - \kappa_{2\omega,s,j})} \tag{3.57}$$

where the definitions of $\kappa'_{2\omega,s,j}$, and $\kappa_{2\omega,s,j}$ are analogous to the expressions in eq. 3.53. The values of the κ's are easily derived from multiple reflection theory, once we divide the multilayer into two parts at interface j, and analyse both parts with the theory of the previous section. For the outgoing wave on the far side we obtain:

$$\begin{pmatrix} E^{+}_{2\omega,p,j} \\ E^{-}_{2\omega,p,j} \\ E^{+}_{2\omega,s,j} \\ E^{-}_{2\omega,s,j} \end{pmatrix} = T^{2\omega}_{forward} \begin{pmatrix} E^{+}_{2\omega,p,m+1} \\ 0 \\ E^{+}_{2\omega,s,m+1} \\ 0 \end{pmatrix} \tag{3.58}$$

with

$$T^{2\omega}_{forward} = \prod_{q=j}^{m} \begin{pmatrix} T^{2\omega,p}_{q} & \ominus \\ \ominus & T^{2\omega,s}_{q} \end{pmatrix} \tag{3.59}$$

where $T^{2\omega,p}_{q}$ and $T^{2\omega,s}_{q}$ are given in equation 3.29. For the second-harmonic wave outgoing on the front side we realize that we solve the multilayer in the backward direction and write:

$$\begin{pmatrix} E'^{-}_{2\omega,p,j} \\ E'^{+}_{2\omega,p,j} \\ E'^{-}_{2\omega,s,j} \\ E'^{+}_{2\omega,s,j} \end{pmatrix} = T^{2\omega}_{backward} \begin{pmatrix} E^{-}_{2\omega,p,0} \\ 0 \\ E^{-}_{2\omega,s,0} \\ 0 \end{pmatrix} \tag{3.60}$$

Notice that the order of the forward and backward fields is interchanged. $T^{2\omega}_{backward}$ is calculated from the equation:

$$T^{2\omega}_{backward} = \prod_{q=j-1}^{1} \begin{pmatrix} T^{2\omega,p}_{q} & \ominus \\ \ominus & T^{2\omega,s}_{q} \end{pmatrix} \tag{3.61}$$

where $T^{2\omega,p}_{q}$ and $T^{2\omega,s}_{q}$ are given in equation 3.29, with the exception that z needs to be replaced by $-z$ in $C^{2\omega}_{j}$. From eq. 3.58 and 3.60 we get expressions of the form:

$$E^{+}_{2\omega,p,j} = \hat{c}^{+}_{p,j} E^{+}_{2\omega,p,m+1} \tag{3.62}$$

$$E^{-}_{2\omega,p,j} = \hat{c}^{-}_{p,j} E^{+}_{2\omega,p,m+1} \tag{3.63}$$

$$E'^{+}_{2\omega,p,j} = \hat{c}'^{+}_{p,j} E^{-}_{2\omega,p,0} \tag{3.64}$$

$$E'^{-}_{2\omega,p,j} = \hat{c}'^{-}_{p,j} E^{-}_{2\omega,p,0} \tag{3.65}$$

where $\hat{c}^{\pm}_{p,j}$ and $\hat{c}'^{\pm}_{p,j}$ are elements of respectively $T^{2\omega}_{forward}$ and $T^{2\omega}_{backward}$, and similar expressions can be given for the s-polarized second-harmonic fields. Looking at eq. 3.53 we realize that $\kappa'_{2\omega,p,j}$, $\kappa_{2\omega,p,j}$, $\kappa'_{2\omega,s,j}$, and $\kappa_{2\omega,s,j}$ are easily calculated from these equations. From eq. 3.64 and 3.65 we derive the ratios:

$$\frac{E^{-}_{2\omega,p,0}}{E'^{+}_{2\omega,p,j} + E'^{-}_{2\omega,p,j}} \quad \text{and} \quad \frac{E^{-}_{2\omega,s,0}}{E'^{+}_{2\omega,s,j} + E'^{-}_{2\omega,s,j}} \tag{3.66}$$

So we can calculate the outgoing second-harmonic fields on the front side. These are the fields that we detect in our reflection geometry. We have verified that at normal incidence the expressions in eq. 3.54 and 3.57 yield the same results, as is to be expected because p- and s-polarization are equivalent at an angle of incidence of 0°. It requires some rewriting of the expressions for the field ratios in eq. 3.53. For the simple situation of one single interface between vacuum and a semi-infinite medium with refractive index n it is easy to show that (at normal incidence):

$$E'^{-}_{2\omega,p,0} = -E'^{-}_{2\omega,s,0} \tag{3.67}$$

where the minus sign is simply the consequence of the fact that we have defined that the x-components of $E^{+}_{\omega,p,j}$ and $E^{-}_{2\omega,p,j}$ have opposite sign, while $E^{+}_{\omega,s,j}$ and $E^{-}_{2\omega,s,j}$ have the same sign. Notice that $E'^{+}_{2\omega,p,0} = E'^{+}_{2\omega,s,0} = 0$, because there exist no forward second-harmonic fields in the vacuum.

3.4 Examples

In this section we shall give two instructive examples. In section 3.4.1 we discuss SHG from interfaces in a system consisting of a semi-infinite substrate covered by a thin top layer. The next section will discuss Magnetization induced SHG from the surface of a semi-infinite ideal metal in vacuum.

3.4.1 Overlayer-thickness dependence of SHG

As a typical example we shall study SHG from a thin gold film on a (non-magnetized) cobalt substrate. Figure 3.5 shows the result of calculations with the multiple reflection model, which has been presented in this chapter.

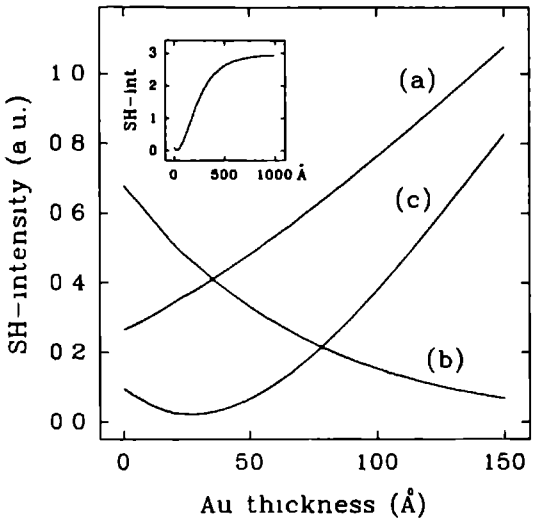

Figure 3.5: *Calculation of second-harmonic intensity emitted from a thin Au film on a Co substrate at normal incidence, as a function of Au film thickness. Only interfacial contributions are included in the calculation. Second-harmonic is generated at the top vacuum/Au interface* ($\chi^{(D)}_{xxx,top}$)*, as well as in the buried Au/Co interface* ($\chi^{(D)}_{xxx,bur}$)*. Curve (a) describes the case* $\chi^{(D)}_{xxx,top} = 1$ *and* $\chi^{(D)}_{xxx,bur} = 0$*, curve (b) is for* $\chi^{(D)}_{xxx,top} = 0$ *and* $\chi^{(D)}_{xxx,bur} = -1.6$*, and curve (c) is for* $\chi^{(D)}_{xxx,top} = 1$ *and* $\chi^{(D)}_{xxx,bur} = -1.6$*. The inset shows curve (c) for a larger film thickness range.*

We consider normal incidence and a fundamental beam with a wavelength of 532 nm. We calculate the fields at the interfaces on the vacuum basis, i.e. we take interface refractive indices: $\hat{n}^i(\omega) = \hat{n}^i(2\omega) = 1$ (see figure 3.4). For the materials we take the optical constants as measured by Johnson and Christy [17], and assume that they change abruptly at the interface. Finally we assume (for simplicity) that both the top and the buried interface have only one nonzero tensor element, respectively $\chi^{(D)}_{xxx,top}$ and $\chi^{(D)}_{xxx,bur}$. Curves (a) and (b) show the calculated second-harmonic intensity for respectively generation at the top vacuum/Au interface and generation at the buried Au/Co interface. Curve (c) shows the results of simultaneous generation at both the top interface and the buried interface.

These calculations illustrate a number of characteristic features that may occur in SHG from multilayers. First of all, curve (a) shows that the contribution of the top interface to the SH-intensity strongly depends on the thickness of the Au film. The total fundamental field at the interface is determined by the sum of the forward and backward fields. The complex amplitude of the backward field depends of course on the dielectric mismatch at the interface. At zero Au thickness we have the dielectric mismatch of a vacuum/Co interface, while for thick Au films we have the mismatch of the Au/vacuum interface. In this particular case, the dielectric mismatches cause a weaker fundamental field at a 'vacuum/Co' interface than at a vacuum/Au interface, and thus an increasing SH-intensity with increasing Au thickness. Of course the phenomenon of dielectric mismatch applies equally well to both the propagation of the fundamental field through the structure, and the propagation c.q. emission of the second-harmonic fields. It turns out that Au and Co have quite similar dielectric properties at 266 nm (the second-harmonic wavelength). This causes the SH-emission from the surface to be similar for a vacuum/Co and a vacuum/Au interface.

Curve (b) shows that the contribution of the buried Au/Co interface to the emitted second-harmonic decreases rapidly as the Au film thickness increases. This effect is due to absorption in the Au film of both the incoming fundamental beam, and the outgoing second-harmonic.

Finally curve (c) shows the result of interference of the SH-fields originating from both interfaces. Since we have chosen opposite signs for the tensor elements of the top versus the buried interface, we may observe destructive interference, as is demonstrated by the initial decrease of curve (c). Notice that the extinction is never perfect, which is caused by phase lag of the contribution from the buried interface with respect to the contribution of the top interface. It is very instructive to consider the ratios of the SH-intensities for the various situations in some detail. Curve (b) shows that a 100 Å film of Au reduces the SH-intensity generated by the buried interface by a factor of five. At this Au thickness we find that the SH-intensities for situations (a) and (c) respectively differ by a factor of two, implying that the presence of the buried interface still plays a very significant role in the total second-harmonic intensity. This is a direct consequence of the fact that we are dealing with interference of the SH-fields and not the SH-intensities. The extinction of the electric fields is less rapid than the extinction of the intensities, because $I \propto E^2$. So, due to field-interference, we have an extended depth-sensitivity.

The inset shows the evolution of curve (c) for larger Au film thicknesses. Notice the initial dip, due to destructive interference, followed by a strong increase of the total SH-intensity. For Au film thicknesses above approximately

500 Å the SH-signal saturates at the intensity that would also be obtained for a Au substrate.

Summarizing the results, we have found that in dealing with SHG from multilayers, three phenomena may be of importance:

1. Impedance mismatch, causing a variation of the fundamental field in the structure and different emission efficiencies of the second-harmonic from different interfaces

2. Absorption in the layers, since this determines the depth sensitivity of the technique

3. Interference of the contributions from the different interfaces.

3.4.2 MSHG from an ideal metal surface

In section 2.2 we have discussed the time-inversion properties of the tensor elements of a magnetized system. We predicted a phase difference of 90° between odd and even tensor elements at frequencies far from resonance. The consequences of this statement may lead to some confusion, because one might naively expect that it would be in contradiction with the observation of magnetization induced effects in SHG. Neglecting details one could describe MSHG by a single interface as:

$$I(2\omega, \mathbf{M}^{\pm}) = |\chi^{(D),even}(\mathbf{M}) \pm \chi^{(D),odd}(\mathbf{M})|^2 I(\omega)^2 \tag{3.68}$$

A phase difference of 90° between $\chi^{(D),even}(\mathbf{M})$ and $\chi^{(D),odd}(\mathbf{M})$ would imply that $I(2\omega, \mathbf{M}^{+}) = I(2\omega, \mathbf{M}^{-})$. However, this is by no means an adequate description of the situation, as it completely neglects the additional phase differences that occur due to the fact that the $\chi^{(D),even}(\mathbf{M})$ and $\chi^{(D),odd}(\mathbf{M})$ tensor elements are excited by different field components.

With the model that we have developed in this chapter it is easy to calculate the second-harmonic fields that are generated at the surface of a semi-infinite metal. In correspondence with the situation in section 3.3, we calculate the fundamental fields in an infinitesimal vacuum sheet, just outside the metal. The interface SH-sources are placed in a nonlinear sheet, positioned within this vacuum sheet (see figure 3.4). For simplicity we choose: $\hat{n}^i(\omega) = \hat{n}^i(2\omega) = 1$.

For p-polarized fields we use eq. 3.17 with eq. 3.18 and 3.19. Because the metal is semi-infinite there will be no backward wave in the metal, so:

$$\begin{pmatrix} E'^{+}_{\omega,p,0} \\ E'^{-}_{\omega,p,0} \end{pmatrix} = \frac{1}{f^{\omega,+}_{0,0}} \begin{pmatrix} f^{\omega,+}_{0,1} \\ -f^{\omega,-}_{0,1} \end{pmatrix} E^{+}_{\omega,p,1} \tag{3.69}$$

with

$$f^{\omega,\pm}_{0,1} = \cos\hat{\theta}_{\omega,1} \pm \hat{n}_1(\omega)\cos\theta_{\omega,0} \tag{3.70}$$

where the indices 0 and 1 refer to respectively the vacuum and the metal. As the nonlinear sheet has the same refractive index as the vacuum sheet, we can now easily calculate the components of the total fundamental field in the nonlinear sheet: $\mathcal{E}_{\omega,p,0}$, using eq. 3.37 , 3.41 and 3.43:

$$\mathcal{E}_{\omega,x,0} = -\frac{2\cos\hat{\theta}_{\omega,1}}{\cos\hat{\theta}_{\omega,1} + \hat{n}_1(\omega)\cos\theta_{\omega,0}} E'^{+}_{\omega,p,0}\cos\theta_{\omega,0} \tag{3.71}$$

$$\mathcal{E}_{\omega,z,0} = \frac{2\hat{n}_1(\omega)\cos\theta_{\omega,0}}{\cos\hat{\theta}_{\omega,1} + \hat{n}_1(\omega)\cos\theta_{\omega,0}} E'^{+}_{\omega,p,0}\sin\theta_{\omega,0} \tag{3.72}$$

In the Drude model the metal has a dielectric constant [18]:

$$\hat{\epsilon}_1(\omega) = 1 - \frac{\omega_p^2}{\omega^2(1 + \frac{i}{\omega\tau})} \tag{3.73}$$

where τ is the relaxation time, and ω_p the plasma frequency. Let us suppose that medium 1 is an ideal metal. An ideal metal has no scatterers, so the relaxation time becomes infinitely long. If we assume that $\omega \ll \omega_p$, we obtain:

$$\hat{\epsilon}_1(\omega) \to -\infty \tag{3.74}$$

Notice that the expression is meant to say that $\hat{\epsilon}_1(\omega)$ has a large negative value, if $\omega \ll \omega_p$, and not really that $\hat{\epsilon}_1(\omega) \to -\infty$. The same reasoning holds for all 'limits' in this section. Since $\hat{\epsilon} = \hat{n}^2 = (n + ik)^2$:

$$n_1(\omega) \to 0 \quad \text{and} \quad k_1(\omega) \to \infty \tag{3.75}$$

As (see page 40),

$$\cos\hat{\theta}_{\omega,1} = \sqrt{1 - [\sin\theta_{\omega,0}/\hat{n}_1]^2} \tag{3.76}$$

we find:

$$\lim_{\substack{n_1 \to 0 \\ k_1 \to \infty}} \cos\hat{\theta}_{\omega,1} = 1 \tag{3.77}$$

and eq. 3.71 and 3.72 can be combined to:[9]

$$\lim_{\substack{n_1 \to 0 \\ k_1 \to \infty}} \mathcal{E}_{\omega,z,0} = \lim_{\substack{n_1 \to 0 \\ k_1 \to \infty}} ik_1 \cos\theta_{\omega,0} \mathcal{E}_{\omega,x,0} \tag{3.78}$$

implying a phase difference of 90° between the x- and z-components of the total fundamental fields in the interface sheet. We can now calculate the reflected second-harmonic intensity using eq. 3.54, 3.44 and 3.45. We obtain:

$$E'^{-}_{2\omega,p,0} = -i\frac{2\omega}{c} 4\pi \frac{P^{sh}_{2\omega,z,1} + \kappa_{2\omega,p,1} \cos\theta_{\omega,0} P^{sh}_{2\omega,x,1}}{(\kappa'_{2\omega,p,1} - \kappa_{2\omega,p,1}) \cos\theta_{\omega,0}} \tag{3.79}$$

with (see eq. 3.36)

$$P^{sh}_{2\omega,k,1} = \chi^{(D)}_{klm,1}(2\omega) \mathcal{E}_{\omega,l,1} \mathcal{E}_{\omega,m,1} \tag{3.80}$$

From eq. 3.53 we calculate the values of $\kappa'_{2\omega,p,1}$ and $\kappa_{2\omega,p,1}$. If the second-harmonic frequency is also far below the plasma frequency, we can use eq. 3.69 and 3.77 to derive:

$$\lim_{\substack{n_1 \to 0 \\ k_1 \to \infty}} \kappa_{2\omega,p,1} = \frac{1}{ik_1 \cos\theta_{\omega,0}} \tag{3.81}$$

$$\lim_{\substack{n_1 \to 0 \\ k_1 \to \infty}} \kappa'_{2\omega,p,1} = -1 \tag{3.82}$$

Eq. 3.82 is obtained after realizing that $E'^{+}_{2\omega,p} = 0$, as we only have a backward SH-field on the outside of the metal. The resulting reflected SH-intensity can be written as:

$$I(2\omega) = K|P^{sh}_{2\omega,z,1} - \frac{i}{k_1} P^{sh}_{2\omega,x,1}|^2 \tag{3.83}$$

[9] Notice that $\lim_{z \to -\infty} \mathcal{E}_{\omega,x,0} = 0$ and $\lim_{z \to -\infty} \mathcal{E}_{\omega,z,0} = 2E'^{+}_{\omega,p,0} \sin\theta_{\omega,0}$, as is to be expected for an ideal metal.

where K is a real constant. Table 2.1 gives the tensor elements for an isotropic interface with a magnetization perpendicular to the plane of incidence. Rewriting eq. 3.80 with eq. 3.78 for this particular system, and assuming a phase difference of 90° between $\chi^{(D),even}$ and $\chi^{(D),odd}$ gives a purely imaginary $P^{sh}_{2\omega,x,1}$, while $P^{sh}_{2\omega,z,1}$ is purely real.[10] So the phase difference between the two terms in eq. 3.83 is either 0° or 180°. This implies that a phase difference of 90°, between odd and even tensor elements does not only give observable magnetization induced effects in SHG, but is for the typical case of an ideal metal even the most 'favorable' situation as it leads to the largest relative changes.

References

[1] B. Koopmans, A. Anema, H.T. Jonkman, G.A. Sawatzky, and F. van der Woude, Phys. Rev. B **48**, 2759 (1993).

[2] Bert Koopmans, *Interface and bulk contributions in optical second-harmonic generation* (Thesis, Rijksuniversiteit Groningen, Groningen, The Netherlands, 1993).

[3] C.W. van Hasselt, M.A.C. Devillers, Th. Rasing, and O.A. Aktsipetrov, accepted for publication in J. Opt. Soc. Am. B.

[4] M.S. Yeganeh, J. Qi, J.P. Culver, A.G. Yodh, and M.C. Tamargo, Phys. Rev. B **46**, 1603 (1992).

[5] B. Dick, A. Gierulski, G. Marowsky, and G.A. Reider, Appl. Phys. B **38**, 107 (1985).

[6] N. Bloembergen and P.S. Pershan, Phys. Rev. **128**, 606 (1962).

[7] *Handbook of optical constants of solids*, edited by E.D. Palik (Academic Press Inc, Orlando, 1985).

[8] P. Yeh, A. Yariv, and C.S. Hong, J. Opt. Soc. Am. **67**, 423 (1977).

[9] A. Yariv, P. Yeh, J. Opt. Soc. Am. **67**, 438 (1977).

[10] P. Yeh, J. Opt. Soc. Am. **69**, 742 (1979).

[10] Autosummation is still implied, and remember that we have used the limit $k_1 \to \infty$ in the sense that k_1 has a large positive value.

[11] D.S. Bethune, J. Opt. Soc. Am. B **6**, 910 (1989).

[12] D.S. Bethune, J. Opt. Soc. Am. B **8**, 367 (1991).

[13] J.E. Sipe, J. Opt. Soc. Am. B, **4**, 481 (1987).

[14] T.F. Heinz, *Nonlinear optics of surfaces and adsorbates* (Thesis, Lawrence Berkeley Laboratory, Berkeley, USA, 1982).

[15] J.D. Jackson, *Classical Electrodynamics*, 2^{nd} edition (John Wiley & Sons, New York, 1975).

[16] Y.R. Shen, *The principles of nonlinear optics* (Wiley, New York, 1984).

[17] P.B. Johnson and R.W.Christy, Phys. Rev. B **9**, 5056 (1974); Phys. Rev. B **6**, 4370 (1972).

[18] N.W. Ashcroft, N.D. Mermin *Solid State Physics* (Holt-Saunders Japan LTD, Tokyo, 1976).

Chapter 4

Experimental introduction

Optical Second-Harmonic Generation (SHG) from interfaces is a very inefficient process. Therefore the experiments require both excitation with the extremely high electric fields that are obtained from a pulsed laser, and detection of the generated second-harmonic light with a sensitive detector like a photomultiplier tube. Due to the enormous difference between the intensities of the reflected fundamental and the generated second-harmonic, and the fact that in general the beams are not spatially separated, proper filtering is always of vital importance. Furthermore, the set up for SHG needs polarizing elements that allow selective detection of the various tensor elements of the system under study. Although many interesting results are obtained in experiments under ambient conditions, better insight often requires the preparation of well defined clean surfaces under Ultra High Vacuum (UHV) conditions.

The initial studies of Magnetization induced Second-Harmonic Generation were done with a system that we built around a pulsed Nd:YAG laser-system. Section 4.1 discusses the relevant details of this set up.

In chapter 6 we describe in situ experiments on thin ferromagnetic films, using a pulsed Ti:Sapphire laser. The set up is discussed in section 4.2. The experiments were done in cooperation with R. Vollmer, A. Kirilyuk, and H. Schwabe, co-workers of J. Kirschner.[1] They provided a UHV chamber with epitaxial growth facilities that will only be discussed briefly, focussing on aspects that might be of importance for future experiments. In section 4.3 we briefly discuss the Magneto-Optical Kerr Effect (MOKE).

[1] Max-Planck-Institut für Mikrostrukturphysik, Halle/Saale, Germany.

4.1 Nd:YAG-laser set up

Figure 4.1 gives a schematic representation of the Nd:YAG laser-system. Two UHV systems are available for the preparation of clean surfaces. However the set up also contains a bench site for experiments under ambient conditions (sample position in figure 4.1). Due to the configuration of the set up, we can operate all 'stations' after changing only a few optical components.

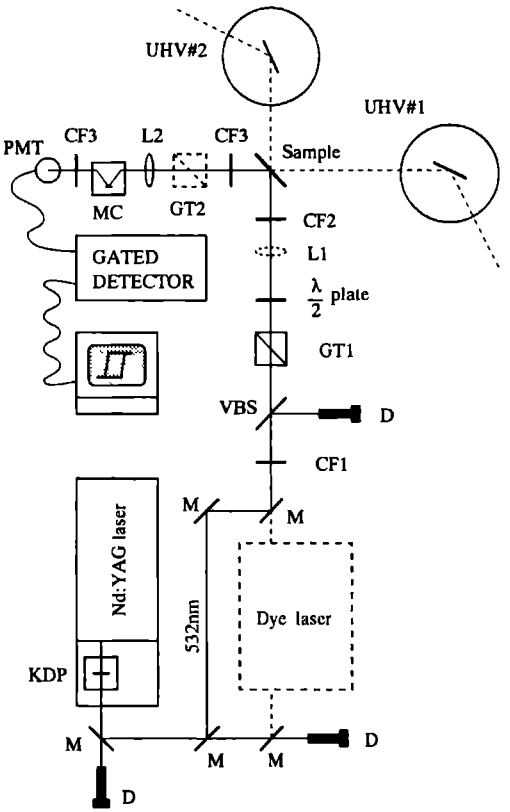

Figure 4.1: *Schematic representation of the Nd:YAG laser-laboratory for Second-Harmonic Generation. KDP - frequency doubling crystal, M - dichroic mirror, D - beam dump, CF- colour filter, VBS - variable beam splitter, GT - Glan Taylor polarizer, L - lens, MC - monochromator, PMT - photomultiplier tube. The sample is at the bench site position.*

4.1.1 Optical set up

The injection seeded Q-switched Neodymium-doped Yttrium Aluminum Garnet laser (Nd:YAG) produces Infrared light pulses with a wavelength of 1064 nm (Spectra Physics, DCR 3). The output beam has a doughnut mode profile, a repetition frequency of 30Hz, a pulse width of about 8 ns, and a maximum pulse energy of about 650 mJ. Injection seeding narrows the linewidth and improves the pulse to pulse stability. Approximately 30 % of the infrared output is frequency doubled to 532 nm in a commercial thermally stabilized KD*P crystal (Spectra Physics, HG-2). The set up contains a Dye laser (Spectra Physics, PDL-2) that must be pumped by the (frequency doubled) Nd:YAG laser. As it is not used in the experiments in this thesis, I shall not describe it in detail. The laboratory is temperature stabilized with an air conditioner in order to improve laser stability.

Reflecting the (collinear) output beams at several dichroic mirrors (M) removes most of the remaining 1064 nm from the optical path, and dumps it into the beam dumps (D). A colour filter BG-39 (CF1) filters out the last remainders of the Infrared light.[2] The laser fluence is adjusted with a variable beam splitter (VBS).[3] It consists of a dielectric substrate covered with alternating layers of respectively $\lambda/2$ and $\lambda/4$ thickness for 532 nm. Varying the angle of incidence changes the interference in the beam splitter, and thus the transmission. The air-spaced Glan-Taylor polarizer (GT1) has an extinction ratio of 10^{-4} and a high damage threshold. It fixes the polarization of the exciting beam independent of the (possibly changing) polarization in the first part of the beam path. The $\lambda/2$-plate for 532 nm rotates the polarization to any preferred orientation (usually s or p). A long focus lens can be used to reduce the beam area on the sample. Before reaching the sample, the light is passed through a GS 3-74 colour filter (CF2). It removes all light with frequencies below 360 nm, thus eliminating the possibility of detecting fields at the second-harmonic wavelength (266 nm) that have not been generated at the sample.

Figure 4.1 shows the configuration that is used in experiments under ambient conditions. The second-harmonic light, generated at the sample, is de-

[2]Of course we could use the 1064 nm output to excite the sample. However, unless there exists a spectroscopic reason to use this wavelength, it is more convenient to use 532 nm as the fundamental and generate second-harmonic with a wavelength of 266 nm, because in the latter case the second-harmonic wavelength is in the Ultra Violet, and it is not necessary to darken the room.

[3]The beam splitter also provides the absolutely necessary reduction of the average pulse intensity of about 450 mJ/cm^2, that would damage nearly any material. In this way the laser always operates at full power, to ensure maximum stability.

tected by the photomultiplier tube (PMT: Hamamatsu, R106UH) after filtering out the reflected fundamental light. Although a simple stack of colour filters (CF3: GS 7-54) would serve this purpose, the detection set up includes a monochromator (MC: Jobin Yvon, H.10 UV) with a maximum spectral resolution of 4 nm. This provides an opportunity to check the presence of luminescence, that might give radiation of the same wavelength (266 nm), but has a much wider band width than the process of second-harmonic generation. The UV-transparent lens L2 focusses the light into the monochromator. Furthermore the detection line includes a UV-transparent Glan-Taylor polarizer (GT2), to analyze the second-harmonic. Because of its poor transmission of only 40 % at 266 nm it is omitted if possible. The complete detection set up has an efficiency of approximately 5 % if GT2 is omitted.

Since we are using a pulsed laser with a low repetition frequency, the PMT-signal must be analyzed by gated electronics. Depending on signal strength we have two options:

(1) Gated Integrating:
This is a standard technique and needs not to be discussed in detail, especially because the experiments in this thesis were done by Gated Photon Counting. The latter technique was developed because at signals much less than 1 photon per laser pulse, the zero point fluctuations of the gated integrator (Stanford Research Systems, SR250) make reliable detection impossible.

(2) Gated Photon Counting (GPC):
This technique exploits the fact that the chances of generating more than one second-harmonic photon in the same pulse, become very small at low signals, and instead of measuring the size of the second-harmonic signal, it becomes sufficient to discriminate whether or not a second-harmonic photon is present.

A tremendous reduction of the background signal, due to the darkcurrent of the PMT, is obtained by using gated photon counting. Analogous to gated integrating, the counter opens only during the very restricted period when a second-harmonic photon is to be expected, which requires triggering the counter with the Nd:YAG laser.

The gated photon counter was easily built from a Hewlett Packard 54510A digital oscilloscope, because we could exploit its special trigger facilities. We connect the trigger output of the laser to channel#1, and the PMT output to channel#2. We choose a configuration that triggers the oscilloscope only if:

1. Both the trigger output of the laser has a value above the trigger level of

channel#1. This is similar to setting the gate. We adjusted the trigger level of channel#1 to obtain a gate width of approximately 50 ns.

2. And the PMT detects a photon, i.e. channel#2 measures a voltage above the trigger c.q. discrimination level.

A special output facility of the oscilloscope gives a trigger pulse whenever this combined event occurs. The number of these latter trigger pulses is easily counted by the computer.

Due to the fact that the photon detection (on channel#2) involves only one discrimination level, it does not distinguish the one photon events from the multiple photon events. This error can be corrected to some extend by applying a scheme that was proposed by Heinz [1]. It is based on the fact that the emission of photons obeys Poisson statistics:

$$P(n) = \frac{\lambda^n}{n!} e^{-\lambda} \tag{4.1}$$

where $P(n)$ is the probability of generating n photo-electrons, and λ is the average number of primary photo-electrons emitted per pulse. If we now introduce Γ, as the fraction of pulses for which at least one photo-electron is produced, we obtain:

$$\Gamma = \sum_{n=1}^{\infty} P(n) = 1 - P(0) = 1 - e^{-\lambda} \tag{4.2}$$

So

$$\lambda = -\ln(1 - \Gamma) \tag{4.3}$$

Figure 4.2 shows the result of a linearity test of the detection method, while including the correction scheme. We have used the set up of figure 4.1 with a silicon wafer as test sample. The SH-countrate versus the square of the input power (P), should yield a linear dependence. We observe that the detection method is linear until countrates of approximately 20 %. The open squares in the figure represent the uncorrected countrates, and show that if we do not apply the correction scheme, we would not only underestimate the signals, but also face first deviations from proper linear behaviour at slightly lower countrates. In our experiments we have always kept the countrates well below 20 %. The GPC method reduces the background level to approximately 1 dark count every 5 minutes, i.e. every 9000 laser shots! We have done experiments on the Co/Au multilayers where the second-harmonic signals were as low as

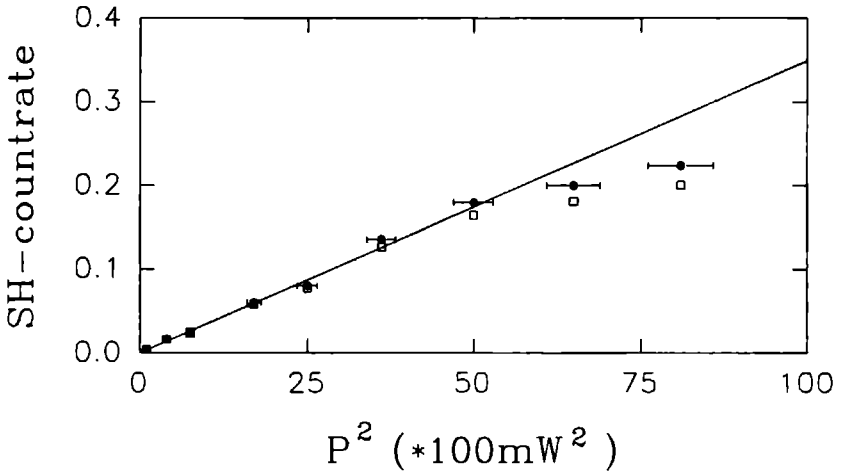

Figure 4.2: *Linearity test of gated photon counting detection system. The open squares represent the measured SH-countrates, the solid circles are obtained after applying the correction formula (eq. 1.3), and show proper linear dependence on the square of the input power until almost 20 %.*

6 photons/minute, while the sample was excited with a pulse intensity of 7 mJcm^{-2} over a beam area of 60mm^2. This implies a conversion rate of: $2I(2\omega)/I(\omega) \sim 10^{-17}$!

It will be clear from figure 4.1 that removing the sample automatically passes the beam to UHV system #2. Replacing it by a mirror reflects the beam to UHV chamber #1. In the latter case we position CF2 between the mirror and the entrance window of UHV #1. For the experiments under UHV conditions we use the same detection set up. Its optical components are placed on a small portable table.

4.1.2 Ultra High Vacuum systems

Both UHV systems in figure 4.1 are equipped with the standard techniques for the preparation and analysis of clean surfaces: Argon Ion Sputtering (AIS), sample annealing, Low Energy Electron Diffraction (LEED), Auger Electron Spectroscopy (AES), and Mass Spectrometry.

This thesis contains no experiments that were done with UHV chamber #2

and a detailed description is therefore superfluous. However, I would like to mention that the system was designed for in situ rotational anisotropy studies with SHG. A standard problem in these type of experiments is the fact that the axis of rotation is usually not parallel to the surface normal. This causes a troublesome precession of the generated second-harmonic beam around the axis of rotation. We have solved the problem by using a manipulator that has three stepper motor-controled rotational degrees of freedom (Vacuum Generators, CTPO) and correcting the wobbling of the sample with an active feedback loop. We put a HeNe aiming beam on the surface of the sample and detect its reflection beam with a four quadrant position detector. Wobbling of the sample, while performing the in plane rotation, causes (small) changes of the HeNe beam position on this detector. These changes are easily detected and can be corrected by appropriate sample manipulations.

UHV system #1 has a base pressure of 2.10^{-10} torr, that was obtained by combining a Turbomolecular pump (Balzers, TPU 270) and a liquid-Nitrogen-cooled Titanium Sublimation Pump. The AIS-gun sputters with a maximum beam energy of 750 eV. The system contains a combined LEED/AES-system (Omicron, Spectaleed). The AES equipment has a 3.5 KeV electron gun and a maximum sensitivity of about half a percent of a monolayer. The mass spectrometer was used for standard gas analysis. Small amounts of gas can be dosed by two leak valves.[4] We have used this system to study the Ni(110) and the Fe(110) surfaces. Both crystals were mounted on different sample manipulators.

Figure 4.3 shows a schematic representation of the sample configuration and the electromagnet as used in the experiments on the Ni(110) surface. Ni(110) has two (111) easy axes lying in the plane of the surface. We have chosen one of them parallel to the direction of the external magnetic field. The sample can be annealed by slow radiative heating, or by fast flashing with 600 eV electrons. Temperatures of 1000 °C are easily obtained, and measured with a K-type thermocouple (TC), that was spot welded on the sample surface. The windings of the coils are isolated with kapton, because it has a low degas rate at elevated temperatures. Due to the fact that the yoke is in direct mechanical contact with the crystal, the nickel is easily magnetized (see figure 7.1). However, a severe disadvantage of the construction was encountered after annealing at very high temparatures (above 700 °C), because thermal expansion led to stress and a distortion of the crystalinity.

A solution to this problem is shown in figure 4.4. It is the sample config-

[4] argon, oxygen and hydrogen are standard.

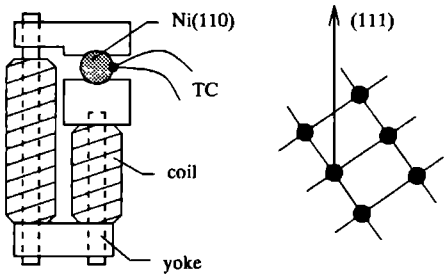

Figure 4.3: *Sample configuration in experiments on Ni(110). The yoke is made out of Armco, the windings of the coil are kapton isolated, TC is a K-type thermocouple. The figure on the right shows the orientation of the crystal.*

uration for the experiments on the Fe(110) surface.[5] This configuration also provides good mechanical contact between yoke and sample, however due to the clamps that fit into small slits that are milled in the sides of the sample, small movements at elevated temperature are allowed.[6] The crystal is annealed by radiative heating. The temperature is measured with a K-type thermocouple (TC), that was clamped in one of the milled slits.

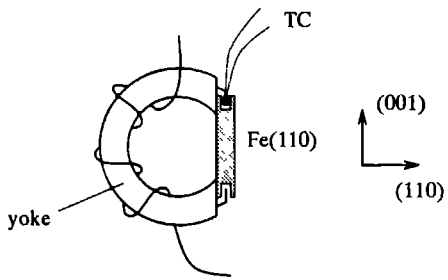

Figure 4.4: *Sample configuration in experiments on Fe(110). The yoke is made out of Armco, the windings of the coil are isolated with glass fibre, TC is a K-type thermocouple. The orientation of the crystal is indicated.*

[5]The crystal and the manipulator were borrowed from J. Kirschner.

[6]This configuration also provides weak stray field, which is important when using electrons. It is however of no relevance in our optical experiments.

4.2 Ti:Sapphire laser set up

In chapter 6 we discuss a series of experiments on epitaxially grown thin ferromagnetic films. The samples were prepared under UHV conditions and studied in situ by the Magneto-Optical Kerr Effect (MOKE) and Magnetization induced Second-Harmonic Generation (MSHG). The second-harmonic signal was generated from the output of a mode-locked Ti:Sapphire laser.

4.2.1 Optical set up

The mode-locked Ti:Sapphire laser (Spectra Physics, Tsunami) is pumped by an Argon Ion laser (Spectra Physics, 2040E, see figure 4.5). The output has a Gaussian mode, a repetition frequency of 82MHz and a pulse width of about 100fs. The output is continuously tunable from 720 to 860 nm.[7] At 800 nm the laser has an average output power of approximately 1.3 W.

The laser fluence is regulated by a set of neutral density filters (NDF). The polarization of the incoming fundamental beam is adjustable with a Soleil/Babinet compensator, that we use as a tunable halfwave plate. A set of lenses (L1) was used to focus the beam on the sample surface, leading to a spot diameter of approximately 100μm. A colour filter OG570 (CF1) removes all light of wavelengths below 570 nm and has the same function as the GS 3-74 filter in the Nd:YAG set up (see page 61). The dashed line in figure 4.5 indicates the beam path for the longitudinal MOKE experiments (see section 4.3). The plane of incidence in the SHG experiments is perpendicular to the optical plane of the MOKE set up, because magnetizing the sample perpendicular to the plane of incidence gives the largest magnetization induced effects in SHG (see section 5.2). The sample is excited with an average power of about 100 mW at 800 nm, leading to a typical pulse intensity of approximately 16μJcm^{-2}.

The inset in figure 4.5 shows a right hand side view of the sample. The magnetization is in the plane of the film, and the detection set up is quite similar to the one used in the experiments with the Nd:YAG laser. Two BG39 colour filters (CF2) filter out the fundamental light, and a UV-transparent lens (L2) focusses the second-harmonic light into the photomultiplier tube (PMT: Thorn EMI, 9789B). We do not need gating as the repetition frequency of the laser is 82MHz and allows semi-continuous detection, using a chopper in combination with a lock-in amplifier to get rid of ambient fluctuations. The Thorn EMI PMT has a much lower dark current than the Hamamatsu PMT

[7] Using a different set of mirrors the Ti:Sapphire can be tuned between 960 nm and 1080 nm.

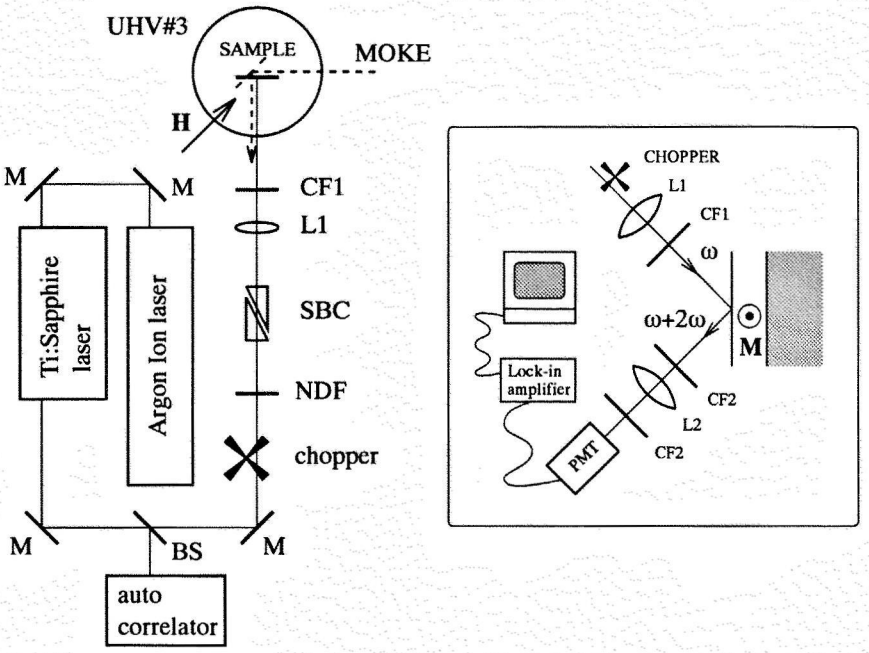

Figure 4.5: *Schematic representation of the Ti:Sapphire set up. The inset on the right shows the sample configuration and the detection set up: M - mirror, BS - beam splitter, NDF - neutral density filter, SBC - Soleil/Babinet compensator used as tunable halfwave plate, L - lens, CF - colour filter, PMT - photomultiplier tube. The dashed line indicates the beam path in the MOKE experiments. The direction of the external magnetic field (**H**) and the induced magnetization (**M**) are indicated.*

used in the Nd:YAG set up, and is therefore much more suitable for the semi-continuous detection method. A monochromator was omitted for practical reasons. We did however use a MC/PMT combination, to verify that the line width of the detected light was of the order of a few nanometers, i.e. limited by the resolution of the monochromator, which implies that we only detect second-harmonic light. Thus it is safe to use only the colour filters (CF2) and omit the monochromator. The detection configuration has an efficiency of about 10 %.

4.2.2 Ultra High Vacuum system

The samples were prepared in a UHV system with a base pressure of 5×10^{-11}torr. The system is equipped with the standard techniques we already mentioned in section 4.1.2. It has two (extra) aspects that I would like to discuss in some detail, as they might be of help in future MSHG experiments:

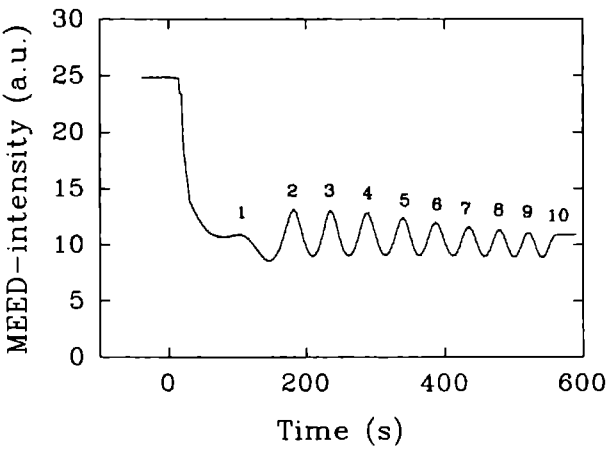

Figure 4.6: *This typical MEED pattern was taken while growing 10 ML of cobalt on Cu(001). A peak in the MEED-intensity corresponds to a full monolayer.*

(1) Epitaxial growth was verified for every film by monitoring the (0,0) Medium Energy Electron Diffraction (MEED) spot intensity while depositing [3, 4]. MEED is the medium energy equivalent of Reflection High Energy Electron Diffraction (RHEED). As the latter technique is discussed in many textbooks [5], it is not necessary to go into details. MEED is based on the fact that the de Broglie wavelength of medium energy electrons (approximately 0.2 Å for electrons with an energy of 2.8 KeV) is shorter than the typical interatomic distance. Therefore MEED is sensitive to corrugations on the atomic scale. Reflecting a medium energy electron beam at grazing incidence[8] from the surface yields an interference pattern that images the structure of the surface. The intensity variations of the (0,0) MEED spot can be measured by a photometer and are a direct measure of the corrugation of the surface,

[8] Angles of incidence larger than approximately 70°.

i.e. the state of the growth. The advantage of MEED in relation to RHEED is that we can easily use the electron gun of the AES equipment.[9] Figure 4.6 shows the MEED-intensity versus time, while growing a 10 monolayer (ML) cobalt film on Cu(001), at a substate temperature of about 100 °C and a constant growth rate. A peak in the intensity indicates the completion of a full monolayer. The growth rate is not very stable until a thickness of about 2 ML, in this specific case, but was usually much better.

(2) The magnetic field was obtained from a coil/yoke construction, where the coil was situated outside the vacuum, thus preventing UHV problems due to degassing of the windings of the coil. The yoke consisted of several cylindrical slabs of μ-metal that guide the magnetic field lines towards the sample, giving a maximum external field of about 70Gauss.

4.3 Magneto-Optical Kerr Effect

The Magneto-Optical Kerr Effect (MOKE) is a well established probe of the magnetic properties of materials [6] and has proven to be extremely useful in recent studies on the exchange coupling in multilayered systems containing ferromagnetic material (see for example Ref. [2, 3]). The Kerr effect involves the magnetization dependent changes of the polarization of light reflected from a magnetic material, caused by spin-orbit coupling, and is observed in materials that have a different reflection coefficient for left- and right-handed circularly polarized light [6, 7]. A typical MOKE set up contains a laser, polarizing elements and a photodiode. The MOKE hysteresis is obtained from detecting the signal at the photodiode versus the magnetization of the sample c.q. the externally applied field. In this section we discuss two set ups that have been used for MOKE experiments, where the magnetization is lying in the plane of the film.

Figure 4.7 shows a simple set up for MOKE experiments. The Glan/Taylor polarizer (GT1) passes p-polarized light. When linearly polarized light is reflected from the surface of a magnetized material, the reflected light is in general elliptically polarized [7]. The optical axis of GT2 makes an angle of 45° with the optical plane. In this configuration we are sensitive to both the changes in the reflectivity and the rotations of the polarization, due to magnetization modulation. These changes are detected by the photodiode (PD) and imaged on an oscilloscope after electronically subtracting the DC back-

[9] It is not necessary to detect the electrons with AES or LEED optics. The reflected electrons in the (0,0) MEED spot can be visualized using a small piece of fluorescent material.

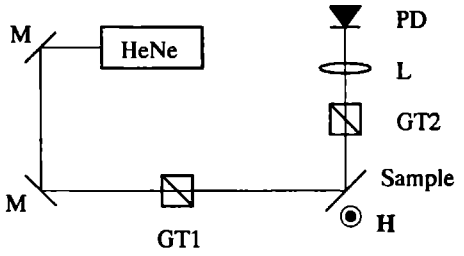

Figure 4.7: *MOKE set up #1: GT - Glan/Taylor polarizer, L - lens, PD - photodiode. The external field is modulated.*

ground signal with a bandpass filter. Modulating the external field gives a rough indication of the hysteresis loop. The method is simple, but not very well defined. Furthermore, it has the strong disadvantage that magnetic saturation, where the magnetization no longer changes with increasing external field, is not properly measured as we suppress the DC signals.

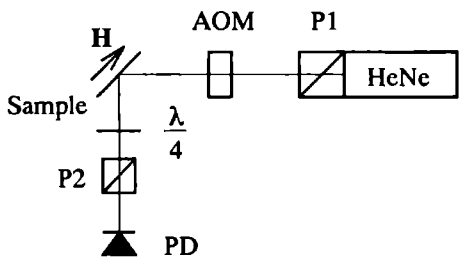

Figure 4.8: *MOKE set up #2: P - polarizer, AOM - Acousto-Optical Modulator, $\lambda/4$ - quarterwave plate, PD - photodiode.*

Figure 4.8 shows a better solution. A polarizer (P1) is glued directly on the unpolarized HeNe-laser, providing an output that is linear polarized at an angle of 45° to the optical plane. The polarization of this light is modulated (at frequency ω) by an Acousto-Optical Modulator (AOM), with its fast axis perpendicular to the plane of incidence. The AOM provides a time-dependent retardation of the light. We have chosen a maximum retardation of $\lambda/4$. Thus we modulate the input between left- and right-handed circularly polarized. The output of the AOM has the Jones vector [7, 8]:

$$\mathbf{E}_{in} = \begin{pmatrix} 1 \\ e^{i\frac{\pi}{2}\sin(\omega t)} \end{pmatrix} \tag{4.4}$$

The concept of Jones vectors is very convenient as every optical component and the reflection of the light from the magnetized sample can be described in terms of matrices. The optical axis of analyzer (P2) is perpendicular to the plane of incidence. The fast axis of the $\lambda/4$-plate is parallel to the optical axis of P2. The intensity that is detected by the photodiode (PD) can be written as:

$$\frac{1}{4}|R^-|^2[1+|\chi|^2+(|\chi|^2-1)\sin\delta - 2Im(\chi)\cos\delta] \tag{4.5}$$

where $\chi \equiv R^+/R^-$ is the polarization variable, and R^+ and R^- are the magnetization dependent reflection coefficients for respectively right- and left-handed circularly polarized light, and $\delta = \pi\sin(\omega t)/2$. The reflected intensity clearly depends on R^+ and R^-, i.e. on the magnetization of the sample. From the intensity and the phase of the modulation of the reflected light, we can deduce χ, from which we can calculate the dielectric tensor of the system.

The same result is obtained if the $\lambda/4$-plate is omitted. However, the combination of P2 and the $\lambda/4$-plate provides a means to compensate the rotation and ellipticity that are introduced by the windows of the UHV chamber.[10]

References

[1] T.F. Heinz, *Nonlinear optics of surfaces and absorbates* (Thesis, Lawrence Berkeley Laboratory, Berkeley, 1982).

[2] M.T. Johnson, S.T. Purcell, N.W.E. McGee, R. Coehoorn, J. aan de Stegge, and W. Hoving, Phys. Rev. Lett. **68**, 2688 (1992).

[3] A. Cebollada, R. Miranda, C.M. Schneider, P. Schuster, and J. Kirschner, J. Magn. Magn. Mat. **102**, 25 (1991).

[4] C.M. Schneider, J.J. de Miguel, P. Bressler, J. Garbe, S. Ferrer, R. Miranda, and J. Kirschner, J. Phys. Suppl. C8, 1657 (1988).

[10] Window induced rotations can be compensated by rotating the polarizer and the quarter wave plate together in the same direction. The ellipticity of the light can be compensated by rotating the quarter wave plate alone. We calibrated the set up by minimizing the PD-signal, while the sample was magnetically saturated in one direction.

[5] see for example M. Prutton, *Surface physics*, 2nd edition (Oxford University Press, New York, USA, 1983).

[6] L.M. Falicov *et al.*, J. Mater. Res. **5**, 1299 (1990).

[7] H. Feil, *Magneto-optical Kerr effect, the relation between optical, transport and electronic properties in magnetic compounds*, (Thesis, Rijksuniversiteit Groningen, Groningen, The Netherlands, 1987).

[8] R.M.A. Azzam, and N.M. Bashara *Ellipsometry and Polarized light* (North Holland Physics Publishing, Amsterdam, 1987).

Chapter 5

MSHG on Co/Au multilayers

In this chapter magnetized multilayers of cobalt and gold are studied by optical Second-Harmonic Generation. The SH-signal depends strongly on the magnetization, and it is shown that the phenomenological theory of chapter 2 offers a good qualitatively description of the dependence of MSHG on the orientation of the magnetization and the polarization of the light. Varying the number of Co/Au interfaces has a pronounced influence on the relative magnetic effects in MSHG. Using the multiple reflection theory of chaper 3, the results could be explained in terms of pure interface contributions, indicating that MSHG is not only sensitive to the highly academical clean surfaces [1], but also to the much more significant buried interfaces.[1]

5.1 Sample preparation and experimental set up

The samples consist of thin films of cobalt and gold, e-beam evaporated at a rate of about 2 Å/s, while the substrate was kept at room temperature.[2] The pressure was 5×10^{-7} Torr while evaporating. The substrates were optical quality glass plates (roughness $\lambda/10$; flatness λ), rinsed in ethanol and blow dried with nitrogen. Four systems, with an increasing number of cobalt/gold interfaces, were studied:

- Sample *A*: glass + 1550 Å Au
- Sample *B*: glass + 500 Å Co + 50 Å Au

[1] Part of this chapter has been published in: Surf. Sci. **287-288**, 747 (1993); J. Magn. Magn. Mat. **121**, 109 (1993); Phys. Rev. B, **50**, 1282 (1994).

[2] The films were prepared by M.W.J. Prins of the Research Institute for Materials, Toernooiveld 1, Nijmegen, The Netherlands.

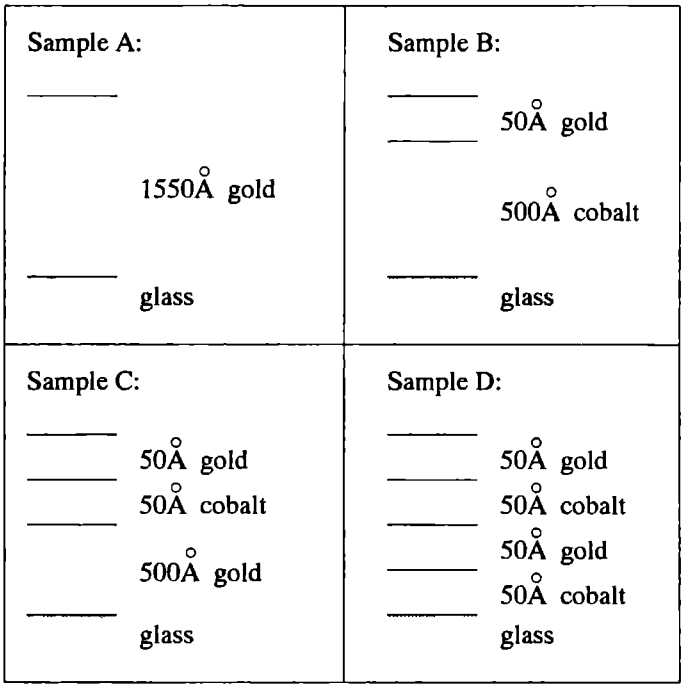

Figure 5.1: *The Co/Au multilayers that are discussed in this chapter.*

- Sample *C*: glass + 500 Å Au + 50 Å Co + 50 Å Au
- Sample *D*: glass + 50 Å Co + 50 Å Au + 50 Å Co + 50 Å Au

The top layer of each system is gold, which protects the cobalt layers, and allows experiments under ambient conditions. Figure 5.1 gives a graphic representation of the samples. Although the films are probably polycrystalline, they are isotropic on the scale of the laser beam area ($\gtrsim$10 mm^2). For the experiments we used the Nd:YAG set up as described in section 4.1 . The fundamental beam has a wavelength of 532 nm, and the SH-signals were measured using Gated Photon Counting (see section 4.1.1). The samples were mounted at the bench site position in figure 4.1 and placed in between the poles of an electromagnet.

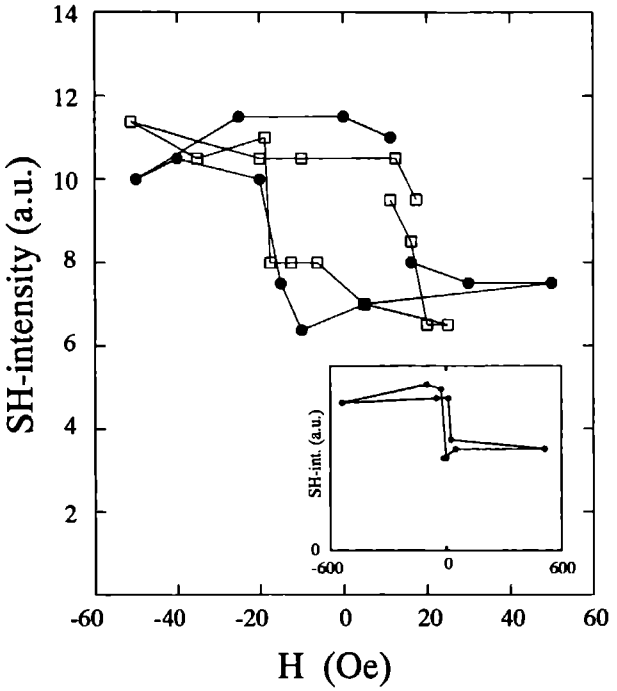

Figure 5.2: $p_{in}p_{out}$ *SH-intensity from sample B as function of applied magnetic field, measured in the transverse configuration. Positive values of* **H** *correspond to an upwards oriented magnetic field. The open squares and filled circles correspond to different sets of data. Inset:* $p_{in}p_{out}$ *SH-intensity for fields up to 600 Oe.*

5.2 Magnetization and polarization dependence

Before discussing the interface sensitivity of MSHG in Co/Au multilayers, we verify that the phenomenological theory of chapter 2 offers a reliable qualitative description of the nonlinear optical properties of these multilayers. The dependence of MSHG on the orientation of the magnetization and the polarization of the light is in good agreement with the theoretical predictions for magnetic interface contributions. The calculated magnetic effects are compared with the results of MOKE on cobalt and MSHG on the clean Fe(110) surface.

5.2.1 Magnetic effects in MSHG

Figure 5.2 shows the $p_{in}p_{out}$ polarized (i.e. both the fundamental and the second-harmonic beam are polarized in the plane of incidence) SH-signal from sample B as a function of the external magnetic field ($\mathbf{H}$).[3] The angle of incidence was 45°, and the pulse intensity of the fundamental beam was about 5 mJcm^{-2}. The magnetization lays in the plane of the film and is perpendicular to the plane of incidence.

We observe a rather square hysteresis with a coercive field of about 20 Oe, which is a reasonable value for these type of films. We verified that the effect is not caused by sample movements. The remanent ($\mathbf{H}$=0) SH-intensity remained constant even after long periods of laser irradiation, showing that the SHG experiments are non-destructive. The inset of figure 5.2 shows the hysteresis for external fields up to 600 Oe. Notice that the vertical axis indicates the SH-intensity, so changing the direction of the magnetization has a large influence on the *total* SH-signal.

We define the relative magnetic effect in MSHG as:

$$\rho(q_{in}q_{out}) \equiv \frac{I(2\omega, q_{in}q_{out}, \mathbf{M}^+) - I(2\omega, q_{in}q_{out}, \mathbf{M}^-)}{I(2\omega, q_{in}q_{out}, \mathbf{M}^+) + I(2\omega, q_{in}q_{out}, \mathbf{M}^-)} \tag{5.1}$$

where $I(2\omega, q_{in}q_{out}, \mathbf{M}^+)$ and $I(2\omega, q_{in}q_{out}, \mathbf{M}^-)$ are the $q_{in}q_{out}$ polarized SH-intensities for opposite directions of magnetization. In this particular situation $\mathbf{M}^+$ refers to upward magnetic saturation of the Co film, while $\mathbf{M}^-$ refers to downward magnetic saturation. From the hysteresis we derive:

$$\rho(pp) \approx -20\ \% \tag{5.2}$$

The magnetic effect in MSHG is much larger than in MOKE. Krinchik and Artemev have measured the transverse (linear) Kerr effect of a thick cobalt film [4]. From their results we derive:[4]

$$\left|\ \rho(pp, MOKE)\ \right| < 1\ \% \tag{5.3}$$

for both the fundamental and the second-harmonic frequency. It is interesting to notice that they observed a maximum transverse Kerr rotation at about

[3] Notice that $\mathbf{H}$ has been inverted in comparison with earlier publications [2, 3], in order to achieve a more uniform description of both the experiments on Co/Au and Co/Cu (see chapter 6).

[4] Notice that their transverse (linear) Kerr effect and our transverse $p_{in}p_{out}$ MSHG are measured in the same experimental configuration.

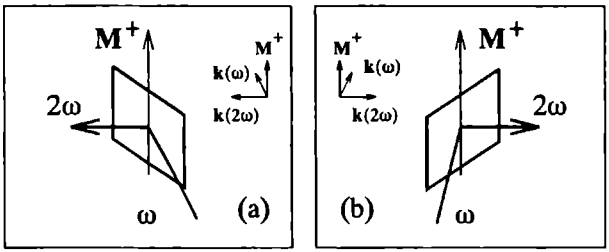

Figure 5.3: *Configurations in transverse MSHG experiments; (a) Right-Handed (RH) transverse configuration, (b) Left-Handed (LH) transverse configuration.*

250 nm (5 eV), which is very close to our second-harmonic wavelength of 266 nm. One might think that the large value of $\rho(pp)$ is caused by a system resonance and that changing the fundamental wavelength leads to smaller values of the relative magnetic effect.
However, our experiments on multilayers of cobalt and copper, as described in chapter 6, were done at fundamental wavelengths of 720-860 nm and we observed even larger values of $\rho(pp)$. In section 5.3 we shall show that the interfaces (between different materials) play a significant role in MSHG from Co/Au multilayers, whereas MOKE probes the bulk properties of the cobalt [5]. Therefore, it is not surprising that there is no simple relation between MOKE and MSHG resonances. Furthermore, Hübner, Pustogowa and Bennemann have calculated the linear Kerr and MSHG (or nonlinear Kerr) spectra for the nickel and iron surface, using quantum mechanics and band theory (see also appendix B). The spectra show no simple correspondence [6, 7], indicating that MOKE and MSHG resonances do not necessarily occur at the same energies.

Reif *et al.* have studied the $p_{in}p_{out}$ MSHG from a clean Fe(110) surface in UHV [1]. If we want to compare the results, we first have to realize that their experiments were done in a different experimental configuration. Figure 5.3(a) shows the configuration that was used while measuring the hysteresis of figure 5.2. We shall call this the Right-Handed (RH) transverse configuration, because at an angle of incidence of 45° ($\mathbf{k}(\omega)$,$\mathbf{k}(2\omega)$,$\mathbf{M}^+$) is a right-handed system:

$$\left(\mathbf{k}(\omega) \times \mathbf{k}(2\omega) \right) \parallel \mathbf{M}^+ \tag{5.4}$$

if $\mathbf{k}(\omega)$ and $\mathbf{k}(2\omega)$ are the wave vectors of the incoming fundamental and outgoing second-harmonic beam respectively.[5] Figure 5.3(b) shows the Left-Handed (LH) transverse configuration, where ($\mathbf{k}(\omega)$,$\mathbf{k}(2\omega)$,$\mathbf{M}^+$) is a left-handed system at an angle of incidence of 45°:

$$\Big(\mathbf{k}(\omega) \times \mathbf{k}(2\omega) \Big) \parallel \mathbf{M}^- \tag{5.5}$$

with identical definitions of $\mathbf{k}(\omega)$ and $\mathbf{k}(2\omega)$. We observed that switching from the RH- to the LH-transverse configuration inverts the values of $\rho(pp)$ and $\rho(sp)$. Comparison of equations 5.4 and 5.5 tells us that the influence of $\mathbf{M}^+$ and $\mathbf{M}^-$ is exchanged in the two configurations, which directly explains the inversion of $\rho(pp)$ and $\rho(sp)$.

The Fe(110) surface gave a relative magnetic effect $\rho(pp) \approx -17$ %, in the LH-transverse configuration at an angle of incidence of 45°, and using the 532 nm output of a Nd:YAG-laser [1], so the effect is approximately equal to our result on the Co/Au multilayer, but has opposite sign.

However, the sign of ρ in the experiments on sample B is a parameter that cannot be predicted from simple arguments, as the total SH-signal of sample B contains contributions from the magnetic Au/Co interface as well as from the nonmagnetic air/Au interface, and possibly also from the deep lying Co/glass interface. Therefore, the total SH-intensity from the entire system must be written as:

$$I_{2\omega,p,out} \propto \Big| \; E_{2\omega,p,out} \; \Big|^2 = \Big| \; \textstyle\sum_j (\hat{\alpha}_{z,j} P^{sh}_{2\omega,z,j} + \hat{\alpha}_{x,j} P^{sh}_{2\omega,x,j}) \; \Big|^2 \tag{5.6}$$

where $E_{2\omega,p,out}$ is the total reflected p-polarized second-harmonic field, and $\hat{\alpha}_{i,j}$ (with $i = x, z$) is a complex constant that is determined by the system parameters 'at' interface j (see equation 3.54), and $P^{sh}_{2\omega,i,j}$ (with $i = x, z$) is the i component of the nonlinear source polarization at interface j. Equation 5.6 shows that the relative magnetic effect is determined by the amplitude and the phase of many unknown tensor elements, as well as by system parameters like layer dimensions and refractive indices.

Large relative magnetic effects in MSHG seem to be quite common, as they have been observed for a variety materials: PtMnSb(111) [8], polycrystalline nickel [9], $Mn_{0.6}Zn_{0.35}Fe_{2.05}O_4$ [10], epitaxially grown Cu on Cu(001) (see chapter 6) and bcc Fe on Cu(001) (see chapter 7).

[5] Even at angles of incidence unequal to 45° we shall still call this the RH-configuration.

polarization combination ($q_{in}q_{out}$)	$I(2\omega, q_{in}q_{out}, \mathbf{M}^+)$ (a.u.)	$I(2\omega, q_{in}q_{out}, \mathbf{M}^-)$ (a.u.)	$\rho(q_{in}q_{out})$ (%)
$p_{in}p_{out}$	72 ± 4	117 ± 9	-24 ± 5
$s_{in}p_{out}$	29 ± 3	9 ± 5	$(-5 \pm 2) \times 10$
$p_{in}s_{out}$	< 2	< 2	$(-1 \pm 7) \times 10$
$s_{in}s_{out}$	< 1	< 1	$(-2 \pm 4) \times 10$

Table 5.1: *SH-intensities and relative magnetic effect for different polarization combinations and opposite directions of magnetization, measured on sample B in the RH-transverse configuration;* $\mathbf{M}^+$ *- upward magnetic saturation,* $\mathbf{M}^-$ *- downward magnetic saturation. The values of* $I(2\omega, q_{in}q_{out}, \mathbf{M}^+)$ *and* $I(2\omega, q_{in}q_{out}, \mathbf{M}^-)$ *are the average (corrected) number of counts in a 500 s time window.*

5.2.2 Polarization dependence in transverse MSHG

A first indication that the phenomenological theory of chapter 2 gives a proper description of these systems follows from measurements of the SH-intensities at different polarization combinations. Table 5.1 shows the results of such experiments on sample B, again using the RH-transverse configuration and an angle of incidence of 45°. We observe clear magnetization induced effects for the $p_{in}p_{out}$ and $s_{in}p_{out}$ polarization combinations. The SH-signals for $p_{in}s_{out}$ and $s_{in}s_{out}$ are two orders of magnitude less than for $p_{in}p_{out}$. The relative magnetic effects $\rho(ps)$ and $\rho(ss)$ are zero within the (large) experimental error.

The observation that the system generates no s-polarized second-harmonic light indicates that an analyser (GT2 in figure 4.1) is not necessary, as was experimentally verified after obtaining equal values of $\rho(pp)$ and $\rho(sp)$ in measurements with and without analyser. Due to its poor transmission of only 40 % at 266 nm, omitting the analyser significantly improves the signal to noise ratio.

The results can be explained qualitatively, while accounting only for the SH-

contributions of the interfaces. This must not be seen as a proof of interface sensitivity of MSHG, as we could equally well explain the observations from bulk contributions. However, we shall show with other experiments (see section 5.3) that the interfaces play a significant role in MSHG from magnetic multilayers. Therefore, it is useful to verify that the results are consistent with the phenomenological theory for magnetized interfaces.

For simplicity we shall at first only account for SHG by the magnetic Au/Co interface. In chapter 3 we related the reflected SH-fields to the nonlinear source polarization at an interface of a multilayer. As we are merely interested in a qualitative analysis of the results it is convenient to rewrite equations 3.54 and 3.57 in a simplified form:

$$E_{2\omega,p,out} = \hat{\alpha}_z P^{sh}_{2\omega,z} + \hat{\alpha}_x P^{sh}_{2\omega,x} \tag{5.7}$$

and

$$E_{2\omega,s,out} = \hat{\alpha}_y P^{sh}_{2\omega,y} \tag{5.8}$$

where $E_{2\omega,p,out}$ and $E_{2\omega,s,out}$ are the reflected p- and s-polarized second-harmonic fields respectively, $\hat{\alpha}_i$ (with $i = x, y, z$) is a complex constant that is determined by the system parameters (see equations 3.54 and 3.57), and:

$$P^{sh}_{2\omega,k} = \chi^{(D)}_{klm}(2\omega)(\mathbf{M})\mathcal{E}_{\omega,l}\mathcal{E}_{\omega,m} \quad \text{with} \quad k,l,m = x,y,z \tag{5.9}$$

where $\chi^{(D)}_{klm}(2\omega)(\mathbf{M})$ represents the magnetization dependent nonlinear susceptibility tensor elements of the Au/Co interface. $\mathcal{E}_\omega$ is the total fundamental field in the nonlinear sheet at this interface and autosummation is implied. The **x**, **y** and **z** axes are as defined at the beginning of chapter 2 (see figure 2.1). The interface is parallel to the **x**,**y**-plane. The **x**-axis is lying in the plane of incidence, and the **z**-axis is normal to the interface. $\mathbf{M}^+$ is parallel to the positive **y**-axis. So, we can describe the nonlinear properties of the Au/Co interface by the set of tensor elements of table 2.1. As $I(2\omega) \propto |E(2\omega)|^2$, magnetization induced effects in the SH-intensity can only be observed if the expressions for $E_{2\omega,p,out}$ or $E_{2\omega,s,out}$ contain both even and odd tensor elements[6] (see chapter 1).

We may now determine the set of tensor elements that could contribute to the SH-intensity at a certain polarization combination. Table 5.2 shows that there are no tensor elements contributing to $p_{in}s_{out}$ and $s_{in}s_{out}$, which is in agreement with the fact that we measure virtually no SHG for these polarization combinations. For the $p_{in}p_{out}$ and $s_{in}p_{out}$ polarization combinations

[6]Remember 'even' and 'odd' refer to 'even' and 'odd' in the magnetization.

polarization combination	p_{in}	s_{in}
p_{out}	$\chi_{xxz}(M\mathbf{y})$, $\chi_{zxx}(M\mathbf{y})$, $\chi_{zzz}(M\mathbf{y})$, $\chi_{xxx}(M\mathbf{y})$, $\chi_{xzz}(M\mathbf{y})$, $\chi_{zxz}(M\mathbf{y})$	$\chi_{zyy}(M\mathbf{y})$, $\chi_{xyy}(M\mathbf{y})$
s_{out}	none	none

Table 5.2: *Tensor elements that could contribute to corresponding polarization combinations in transverse MSHG experiments. The top rows of elements for the $p_{in}p_{out}$ and $s_{in}p_{out}$ combinations are even in the magnetization, while the second rows are odd ($\chi_{jkl}(M\mathbf{y}) = \chi_{jlk}(M\mathbf{y})$).*

we detect both even an odd tensor elements, explaining the magnetization induced changes of the reflected p-polarized SH-intensity.

Although we have excluded all interface contributions, except those from the magnetic Au/Co interface, it is easy to show that taking into account all interfaces does not alter the conclusions of the foregoing analysis. The complete multilayer contains three interfaces: (1) a nonmagnetic air/Au interface, (2) a magnetic Au/Co interface, and (3) a magnetic Co/glass interface. Including all three interfaces merely increases the number of independent tensor elements (even and odd) that could contribute to the $p_{in}p_{out}$ and $s_{in}p_{out}$ polarization combinations. Furthermore, none of these interfaces generates s-polarized second-harmonic light (see also table 2.2). So, all results are well explained by the phenomenological theory for magnetized interfaces.

5.2.3 Longitudinal versus transverse MSHG

Changing the experimental configuration from transverse (magnetization perpendicular to the plane of incidence, $\mathbf{M} = M\mathbf{y}$) to longitudinal (magnetization in the plane of incidence, $\mathbf{M} = M\mathbf{x}$) does not alter the system, as the unmagnetized sample is isotropic, but it does change the set of tensor elements that

polarization combination	p_{in}	s_{in}
p_{out}	$\chi_{xxz}(M\mathbf{x})$, $\chi_{zxx}(M\mathbf{x})$, $\chi_{zzz}(M\mathbf{x})$	$\chi_{zyy}(M\mathbf{x})$
s_{out}	$\chi_{yxx}(M\mathbf{x})$, $\chi_{yzz}(M\mathbf{x})$	$\chi_{yyy}(M\mathbf{x})$

Table 5.3: *Tensor elements that could contribute to corresponding polarization combinations in longitudinal MSHG experiments* ($\chi_{jkl}(M\mathbf{x}) = \chi_{jlk}(M\mathbf{x})$).

can be detected in the various polarization combinations. In the longitudinal configuration we measured no magnetization induced effects in any of the standard polarization combinations. Table 5.3 shows that the $p_{in}p_{out}$ and $s_{in}p_{out}$ polarization combinations detect exclusively even tensor elements, while the $p_{in}s_{out}$ and $s_{in}s_{out}$ polarization combinations detect exclusively odd tensor elements.[7] This means that we expect no magnetization induced effects in the SH-signal, which is in agreement with our experimental observations.

It is easy to show that magnetization induced effects could be present for the $m_{in}p_{out}$ polarization combination (i.e. the angle between the polarization of the fumdamental beam and the optical plane is 45°, 'm' means 'mixed'). At an angle of incidence of 35° this polarization combination gave low SH-signals and a small, but detectable magnetization induced effect $\rho(mp) = 6 \pm 4$ %.[8]

Because the Au/Co multilayers are isotropic there is no real difference between the systems with $\mathbf{M} = M\mathbf{x}$ and $\mathbf{M} = M\mathbf{y}$. Once we know the tensor elements $\chi^{(D)}_{jkl}(M\mathbf{x})$, replacing x by y and visa versa immediately gives the

[7]Notice that in the longitudinal case ($\mathbf{M} \parallel \mathbf{x}$), odd and even correspond with an odd or even number of times the index y. $\chi_{zyz}(M\mathbf{x})$ is not enlisted in table 5.3, as it is not excited in any of these polarization combinations.

[8]We used the configuration of figure 5.3(b), but with $\mathbf{M}^+ \parallel \mathbf{k}_x(\omega)$, m is the mixed polarization that is obtained after a 45° counter clockwise rotation from s_{in}, while looking along the incoming fundamental beam.

elements of the other configuration $\chi^{(D)}_{jkl}(M\mathbf{y})$. Comparing tables 5.2 and 5.3 tells us that it is much easier to determine the values of the individual tensor elements from experiments in the longitudinal ($\mathbf{M} = M\mathbf{x}$) configuration. $\chi^{(D)}_{yyy}(M\mathbf{x})$ and $\chi^{(D)}_{zyy}(M\mathbf{x})$ are directly determined from the $s_{in}s_{out}$ and $s_{in}p_{out}$ polarization combinations respectively, while the angle of incidence dependence of $p_{in}s_{out}$ gives $\chi^{(D)}_{yxx}(M\mathbf{x})$ and $\chi^{(D)}_{yzz}(M\mathbf{x})$. The angle of incidence dependence of the $p_{in}p_{out}$ polarized SH-intensity gives two relations between the elements $\chi^{(D)}_{xxz}(M\mathbf{x})$, $\chi^{(D)}_{zxx}(M\mathbf{x})$ and $\chi^{(D)}_{zzz}(M\mathbf{x})$. Although explicit determination of the relative phase of the elements is still necessary and the presence of several interfaces, whether magnetic or not, will of course make the analysis more involved, the longitudinal configuration is nevertheless preferable for determining the amplitudes of the tensor elements, which will be of vital importance in future experiments.

5.3 Interface sensitivity in Co/Au multilayers

In the previous section we have seen that MSHG is sensitive to the magnetization of a Co/Au multilayer. We have given a qualitative explanation of the experimental results using the phenomenological theory of chapter 2 and gained some confidence in its validity. Although all observations could be explained from (magnetic) interface contributions, this is by no means a proof of interface sensitivity of MSHG, as the results are equally well explained by the set of nonzero bulk tensor elements of table 2.4.

In order to verify whether or not MSHG is interface sensitive we studied samples containing different numbers of Au/Co interfaces (samples *A*-*D* of figure 5.1). If the technique is interface sensitive this should have a pronounced influence on the observed magnetization induced effects.

It should be stressed that the detailed interface structure, and the choice of the materials are at this stage neither a real issue nor of primary relevance. Interface sensitivity is based on the breaking of the macroscopic inversion symmetry at interfaces. For the Co/Au systems, all metal films have an average inversion symmetry, whether they consist of large single domains or small microcrystallites. In relation to the choice of the materials it may be pointed out that Co/Au multilayers are suitable candidates for an experimental verification of theories about the oscillatory exchange interaction [11].

For the pure gold film of sample *A* magnetization induced effects are not expected. This is indeed observed, as $\rho(pp) = (1 \pm 4)$ %. Figure 5.4 shows the results of $p_{in}p_{out}$ polarized MSHG experiments in the RH-transverse configu-

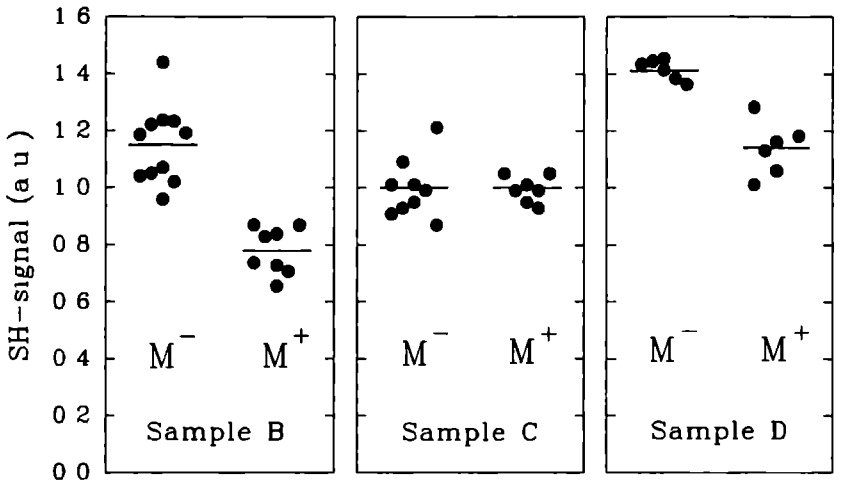

Figure 5.4: *Magnetization induced Second-Harmonic Generation from Co/Au multilayers containing different numbers of magnetic Co/Au interfaces; sample B contains 1 Co/Au interface, sample C contains 2 Co/Au interfaces, and sample D contains 3 Co/Au interfaces.*

ration on samples B,C and D at an angle of incidence of 45° (see also Ref. [12]). The signals were normalized to the SH-intensities from sample C, that shows no magnetization induced changes of the SH-intensity (i.e. no MSHG). Table 5.4 summarizes the results. For sample B we find of course a similar value for $\rho(pp)$ as in the previous section. Sample C has two identical but mirrored interfaces between cobalt and gold (see figure 5.1). We have shown in section 2.3 that the tensor elements of mirrored interfaces have opposite phase.

Therefore, the results on sample C could be explained by the fact that the two Au/Co interfaces cancel each other. Combined with the large SH-signal from the air/Au interface (the $p_{in}p_{out}$ SH-intensity from the pure gold film (sample A) was about thirty times higher than from the samples B,C and D) this would lead to small values of ρ. The idea is supported by the experiments on sample D, that contains three Au/Co interfaces, and where the magnetic effect 'reappears'. However, such an argument is dangerous, as $\rho(pp)$ equals zero for sample C could also mean that the Co film has a poor quality and is not properly magnetized.

A solution to the dilemma might follow from experiments at different angles of incidence. If the Co layer is non-magnetic $\rho(pp)$ will remain zero for

Sample	$I(2\omega, p_{in}p_{out}, \mathbf{M}^+)$ (a.u.)	$I(2\omega, p_{in}p_{out}, \mathbf{M}^-)$ (a.u.)	$\rho(p_{in}p_{out})$ (%)
B	0.78 ± 0.08	1.15 ± 0.14	-19 ± 8
C	1.00 ± 0.05	1.00 ± 0.10	0 ± 6
D	1.14 ± 0.09	1.41 ± 0.04	-11 ± 4

Table 5.4: *$p_{in}p_{out}$ SH-intensities and relative magnetic effects for samples B,C and D. We used the RH-transverse configuration and an angle of incidence of* 45°.

all angles. However, it is very unlikely that the cancellation of the two Au/Co interfaces in system C is 'perfect' at all angles. Furthermore, SHG by the air/Au interface reduces for smaller angles of incidence (and should be equal zero at normal incidence, see table 2.2). Consequently the contributions by the Au/Co interfaces become relatively larger. So, if the Co film is properly magnetized, sample C should show observable MSHG at small angles of incidence.

Figure 5.5 presents the results of experiments on the pure Au film and the magnetic multilayers B,C and D in the LH-transverse configuration at near normal incidence and $p_{in}p_{out}$-like polarization (i.e. the polarization is perpendicular to the magnetization). The pulse energy was kept below 7 mJcm^{-2}, and the beam area was about 0.6 cm^2. For each sample we measured the second-harmonic intensities for upward ($\mathbf{M}^+$) and downward ($\mathbf{M}^-$) magnetic saturation.

Now we do observe a magnetization induced effect in sample C, which proves that the 50 Å Co film is indeed magnetized. As is to be expected, the signal from the Au film is not dependent on the magnetization. The inversion of the $I(2\omega, pp, \mathbf{M}^+)$ and $I(2\omega, pp, \mathbf{M}^-)$ levels between samples B and C and between samples C and D is most striking. In combination with the results of the experiments at 45° incidence this is an extremely strong indication

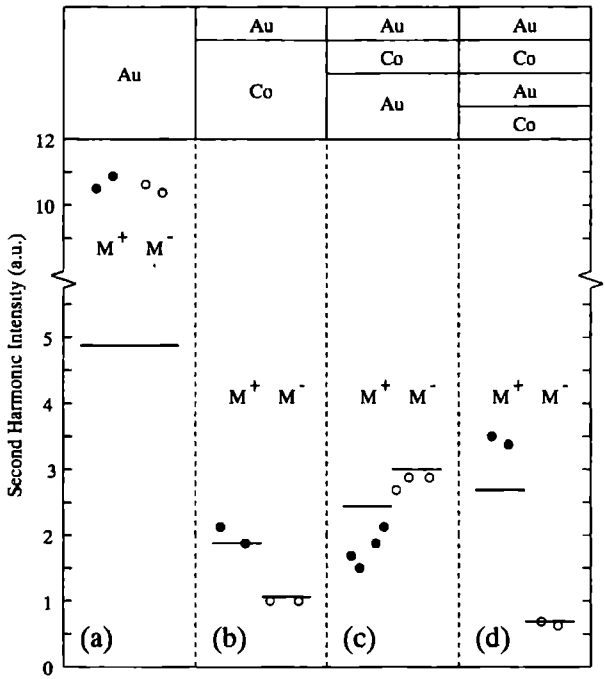

Figure 5.5: *LH-transverse MSHG at near normal incidence and $p_{in}p_{out}$-like polarization. The filled and open circles represent SH-intensities for upward ($\mathbf{M}^+$) and downward ($\mathbf{M}^-$) magnetic saturation respectively; (a) Sample A: no Au/Co interface, (b) Sample B: 1 Au/Co interface, (c) Sample C: 2 Au/Co interfaces, (d) Sample D: 3 Au/Co interfaces. The first 200 Å of each system are indicated at the top of the figure. The solid lines are the result of the model calculations in this section.*

that the interfaces play a significant role.[9] We observe that sample D gives a much larger magnetic effect than samples B and C. Furthermore, we find no correlation between the measured signals and the thicknesses of the cobalt or gold layers. For example, sample D gives a larger magnetic effect than sample B, which contains five times more Co. This leads to the reasonable assumption that the bulk (read $\chi^{(Q)}_{xxzx}(M\mathbf{y})$, see table 2.4) contributes much less than the interfaces. This assumption is strengthened by the MSHG experiments on

[9]We verified in all experiments that sample movements were not causing the effects, by checking the magnetization independence of position and/or intensity of the reflected fundamental beam.

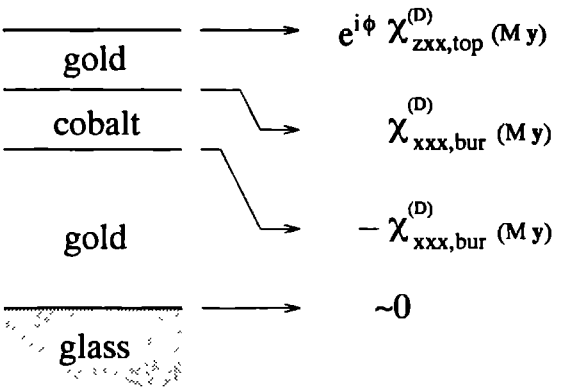

Figure 5.6: *The interface contributions to the $p_{in}p_{out}$ SH-field from sample C in the transverse configuration at near normal incidence.*

Co/Cu, as described in chapter 6, where we varied the thickness of the Co film continuously and observed that the relative magnetic effect remained constant after only a few monolayers.

We shall show that the results of figure 5.5 can be explained by pure interface contributions and the theory of chapter 3, which we consider as indirect proof of the interface sensitivity of MSHG.

All four systems contain only two types of interfaces: air/Au and Au/Co. The contributions from the Co/glass and the Au/glass interfaces are negligible for samples A,B and C, because of the thick metal layer between the air/Au and metal/glass interfaces (1550 Å, 550 Å and 600 Å respectively). Furthermore, we have measured the contributions of the comparable Co/quartz interface by exiting from the quartz side. We have concluded that the contributions from the Co/glass-interface in sample D (where the total metal layer thickness is only 200 Å) are also negligible.

For the air/Au-interface there ought to be no second-harmonic generation for normal incidence and $p_{in}p_{out}$-like polarization (see table 2.2: $\chi^{(D)}_{xxx}$ is zero for an isotropic non-magnetic interface). However, the experiments on the pure Au film show significant SH-signal in this configuration. This can be explained by the experimental limitations, allowing a minimum angle of incidence of 4°. In view of the fact that the SH-signal from sample A, at an angle of incidence of 45°, was about thirty times higher than from the other samples,

the air/Au interface could still give a significant contribution. To first order approximation we excite $\chi^{(D)}_{xxz}$ and $\chi^{(D)}_{zxx}$. Notice that none of these elements depends on the magnetization, as they belong to the non-magnetic air/Au interface. We shall analyse the results as though $\chi^{(D)}_{zxx}$ were the strongest tensor element. However, similar results can be obtained with $\chi^{(D)}_{xxz}$, and in fact with any combination of the two elements.

The analysis of the multilayers is now fairly simple. As an example we shall discuss sample C in detail. The treatment of the other systems is straightforward. Sample C contains a non-magnetic air/Au interface and two buried magnetic Au/Co interfaces (see figure 5.6). In the present configuration we detect the even tensor element $\chi^{(D)}_{zxx}$ at the air/Au interface (to be called $\chi^{(D)}_{zxx,top}$), and the odd element $\chi^{(D)}_{xxx}(M\mathbf{y})$ at the buried Au/Co interfaces (to be called $\chi^{(D)}_{xxx,bur}(M\mathbf{y})$). The tensor elements at the two Au/Co interfaces have exactly opposite phase, but the phase difference ϕ between $\chi^{(D)}_{zxx,top}$ and $\chi^{(D)}_{xxx,bur}(M\mathbf{y})$ is unknown. SHG from the Au/glass interface is negligible. Inverting the magnetization changes the sign of all $\chi^{(D)}_{xxx,bur}(M\mathbf{y})$ in the system. So, the entire system is described by only three independent parameters: $\chi^{(D)}_{zxx,top}$; $\chi^{(D)}_{xxx,bur}(M\mathbf{y})$ and ϕ. In fact these parameters describe all four systems.

The SH-intensities for upward and downward magnetic saturation were calculated with a computer program that contains the theory of chapter 3. We have used the indices of refraction for bulk materials as measured by Johnson and Christy [13] (see table 5.5). Although one might argue whether or not bulk refractive indices accurately describe the optical properties of thin films, the general observation is that such an approach leads to good results [14]. The glass substrates have a refractive index of about 1.5 and a thickness of about 2 mm. We do not consider the influence of reflections from the far side of the glass substrate. In samples A,B and C its influence is negligible because of the strong absorption in the thick metal layers. In sample D it could have a minor influence (the total film thickness is only 200 Å), that is however neglected in the present analysis. In order to prevent unwanted reflections from the farside of the glass substrate in the calculations we introduce a sligthly complex refractive index of the glass $n(\omega) = n(2\omega) = 1.5 + i0.002$. This does not alter the boundary conditions at the metal/glass interfaces, but the absorption in the substrate reduces the reflections from its far side to zero.

As the refractive indices of the interfaces: $\hat{n}^i(\omega)$ and $\hat{n}^i(2\omega)$ may be interpreted as scaling factors of the tensor elements (see section 3.3), we have taken both equal to unity for simplicity. We adjust $\chi^{(D)}_{zxx,top}$; $\chi^{(D)}_{xxx,bur}(M\mathbf{y})$

material	wavelength	refractive index
Au	532 nm	$0.52 + i2.25$
	266 nm	$1.37 + i1.78$
Co	532 nm	$2.01 + i3.73$
	266 nm	$1.44 + i2.03$

Table 5.5: *Refractive indices of gold and cobalt at fundamental and second-harmonic wavelengths, data from Johnson and Christy [7].*

and ϕ for optimal description of the SH-signals of all four systems, i.e. we describe 7 SH-intensities by 3 free parameters. The results of our calculations for samples *A*-*D* are indicated by the solid lines in figure 5.5. The values for the fit parameters are enlisted in table 5.6 .

$\left\| \chi^{(D)}_{xxx,bur}(M\mathbf{y})/\chi^{(D)}_{zxx,top} \right\| = 0.27$	$\phi = 40°$

Table 5.6: *Results of fitting* $\chi^{(D)}_{xxx,bur}(M\mathbf{y})$, $\chi^{(D)}_{zxx,top}$ *and* ϕ *to the experiments on Co/Au multilayers, using multiple reflection theory.*

The correspondence between calculated and measured SH-intensities is rather good for all systems, except the pure gold film, where the difference is a factor of two. The model clearly describes the inversion of $I(2\omega, pp, \mathbf{M}^+)$ and $I(2\omega, pp, \mathbf{M}^-)$ between samples *B* and *C*, and between samples C and *D*. Furthermore, it does explain that sample *D* gives a larger relative magnetic effect than sample *B*. Although surprising and counterintuitive, as *C* involves deeper interfaces, it is purely the result of multiple reflections in these

multilayer systems.

Notice that the value of $\chi^{(D)}_{xxx,bur}(M\mathbf{y})/\chi^{(D)}_{zxx,top}$ is close to the estimated value for the clean cobalt surface (see appendix B):

$$\left| \chi^{(D),odd}/\chi^{(D),even} \right|_{Co} = 0.22 \tag{5.10}$$

However, one cannot directly compare these values, as $\chi^{(D)}_{xxx,bur}(M\mathbf{y})$ and $\chi^{(D)}_{zxx,top}$ belong to the Au/Co and air/Au interfaces respectively. But it is quite satisfying that ratios are of the same order of magnitude.

We found that the calculated values are not critically dependent on the exact layer thicknesses and the chosen set of (bulk) refractive indices. Varying the film thickness by as much as 20 percent, changes the reflected SH-intensities by only 10 percent. Using the set of (bulk) refractive indices of Ref. [15] (Au: $\hat{n}(532\text{ nm}) = 0.35 + i2.13$, $\hat{n}(266\text{ nm}) = 1.28 + i1.66$; Co: $\hat{n}(532\text{ nm}) = 1.99 + i3.54$, $\hat{n}(266\text{ nm}) = 1.25 + i1.93$) leads to an equally good description of the experiments.

The phase difference ϕ between the tensor elements is more critical, as inversion is only observed for values of ϕ between 33° and 55°. So, the value of ϕ is rather crucial for observing inversion.

In an earlier publication we found $\phi = 88°$ after using a preliminary version of the model [3]. That version accounted for the multiple reflections of both fundamental and SH-light, but did not treat the nonlinear boundary conditions at the interfaces. This value of ϕ was to be expected, because the time-inversion properties of $\chi(\mathbf{M})$ predicted a phase difference of $\phi = 90°$. However, as discussed in section 2.2, this argument is only valid if dissipation is negligible. A brief look at the dielectric constants tells us that this is probably not the the case, as the energy of the second-harmonic photons is lying near the interband transition of Au [15]. This implies that the phase difference between odd and even elements is no longer a priori determined, and a deviation from 90° seems likely. However, it is of the utmost importance that the phase differences between the tensor elements are directly measured in future experiments [16-18].

With the value for $\chi^{(D)}_{zxx,top}$ from the fit, we underestimated the second-harmonic signal from the pure Au film by a factor of two. This difference could be caused by bulk contributions from the gold. However, we have combined the fit values for $\chi^{(D)}_{xxx,bur}(M\mathbf{y})/\chi^{(D)}_{zxx,top}$ and ϕ with the value for $\chi^{(D)}_{zxx,top}$ that follows directly from the measurements on the pure gold film ($\chi^{(D)}_{zxx,top}$ becomes a factor $\sqrt{2}$ larger). This overestimates all SH-intensities from the multilayer systems B,C and D by roughly a factor of 2, indicating that the

difference between the experimental and calculated values for sample A might very well be caused by an as yet unknown scaling problem. Furthermore, we have analysed these systems while allowing for an even contribution by the Au/Co interfaces. As the angle of incidence is not exactly zero $\chi^{(D)}_{zxx,bur}$ might contribute. This extra parameter improves the results. Whatever the explanation is, the general argument remains that interface contributions are most significant, as they determine the inversion, and the increase of the relative magnetic effect in sample D.

It is instructive to consider the theoretical thickness dependence of the SH-intensities and the relative magnetic effect. Increasing the thickness of one of the layers pushes part of the multilayer backwards, and due to the strong absorption of light in the metal layer, the influence of the interfaces in this part will gradually disappear. So, from an optical point of view, there is no distinction between samples B and C, if the thickness of the Co layer in C is larger than a few hundred Angstroms.

Figure 5.7(a) shows the result of increasing the thickness of the deepest Co layer in sample D from 10 to 600 Å. We find that the relative magnetic effect decreases rapidly from 80 % to 20 % over the first 200 Å, whereafter it remains constant (solid line in figure 5.7(a)). So, the presence of the Co/glass interface strongly enhances the relative magnetic effect even though the interface itself does not generate any second-harmonic light. This is purely the result of the multiple reflections in the system. For comparison we have also shown the experimental data.

In figure 5.7(b) we increased the thickness of the deepest Au layer in sample D. At small Au thicknesses $\rho(pp)$ has a high value, it becomes zero at approximately 200 Å, whereafter it reaches a negative minimum value of -10 %, i.e. we have inversion. As was expected we have 'converted' sample D into sample C. The points at 550 Å indicate the experimental results on sample C.

Increasing the thickness of the Co layer in sample C should convert the system into sample B. This is indeed the case, as is shown in figure 5.7(c). Notice that the inversion of $\rho(pp)$ is only present up to Co film thicknesses of about 100 Å, and that $\rho(pp)$ goes to zero if the cobalt thickness goes to zero. This is to be expected as the two Au/Co interfaces will cancel exactly at zero Co thickness. At 550 Å we have indicated the experimental results on sample B.

Figure 5.7(d) shows the result of increasing the Au film thickness in sample B. $\rho(pp)$ reaches a maximum value of about 40 % at a Au thickness of approximately 100 Å, whereafter it drops gradually to zero, the 'relative magnetic effect' of a pure gold film (sample A).

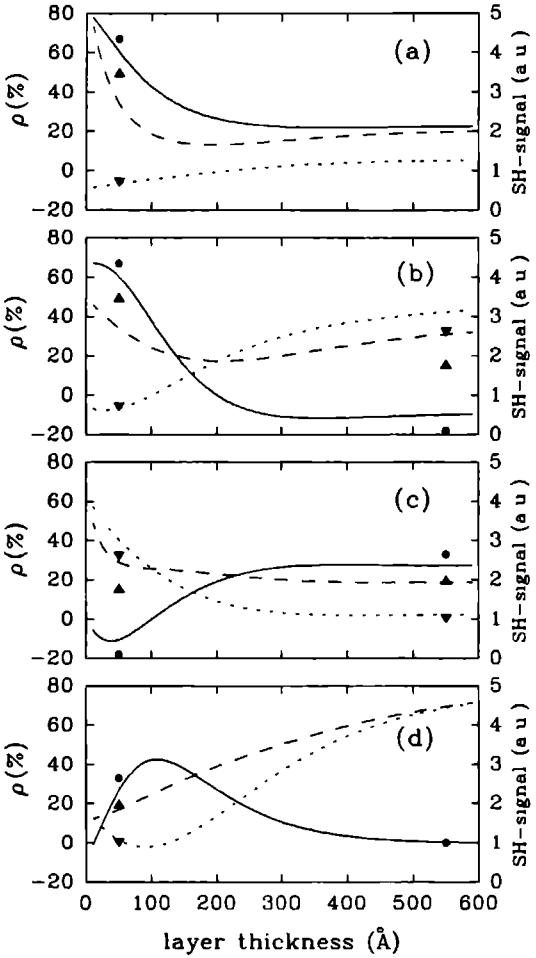

Figure 5.7: *Result of model calculations of thickness dependence of the SH-intensity and relative magnetic effect in various Co/Au multilayers. The wavelength of the fundamental beam is 532 nm. The refractive indices and the relevant tensor elements are enlisted in tables 5.5 and 5.6 respectively: solid lines - $\rho(pp)$, dashed lines - $I(2\omega, pp, \mathbf{M}^+)$, dotted lines - $I(2\omega, pp, \mathbf{M}^-)$; dots - $\rho(pp)$ experimental, upward triangles - $I(2\omega, pp, \mathbf{M}^+)$ experimental, downward triangles - $I(2\omega, pp, \mathbf{M}^-)$ experimental: (a) Thickness scan deepest Co layer in sample D, (b) Thickness scan deepest Au layer in sample D, (c) Thickness scan Co layer in sample C, (d) Thickness scan Au layer in sample B.*

The results clearly indicate that it would be very interesting to study the layer thickness dependence in detail, as it will be an excellent check of both the validity of the multiple reflection model in general, and the analysis of the multilayers in this section. A magnetic two layer system similar to sample *B* seems preferable, as it contains a limited number of tensor elements. Experiments on Fe(001) covered by a chromium wedge are already in progress. Verification of the model is essential, because the tensor elements at the interfaces could then be derived from the total reflected SH-intensities. The final step would than be to relate these macroscopic elements to the microscopic structural, electronical and magnetic properties of the interfaces.

Another important conclusion of the results in figure 5.7 is the fact that the relative magnetic effect in MSHG can be strongly enhanced by adjusting layer thicknesses, i.e. the signal to noise ratio is improved. Enhancement of the magneto-optical performance of multilayers by systematically adjusting the layer thicknesses is a well known concept from linear Kerr studies [19-21]. The conclusion is of course most relevant if MSHG is ever going to be applied in data storage.

5.4 Conclusion

We have observed that the reflected second-harmonic signal from Co/Au multilayers depends strongly on the magnetization. The relative intensity changes in MSHG are more than one order of magnitude higher than in comparable MOKE experiments. We have shown that the phenomenological theory for Magnetization induced Second-Harmonic Generation (MSHG) from interfaces in magnetic multilayers accurately describes the experimental results.

To verify interface sensitivity we studied sytems containing different numbers of Au/Co interfaces. At near normal incidence we observed that both the number of interfaces and the direction of the magnetization have a pronounced influence on the measured second-harmonic signal. The most important result is the inversion of $I(2\omega, pp, \mathbf{M}^+)$ and $I(2\omega, pp, \mathbf{M}^-)$ between the samples containing 1 and 2 Au/Co interfaces and again between the samples with 2 and 3 interfaces. This cannot be explained in terms of bulk induced effects. Furthermore, we observed no correlation between the bulk amounts of Co or Au and the measured signals. However, the results are accurately described in terms of interface contributions and the multiple reflection model of chapter 3. We consider this as indirect proof of interface sensitivity.

We have argued that the longitudinal configuration is preferable to determine the amplitudes of the tensor elements, although this configuration does

in general not lead to magnetization induced effects in the SH-signal (experiments along these lines are already in progress).

It seems extremely useful to study the layer thickness dependence of MSHG from multilayers, as it will check the accuracy of the multiple reflection model of chapter 3. An accurate model is of vital importance, as it deduces the values of the tensor elements from the reflected SH-intensities. Relating these macroscopic tensor elements to the microscopic structural, electronical and magnetic properties of the buried interface leads to the ultimate goal: using MSHG as an external macroscopic probe for the microscopic magnetic properties of buried interfaces.

References

[1] J. Reif, J.C. Zink, C.M. Schneider, and J. Kirschner, Phys. Rev. Lett. **67**, 2878 (1991).

[2] G. Spierings, V. Koutsos, H.A. Wierenga, M.W.J. Prins, D. Abraham, and Th. Rasing, Surf.Sci. **287-288**, 747 (1993).

[3] H.A. Wierenga, M.W.J. Prins, D.L. Abraham, and Th. Rasing, Phys. Rev. B **50**, 1282 (1994).

[4] G.S. Krinchik and V.A. Artemev, Sov. Phys. JETP **26**, 1080 (1968); *Laser Handbook volume I*, edited by F.T. Arecchi and E.O. Schulze-Dubois (North Holland Publishing Company, Amsterdam, 1972), p 1025.

[5] L.M. Falicov *et al.*, J. Mater. Res. **5**, 1299 (1990).

[6] W. Hübner, Phys. Rev. B **42**, 11553 (1990).

[7] U. Pustogowa, W. Hübner, and K.-H. Bennemann, Phys. Rev. B **48**, 8607 (1993).

[8] J. Reif, C. Rau, and E. Matthias, Phys. Rev. Lett. **71**, 1931 (1993).

[9] K. Böhmer, J. Hohlfeld, and E. Matthias, to be published.

[10] Th. Rasing, and H.A. Wierenga, accepted for publication in Ferroelectrics.

[11] M.T. Johnson, S.T. Purcell, N.W.E. McGee, R. Coehoorn, J. aan de Stegge, and W. Hoving, Phys. Rev. Lett. **68**, 2688 (1992).

[12] G. Spierings, V. Koutsos, H.A. Wierenga, M.W.J. Prins, D Abraham, and Th. Rasing, J. Magn. Magn. Mat. **121**, 109 (1993).

[13] P.B. Johnson and R.W.Christy, Phys. Rev. B **9**, 5056 (1974); Phys. Rev. B **6**, 4370 (1972).

[14] J. Inglesfield, *private communication.*

[15] J.H. Weaver *et al.*, *Physics Data: Optical constants of metals, Nr 18-1 and Nr 18-2*, (H. Behrens and G. Ebel, Karlsruhe, 1981).

[16] H.W.K. Tom, *Studies of surfaces using optical second-harmonic generation* (Thesis, University of California, Berkeley, 1984).

[17] E. Schwarzberg, and G. Berkovic, Mol. Liq. Cryst. Sci. Technol. - Sec. B: Nonlinear Optics **4** (1993).

[18] G. Berkovic, and E. Shvartsberg, Appl. Phys. B **53**, 333 (1991).

[19] M. Mansuripur, G.A.N. Connell, J.W. Goodman, J. Appl. Phys. **53**, 4485 (1982).

[20] R. Atkinson, I.W. Salter, and J. Xu, J. Magn. Magn. Mat. **102**, 357 (1991).

[21] R. Atkinson, I.W. Salter, and J. Xu, Appl. Opt **31**, 4847 (1992).

Chapter 6

MSHG on Co/Cu multilayers

Magnetization induced optical Second-Harmonic Generation in combination with the Magneto-Optical Kerr Effect (MOKE) was used to study thin Co films of thicknesses between 1 and 20 monolayers (ML) grown on a Cu(001) substrate. The relative magnetic effect ρ, as determined from MSHG reaches a constant value at 6 ML, in contrast with the MOKE signal that increases linearly with thickness. From their different behavior with Co film thickness we get direct information about the interface sensitivity of MSHG. Similar results are obtained in experiments on Cu/Co/Cu trilayers. Modifying the vacuum/Co interface by gas adsorption yields the relative contributions of the vacuum/Co and the Co/Cu(001)-substrate interfaces. Below 6 ML, ρ shows an oscillatory-like behavior that may be related to quantum well states. When growing up to 15 ML Cu on top of 10 ML Co/Cu(001), these oscillations become very pronounced.[1]

6.1 Introduction

In the previous chapter we discussed MSHG experiments on magnetized multilayers of cobalt and gold, where the individual slabs had a typical thickness of about 50 Å. However, many interesting phenomena, like antiferromagnetic coupling and the giant magneto-resistance, are observed in ultrathin film systems with typical slab thicknesses of only a few monolayers [1-4]. It is well known that the interfaces play a significant role in the precise magnetic properties of such multilayers [1,4-6]. Therefore, an interface sensitive optical probe like MSHG could become a powerful tool in studies of the electronic and magnetic properties of these systems.

[1]Parts of this chapter wil be published in Phys. Rev. Lett, and J. Magn. Magn. Mat.

The main goal of this chapter is to show that MSHG is sensitive to the magnetic interfaces in epitaxially grown ultrathin films. The precise dependence of MSHG on for example the interface roughness and the microscopic electronic and magnetic properties is left to future experiments. We have chosen the Co/Cu(001) system as a first candidate, because it is well known for its epitaxial growth.

We show the interface sensitivity of MSHG directly from experiment, by comparing the cobalt film thickness dependence of the longitudinal Magneto-Optical Kerr Effect (MOKE), and the $p_{in}p_{out}$ and $s_{in}p_{out}$ polarized MSHG. It is well known that MOKE has a characteristic linear dependence on magnetic film thickness for very thin films. In section 6.3 we shall describe the Co film thickness dependence of MOKE on Co/Cu films, and introduce a simple model that accounts for the results. The Co film thickness dependence in MSHG is completely different, and proofs the interface sensitivity of the technique, as shall be discussed in section 6.4. Furthermore, we have observed that the relative magnetic effect in MSHG from these systems, changes dramatically on adsorbing a few Langmuirs of gas. This is a second and independent proof of the interface sensitivity of MSHG.

In section 6.6 we give a preliminary theoretical analysis. It is shown that the multiple reflection theory of chapter 3 leads in principle to a proper description of the results. Finally, we discuss the possible relation between the observed oscillations in the relative magnetic effect and the existence of quantum well states in cobalt and copper. The experiments were done in cooperation with R. Vollmer,[2] A. Kirilyuk[1], W. de Jong,[3] H. Schwabe[1], and J. Kirschner[1].

6.2 Sample preparation and experimental set up

We have studied three sets of samples:

1. Co/Cu(001) with varying cobalt film thickness.
2. 10 ML Cu/Co/Cu(001) with varying cobalt film thickness.
3. Cu/10 ML Co/Cu(001) with varying copper film thickness.

The samples were prepared in the UHV system of the Halle group (see section 4.2.2). It had a base pressure of 5×10^{-11} torr. Cleaning the Cu(001) substrate

[2]Max-Planck-Institut für Mikrostrukturphysik, Halle/Saale, Germany.
[3]Research Institute for Materials, Toernooiveld 1,Nijmegen, The Netherlands.

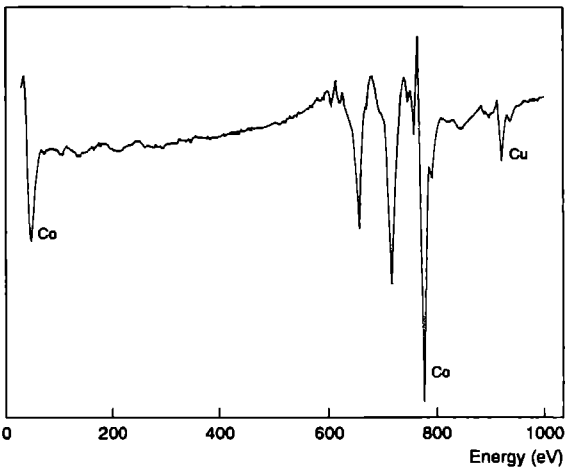

Figure 6.1: *Typical AES spectrum of a Co film on Cu(001). The height of the Cu(920 eV) peak decreases with increasing Co film thickness; this spectrum has been obtained from 10 ML Co/Cu(001).*

consisted of several cycles of Ar^+ sputtering followed by annealing at 400 °C. The Co films were grown at a rate of approximately 1 ML/minute, while the Cu(001) substrate was kept at a temperature of approximately 100 °C. The Cu overlayers were grown at the same rate, while the substrate was kept at about 70 °C. It has been shown that both the growth of Co on Cu(001) and the growth of Cu on Co(001) is pseudomorphic [2, 7, 8]. Epitaxial growth was verified for every film by monitoring the (0,0) Medium Energy Electron Diffraction (MEED) spot intensity while depositing (see section 4.2.2). After preparation the film quality was checked by Auger Electron Spectroscopy (AES); all contaminations were below 1 atomic %, except carbon, which was typically 2-3 atomic % (see figure 6.1).

For the SHG experiments we used the experimental set up of section 4.2. The output of the Ti:Sapphire laser has a wavelength of 800 nm, unless explicitly stated otherwise. The pulse intensity of the incoming beam was about 16 μJcm^{-2}. At an angle of incidence of 35°, we have studied the $p_{in}p_{out}$ polarization combination (i.e. both fundamental and second-harmonic beams are polarized in the plane of incidence) as well as $s_{in}p_{out}$ (i.e. the fundamental beam is polarized perpendicular to the plane of incidence). No analyser was needed, because the s-polarized SH-output was negligible, which is in accordance with the theory and the experimental observations on Co/Au mul-

tilayers (see table 5.2). The magnetization is parallel to the [110] direction of the Co film, the easy axis of the film, and perpendicular to the optical plane. The direction of $\mathbf{M}^+$ is parallel to the direction of the vector product of the wave vector of the incoming light and the surface normal, which corresponds to the RH-transverse configuration of figure 5.3(a).

6.3 Co film thickness dependence in MOKE

Before describing and analysing the results of the MSHG experiments, it is very useful to consider first the results of the linear MOKE experiments on the Co/Cu multilayers. MOKE is a powerful tool to study the magnetic properties of thin film systems. A proper theoretical analysis involves extended theory that accounts for Kerr effects (rotation due to reflection from a magnetic film) and Faraday rotations (rotations due to transmission through a magnetic film) [9-12], which is however far beyond the scope of this thesis. We use MOKE as a simple probe for the film quality. Whereas AES checks the chemical quality of the film, MOKE verifies whether or not the film is properly magnetized.

The MOKE hysteresis were taken in the longitudinal configuration at an angle of incidence of 45°, with the external magnetic field applied along the easy axis of the Co film. We used MOKE set up #2 as described in section 4.3 .

Figure 6.2 shows the amplitude of the MOKE square hysteresis at zero field (M_r) as a function of the Co film thickness for Co on Cu(001). We find that 1 ML of Co is magnetically dead, which is due to the fact that the Curie temperature of the atomic monolayer is far below 0 °C [39, 40].[4] For Co film thicknesses equal to or larger than 3 ML the Curie temperature is far above room temperature [39, 40]. In the latter case we find that M_r is almost perfectly proportional to the Co film thickness. This is a well established observation in linear magneto-optics [2, 9, 10, 13] and known as the thin-film additivity law for the Kerr effect [10]. The law is directly applicable for film thicknesses far below the penetration depth of the HeNe-light, which is of the order of 100 Å in metals. However, 1 monolayer of cobalt has a thickness of 1.8 Å [14], so the contributions from for example the deepest monolayer in the 20 ML Co film will be significantly reduced due to absorption (the HeNe-beam has to pass through $2 \times 36 = 72$ Å of Co).

In a first order approximation we may account for this effect by applying the exponential law of absorption [15, 16].[5] Let us consider an infinitesimal layer of thickness dz at a position z within the cobalt layer, where the **z**-axis is

[4] Remember that the MOKE and MSHG experiments where done at roomtemperature.

[5] Also known as Lambert's, Beer's or Bouguer's law.

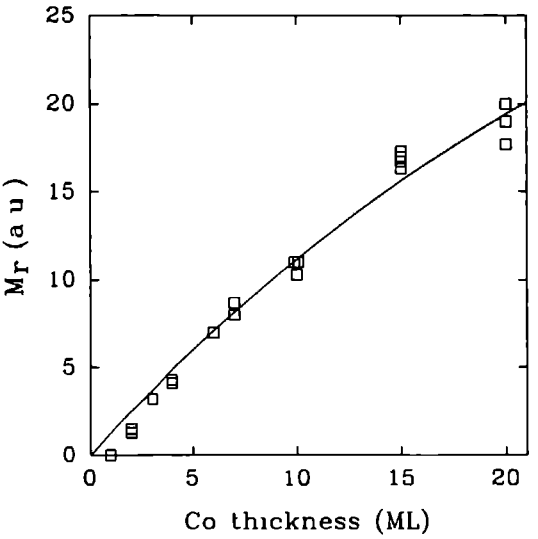

Figure 6.2: *Co film thickness dependence of the amplitude of the MOKE hysteresis (M_r) for the Co/Cu(001) bilayers; squares - MOKE data, solid line - result of simple fit using exponential law of absorption.*

perpendicular to the plane of the film, and the origin is at the vacuum/cobalt interface. Due to the high refractive index of cobalt ($\hat{n}_{Co}(633\text{ nm}) = 2.21 + i4.17$ [17]) it is a good approximation to take the angle of propagation in the Co layer equal to zero. So, the intensity of the light at position z may be expressed as:

$$I(z) = I(0)e^{2i\hat{k}z} \quad \text{with} \quad \hat{k} = 2\pi\hat{n}/\lambda_0 \tag{6.1}$$

Every position in the layer is equivalent, so every sheet dz gives the same partial rotation of the polarization ($\pm m$). The rotated light at position z has to travel back to the vacuum/Co interface before leaving the layer. So, the contribution to the 'Kerr' signal from the infinitesimal sheet dz may roughly be described as:

$$I_{out}(z) = I(0)e^{2i\hat{k}z} \cdot mdz \cdot e^{2i\hat{k}z} \tag{6.2}$$

The total 'Kerr' induced intensity of a film (or the amplitude of the MOKE hysteresis) is obtained after integrating equation 6.2:

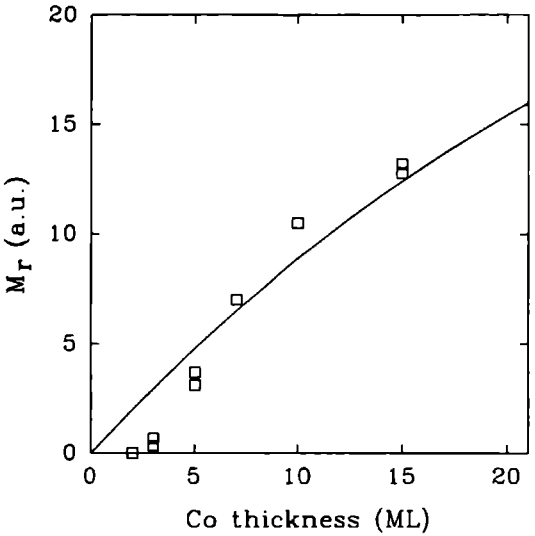

Figure 6.3: *Co film thickness dependence of the amplitude of the MOKE hysteresis (M_r) for the 10 ML Cu/Co/Cu(001) trilayers; squares - MOKE data, solid line - result of simple fit using exponential law of absorption.*

$$M_r(d) = K(e^{4\pi\imath\hat{k}d} - 1) \tag{6.3}$$

where $M_r(d)$ is the amplitude of the hysteresis for a film of thickness d, and K is a constant, that contains m. The solid line in figure 6.2 shows the result of fitting K in equation 6.3 to the data for Co film thicknesses $\leq$3 ML ($K = 38.7$). We conclude that this simple approach, that contains only one free parameter, describes the results rather well.

The same approach can be used to explain the results of the MOKE experiments on the 10 ML Cu/Co/Cu(001) trilayers. The copper overlayer only reduces the 'Kerr' signal due to absorption. Figure 6.3 shows the Co film thickness dependence of M_r for these systems. Schneider *et al.* have reported the reduction of the Curie temperature of a 2 ML Co film to below room temperature, upon growth of a copper overlayer [39]. This is consistent with our observation that the cobalt in 10 ML Cu/2 ML Co/Cu(001) is magnetically dead. Similar results for other Co film thicknesses have not been reported, however, the low value of M_r at 3 ML Co may be related to a lowered Curie temperature. For Co film thicknesses larger than 3 ML, M_r is again nearly

linear to the thickness. The solid line and the dashed line are the result of fitting equation 6.3 to the data ($K = 31.7$).

Although the result is quite satisfying, the data are somewhat suggestive towards the presence of magnetically dead Co monolayers at the Co/Cu interfaces. However, Cebollada *et al.* have studied ferromagnetically and antiferromagnetically coupled Co layers in Co/Cu/Co/Cu(001) multilayers, that were prepared under exactly the same conditions [2]. Their results show that a 7 ML Cu spacer layer causes antiferromagnetic coupling between the Co films. It has been shown that the thin film additivity law is also valid for systems containing several magnetic layers separated by non-magnetic spacer layers, where the total magneto-optical effect is the sum of the effects of all magnetic layers [10].[6] While the buried Co film had a thickness of 3 ML, they observed that the reduction of the magneto-optical effect was proportional to the thickness of the top Co film, and that it required an equally thick top Co film to obtain zero magneto-optical effect by the total multilayer. As the buried Co film has two Co/Cu interfaces, while the top Co layer has only one, this shows that the presence of dead layers is unlikely.

Furthermore, in the presence of a magnetically dead Co monolayer, the buried Co/Cu interface would be essentially non-magnetic. However, MSHG experiments on Co/Cu(001) indicate that this is probably not the case, as we observe magnetic contributions by the buried Co/Cu interface (see section 6.4).

We have done a few experiments on Co/Cu(001) systems with Co film thicknesses above 20 ML. We shall see that the analysis of the MOKE experiments in the $0 - 100$ ML range requires improving the simple model as summarized in equation 6.3. However, it is useful to keep in mind that absorption is still the major cause of the deviation from perfect linear dependence of M_r on film thickness.

Figure 6.4 shows the result of MOKE experiments on Co films up to 100 ML (it also includes the data of figure 6.2). We observe that M_r saturates after about 40 ML. Although the shallow maximum at 50 ML is negligible within the experimental accuracy, its presence has been reported in experiments on several systems (Fe on Au(001) [9], Fe, Ni and Co on Ag [13]). The M_r versus film thickness curves can be divided into three regions. The linear part, at low film thicknesses, is caused by Faraday rotations of the light on traversing the magnetized film, while the saturation part, at large film thicknesses is caused by the Kerr effect. In the intermediate region both effects play a role [9]. It

[6] Although, recently Atkinson *et al.* have shown that the correct formulation of the first-order magneto-optical effect from such systems requires some special care [11].

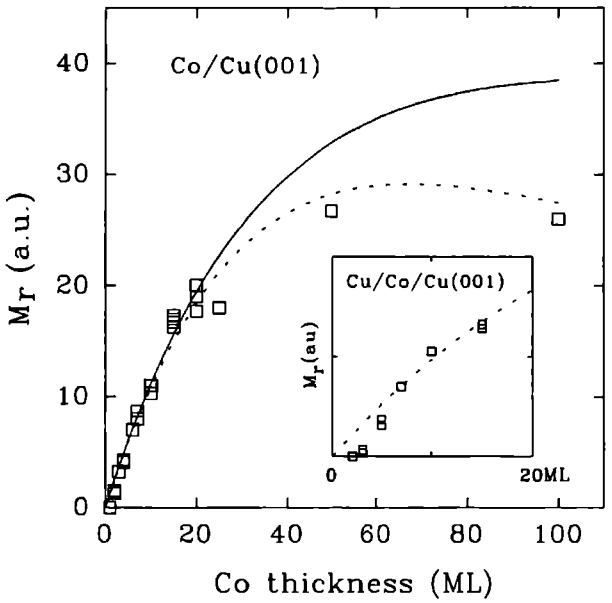

Figure 6.4: *Co film thickness dependence of the amplitude of the MOKE hysteresis (M_r) for the Co/Cu(001) bilayers; squares - MOKE data, solid line - extrapolation of solid line in figure 6.2, dotted line - result of fit with multiple reflection theory. Inset: MOKE on 10 ML Cu/Co/Cu(001) trilayers; squares - MOKE data, dotted line - directly calculated from the Co/Cu(001) fit using multiple reflection theory.*

has been shown that the maximum value of M_r in these systems occurs at a ferromagnetic film thickness, that produces a minimum in the reflectivity of the system [9, 13].

The solid line in figure 6.4 is the result of extrapolating the solid line in figure 6.2, i.e. the fit that resulted from using the exponential law of absorption. This approach overestimates the values of M_r for the thick Co films and cannot account for a maximum. However, we completely neglected the multiple reflections of the light. The observation that the maximum of M_r is related to a minimum in the reflectance suggests that the multiple reflections are important for the magneto-optical properties of such systems, which is indeed verified by complete theories for magnetic multilayers [10,18-20].

We may use the theory of section 3.2 to account for the multiple reflections. Equation 3.33 gives the reflectance of the multilayer, as it relates the forward and backward fields at the front side of the system. For p-polarized light we obtain:

$$R_{pp} = \left| \frac{E^-_{\omega,p,in}}{E^+_{\omega,p,in}} \right|^2 \tag{6.4}$$

We introduce a slightly magnetization dependent (bulk) refractive index for the Co film:

$$\hat{n}_{Co}(\mathbf{M}^{\pm}) = \hat{n}_{Co}(0) \pm Re\left(\hat{\delta} \cdot \hat{n}_{Co}(0)\right) \tag{6.5}$$

where $\hat{n}_{Co}(0)$ is the refractive index of unmagnetized cobalt, and $\hat{\delta}$ is a complex number, with $|\hat{\delta}|^2 \ll 1$. We may now calculate the reflectance for positive and negative magnetization, using $\hat{n}_{Co}(\mathbf{M}^+)$ and $\hat{n}_{Co}(\mathbf{M}^-)$ respectively. The difference between the reflectances of the complete system at $\mathbf{M}^+$ and $\mathbf{M}^-$ is a direct measure of the MOKE amplitude M_r:

$$M_r = K\left(R_{pp}(\mathbf{M}^+) - R_{pp}(\mathbf{M}^-) \right) \tag{6.6}$$

where K is a constant, and $R_{pp}(\mathbf{M}^+)$ and $R_{pp}(\mathbf{M}^-)$ are the reflectances for positive a negative magnetization respectively. This is in fact a simplified version of the analysis by Moog *et al.* [9] and Lissberger *et al.* [18, 21].

The dashed line shows the fit with $\hat{\delta} = 0.01$, $K = 4820$, and the refractive indices: $\hat{n}(633\text{ nm}) = 2.21 + i4.17$ for cobalt and $\hat{n}(633\text{ nm}) = 0.27 + i3.45$ for copper [17]. For thick Co films the agreement with experiment is much better than in the previous analysis, i.e. using equation 6.3. For films up to 20 ML the methods give identical results. So, taking into account the multiple reflections leads to a satisfying description of the MOKE results over the entire range of Co film thicknesses.

At small values the real part of $\hat{\delta}$ has the character of a scaling factor, and does not influence the curvature.[7] So, in fact the entire curve is determined after fitting only one free parameter ($K \cdot Re(\hat{\delta})$).

The inset of figure 6.4 shows once more the data of the MOKE experiments on the 10 ML Cu/Co/Cu(001) samples. The dashed line in the inset has been calculated from equation 6.6, using $\hat{\delta} = 0.01$, $K = 4820$, and the multiple

[7]Giving $\hat{\delta}$ a small imaginary part improves the description of the results on the thick films, and does not affect the results for the thin films.

reflection theory for the trilayer system. We obtain an excellent description of the data without further fitting.

In conclusion, we have found that the films are properly magnetized, as they show standard Kerr rotation dependence on Co film thickness. We have developed a simple, but reliable model, that gives a good description of the experimental results, especially for Co film thicknesses above about 5 ML. The model accounts for multiple reflections in the multilayer, and uses bulk refractive indices for the materials. The conclusion that bulk refractive indices accurately describe the optical properties of films above about 5 ML is quite common [22]. For the Co/Cu(001) system it is also supported by Angle-Resolved Ultraviolet Photoemission Spectroscopy (ARUPS). Experiments by Schneider *et al.* have shown that the electronic structure of 5 ML Co on Cu(001) is already bulk-like [7].

Recently Kuzik *et al.* have shown that the (optical) properties of thin niobium and copper films are oscillatory functions of the film thickness in the 0-40 Å regime [23]. Although we have no indication of such a phenomenon, it stands to reason that the properties (for example the refractive index) of extremely thin films (in this case < 5 ML) differ from the bulk properties. This would explain the difference between theory and experiment at very low film thicknesses.

In the analysis of the MSHG experiments on Co/Cu multilayers in the following section we shall use bulk refractive indices without further comments. We shall see that also for the nonlinear optical case, above film thicknesses of 6 ML, the results can be described by multiple reflection theory, treating thin films as bulk media.

6.4 Interface sensitivity of MSHG

In this section we shall discuss the interface sensitivity of Magnetization induced Second-Harmonic Generation in Co/Cu multilayers. We describe the Co film thickness dependence of MSHG on Co/Cu(001) and 10 ML Cu/Co/Cu(001). The MOKE and MSHG data in the previous and present section, respectively, were taken on the same films. Comparing the results of MOKE and MSHG experiments gives direct proof of interface sensitivity. Furthermore, we study the dependence of MSHG from Co/Cu(001) on gas adsorption, as it is well known that this usually strongly reduces SHG from metal surfaces [24].

As a first and typical result on the Co/Cu(001) systems, figure 6.5 shows the MOKE and MSHG hysteresis measured on a 15 ML Co film at room

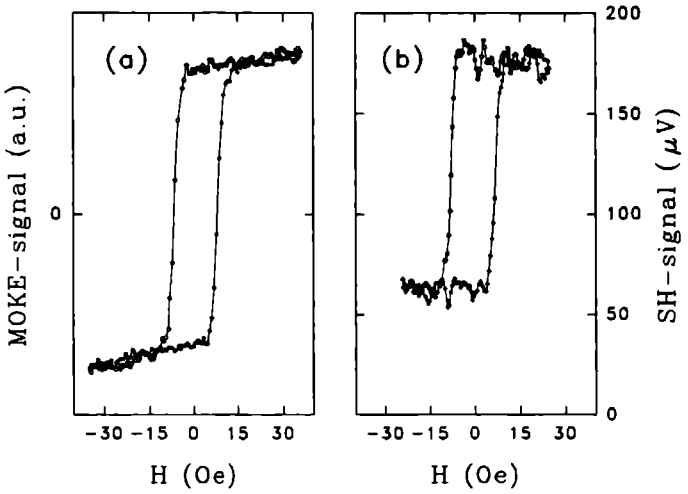

Figure 6.5: *Hysteresis for 15 ML Co on Cu(001): (a) longitudinal MOKE, (b) $p_{in}p_{out}$ MSHG. Both are the result of averaging over 4 cycles taking 1 minute each. Notice that (b) shows the total SH-signal.*

temperature. The SH-signal has been expressed in microVolts, i.e. the voltage that is found after running the output current of the photomultiplier tube through a 1MΩ load resistance. They may be interpreted as arbitrary units, but allow easier comparison of the SH-intensities in different experimental configurations. Both hysteresis are rectangular and have equal coercive fields, within the experimental accuracy. The magnetization induced changes in the SH-intensity are again very high. From the MSHG hysteresis we derive a relative magnetic effect (see equation 5.1, but with the exception that $\mathbf{M}^+$ and $\mathbf{M}^-$ refer now to the remanent magnetization): $\rho(pp, 15\text{ ML}) = 47\ \%$. This value is of the same order of magnitude as in the experiments on the Co/Au multilayers (see chapter 5) and on the Fe(110)-surface using the 532 nm output of a Nd-YAG laser [25], and again much higher than the corresponding value in MOKE (see equation 5.3).

6.4.1 Co film thickness dependence in MSHG

The Co film dependence of MSHG is completely different from MOKE. Figure 6.6 shows the relative magnetic effects in MSHG. We observe that $\rho(pp)$ changes only up to 6 ML, after which it becomes nearly constant and varies only a few percent for Co layers ranging from 6 to 20 ML. We also observe a

rapid increase of $\rho(sp)$ until 4 ML (see figure 6.6(b)), but in contrast to $\rho(pp)$, $\rho(sp)$ drops down to nearly zero at 6 ML, where it changes sign and remains nearly constant for thicker cobalt films. The behavior of $\rho(pp)$ and $\rho(sp)$ is completely different from the linear dependence on film thickness observed in MOKE.

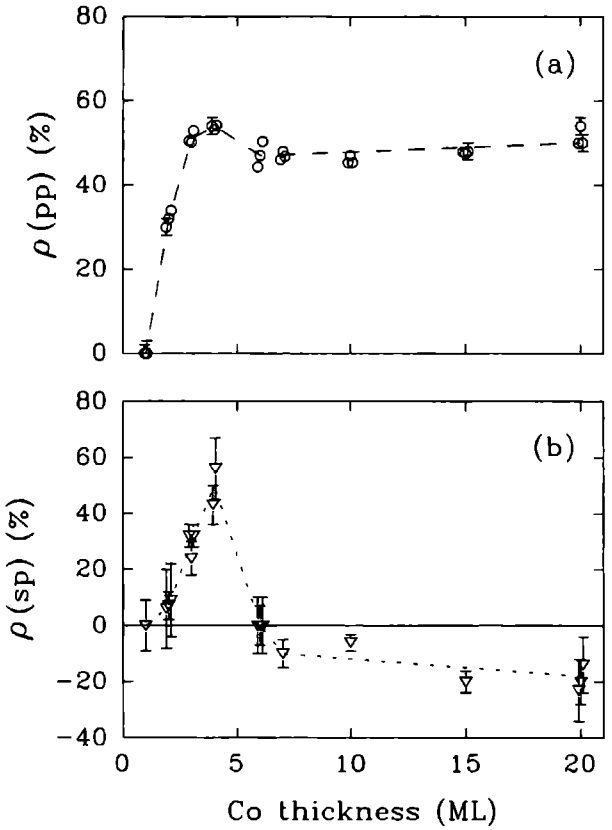

Figure 6.6: *Co film thickness dependence of the relative magnetic effects in MSHG from Co/Cu(001); (a) circles - $\rho(pp)$; (b) triangles - $\rho(sp)$. The dashed lines are guides to the eye.*

These results proof that the SH-signal is generated by the interfaces, because:

1. $\rho(pp)$ and $\rho(sp)$ are nearly constant for Co films above 6 ML. As the film thickness is small on the scale of the wavelength this is exactly

what one would expect if the SH-fields are generated by the interfaces. The result is entirely different from MOKE, where the magnetic effect was proportional to the film thickness (see section 6.3).

2. $\rho(pp)$ and $\rho(sp)$ depend strongly on Co film thickness in the 1-6 ML regime. It is generally believed that an interface has a typical thickness of 2-3 ML. In other words the interface states have a width of 2-3 ML. Therefore, one would expect overlap of the wave functions of the vacuum/Co and Co/Cu(001) interfaces until Co film thicknesses of roughly 4-6 ML. In this regime the interfaces cannot be considered independent and must be treated as one complete system. For thicker films, the interfaces become independent as their wave functions no longer overlap. In section 6.7 we shall discuss that the observation might be related to quantum well states in the Co film.

The previous arguments are supported by the Co film thickness dependence of the absolute SH-signals. Figure 6.7 shows the $p_{in}p_{out}$ and $s_{in}p_{out}$ SH-intensities for both $\mathbf{M}^+$ and $\mathbf{M}^-$ as a function of Co film thickness. The circles and squares correspond to two different sample positions.

The $p_{in}p_{out}$ SH-intensity variations with sample position are quite large (at least of the order of 20 %, see figure 6.7(a)), which is due to surface inhomogeneities of the substrate, and the fact that we excited with a focused beam.[8] However, within the experimental limitations we observe that the $p_{in}p_{out}$ SH-intensity depends strongly on Co film thickness over the first three monolayers. For Co film thicknesses of 3-20 ML we observe, that while the ferromagnetic film thickness increases by nearly a factor of seven, the SH-intensity remains constant within roughly a factor of two.
For clarity, only one set of data has been shown for the $s_{in}p_{out}$ polarization combination (see figure 6.7(b)). The SH-intensity variations with sample position for this polarization combination are at least of the order of 30 %. In contrast to $p_{in}p_{out}$, the $s_{in}p_{out}$ SH-intensity does not change very much in the 0-3 ML range, but for Co film thicknesses of 3-20 ML we observe again that the SH-intensity remains constant within roughly a factor of two.

We have verified that the SH-intensity generated by clean Cu(001) does not depend on the magnetic field. Comparison of the $p_{in}p_{out}$ SH-intensity from the Cu(001) substrate and $I(2\omega, pp, \mathbf{M}^-)$, the lowest signal from Co/Cu(001), shows that the latter is about one order of magnitude higher for all Co film thicknesses. Thus we may directly conclude that the bulk of the copper crystal

[8] The value of ρ is less sensitive to inhomogeneities, as it represents a relative effect.

does not contribute significantly to the $p_{in}p_{out}$ SH-intensity. For the $s_{in}p_{out}$ polarization combination the difference between the SH-intensities of the clean Cu(001) substrate and the Co/Cu(001) films is small. Therefore, contributions by the bulk of the Cu crystal cannot a priori be excluded in the discussion of this polarization combination. However, the results in figure 6.6(b) strongly suggest that bulk contributions are relatively unimportant.

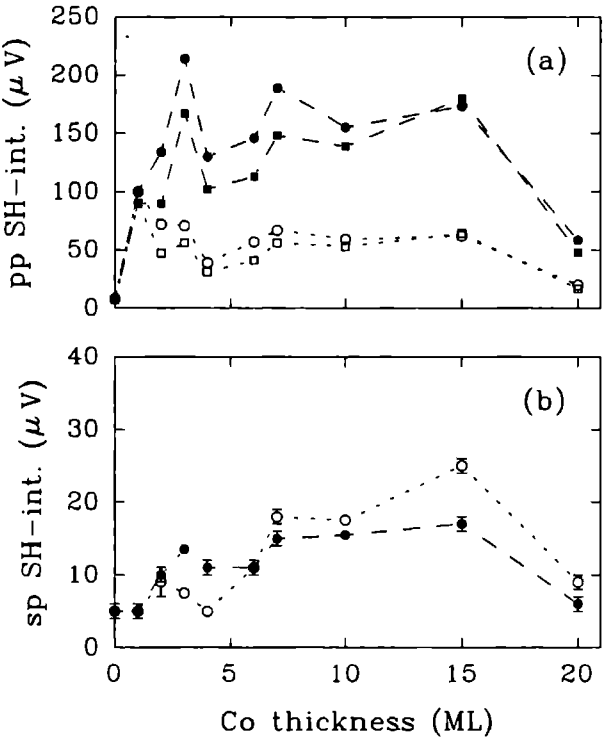

Figure 6.7: *The Co film thickness dependence of the SH-intensities from Co/Cu(001); (a) $p_{in}p_{out}$ SH-intensity; (b) $s_{in}p_{out}$ SH-intensity; filled circles - $I(2\omega, qq, \mathbf{M}^+)$ at position #1, filled squares - $I(2\omega, qq, \mathbf{M}^+)$ at position #2, open circles - $I(2\omega, qq, \mathbf{M}^-)$ at position #1, open squares - $I(2\omega, qq, \mathbf{M}^-)$ at position #2. The dashed lines are guides to the eye.*

One might argue that even if the second-harmonic light would be generated entirely by the bulk, ρ could be constant, simply as a consequence of its definition. Because, if both $I(2\omega, qq, \mathbf{M}^+)$ and $I(2\omega, qq, \mathbf{M}^-)$ scale equally with

Co film thickness, ρ would be independent of film thickness (see equation 5.1) even though the SH-signal is generated by the bulk. However, the observation that the absolute SH-intensities are by no means proportional to the Co film thickness indicates that this is certainly not the case (see figure 6.7). Furthermore, the next section gives direct experimental proof that the vacuum/Co interface plays a significant role in MSHG.

6.4.2 Dependence on gas adsorption

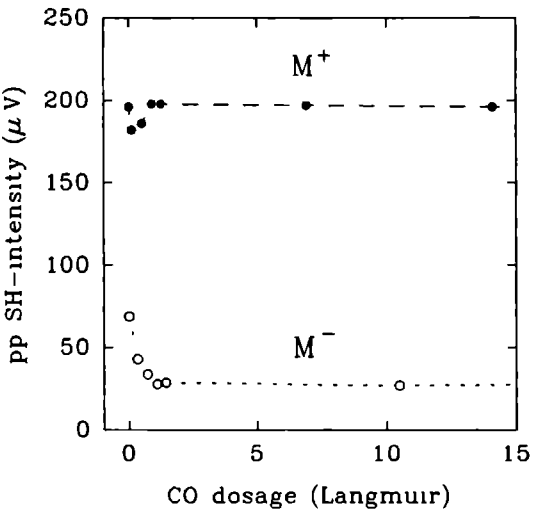

Figure 6.8: *The $p_{in}p_{out}$ SH-intensities of a 7 ML Co-film on Cu(001) for positive and negative magnetic saturation as a function of CO-dosage. The signals at 15L CO remain constant until at least 40L.*

The SH-signal from the Co/Cu(001) is, in principle, the superposition of the contributions from two interfaces, the vacuum/Co and the Co/Cu(001) interface. To gain some insight in the relative strength of the SH-signal from these two interfaces we measured the SH-signal from a Co film on Cu(001) as a function of carbonmonoxyde exposure. Figure 6.8 shows the $p_{in}p_{out}$ SH-intensities of a 7 ML Co film on Cu(001) for positive and negative magnetization as a function of CO dosage. We observe that the signals change until a dosage of 1 Langmuir (1L=10^{-6} torr.sec), hereafter they become constant until at least 40L. The original value of $\rho(pp) = 48$ % has increased to $\rho(pp) = 75$ %. Comparable effects have been observed on adsorbing oxygen, on sputtering, and for different Co film thicknesses (see table 6.1):

- Exposing a 10 ML Co film to 1 Langmuir of carbonmonoxyde changes the value of $\rho(pp)$ to 75 %.
- We observed that $\rho(pp)$ of a 15 ML Co film increased to 70 % after sputtering at 500 eV. Sputtering reduced the initial MEED-intensity by a factor of two, indicating surface roughening. However, during sputtering the surface became contaminated by roughly 6 atomic % carbon.[9] So, the surface modification is not exclusively structural.
- Exposing a 20 ML Co film to a few Langmuirs of oxygen increased the value of $\rho(pp)$ to 66 %. For unknown reasons, the initial value of $\rho(pp)$ = 37 % was too low for this specific 20 ML Co film. However, the increase of the relative magnetic effect on oxidation is clear.

Co film thickness	$\rho(pp)$ before (%)	Surface treatment	$\rho(pp)$ after (%)
7 ML	47.9 ± 0.7	1 Langmuir CO	74.3 ± 0.8
		2-40 Langmuir CO	75 ± 2
10 ML	52 ± 3	1 Langmuir CO	75 ± 8
		10 Langmuir CO	79 ± 8
15 ML	47 ± 1	Sputter at 500 eV	70 ± 2
20 ML	37 ± 3	few Langmuirs of O_2	66 ± 3

Table 6.1: *Dependence of the relative magnetic effect in $p_{in}p_{out}$ MSHG on modifying the vacuum/Co surface in Co/Cu(001).*

The sensitivity to gas adsorption is a second independent proof of the interface sensitivity of MSHG.

[9]The AES spectrum showed no oxygen within the experimental resolution of about 1 atomic %. Therefore, the sample surface is not contaminated by carbonmonoxyde.

It is well known that gas adsorption usually strongly reduces SHG from metal surfaces [24]. The fact that all surface treatments of the various Co/Cu(001) systems invoked a similar result, strongly suggests that certain contributions by the vacuum/Co interface are reduced to (nearly) zero.

We have observed in other experiments that a dosage of a few Langmuirs of O_2 to magnetized Ni(110) and Fe(110) crystals reduces the total $p_{in}p_{out}$ SH-signal, generated from a 532 nm Nd-YAG beam, by up to a factor of 20 depending on initial cleanliness (see also chapter 7). Therefore, we come to the reasonable conclusion that gas adsorption eliminates all SH-contributions by the vacuum/Co interface, and not only the elements that are odd in the magnetization, as was suggested by Reif *et al.* [25].

The value of $\rho(pp)$ after adsorption gives the magnetization induced effect of the buried Co/Cu interface exclusively. All surface treatments of table 6.1 changed the absolute SH-intensities by less than a factor of three, indicating that both the vacuum/Co and the Co/Cu(001) interface contribute significantly to the total SH-intensity.

6.4.3 Thick Co films

We have studied a few Co films with thicknesses above 20 ML. In section 6.3 we have shown that these films are properly magnetized. Figure 6.9 shows the results for $p_{in}p_{out}$ and $s_{in}p_{out}$ MSHG in the 6-100 ML range. The strong changes of both $\rho(pp)$ and $\rho(sp)$ in the 20-100 ML range are not expected after the film thickness independence in the 6-20 ML range.

The effect is most probably not caused by structural changes of the film. LEED verified that the 100 ML Co film still has the fcc structure, so the phase transition to hcp (the natural crystal lattice of cobalt) has not yet taken place. Furthermore, we observed MEED oscillations while growing a few extra Co layers on the 100 ML cobalt film, indicating that the vacuum/Co interface is still smooth on the atomic scale.

However, the AES spectrum of the 100 ML film showed 5 atomic % of oxygen and 5 atomic % of carbon. This is more than the amounts that were observed after the adsorption experiments in the previous section. We therefore conclude that the Co/vacuum interface of the 100 ML film does not generate any second-harmonic light. The contamination is probably a consequence of the long period of increased pressure during growth.

MSHG by the buried Co/Cu interface exclusively, implies a value of $\rho(pp)$ of about 75 % and low SH-intensities, due to absorption in the 100 ML film. This is in good agreement with the experimental results: $I(2\omega, pp, \mathbf{M}^+) \approx 9\ \mu$V, $I(2\omega, pp, \mathbf{M}^-) \approx 1\ \mu$V, and $\rho(pp, 100\text{ ML}) \approx 80$ %. The positive value

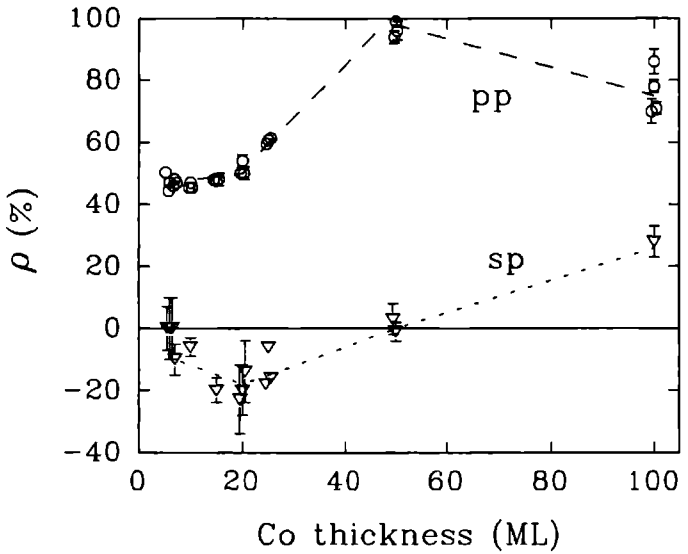

Figure 6.9: *Co film thickness dependence of the relative magnetic effects in MSHG from Co/Cu(001); circles - $\rho(pp)$, triangles - $\rho(sp)$. The dashed lines are guides to the eye.*

of $\rho(sp)$ at 100 ML agrees well with the one value we have for a contaminated Co surface. It stems from the sputter experiment on the 15 ML Co film in section 6.4.2.

The AES spectra on the 25 and 50 ML Co film show a growing amount of oxygen and carbon at the surface, although not as much as on the 100 ML Co. The values of $\rho(pp)$ and $\rho(sp)$ for the 25 and 50 ML Co film must probably be explained by the fact that we have an ill-defined system, as their vacuum/Co interfaces do still generate some SH-light. It is interesting that we have obtained the maximum possible relative magnetic effect of 100 % (for the 50 ML film).

6.4.4 Cu/Co/Cu(001) trilayers

We have studied MSHG from 10 ML Cu/Co/Cu(001) trilayers. The dependence of $\rho(pp)$ and $\rho(sp)$ on Co film thickness are shown in figure 6.10. We observe that $\rho(pp)$ increases until a thickness of 5 ML, hereafter it saturates at a value of 23 %. The Co film thickness dependence is similar to what we observed in the Co/Cu(001) bilayers, which is to be expected if SHG by the

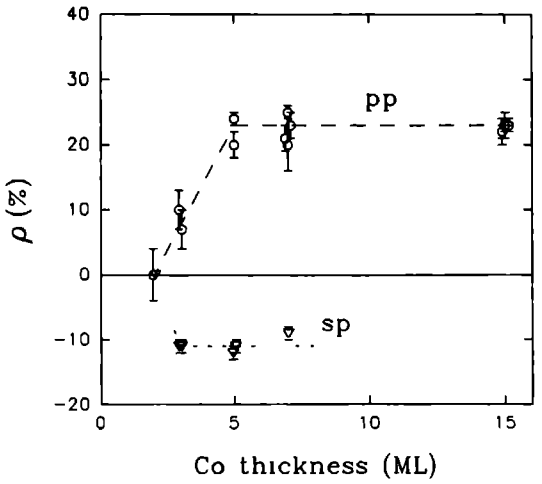

Figure 6.10: *Co film thickness dependence of the relative magnetic effects in MSHG from 10 ML Cu/Co/Cu(001); circles - $\rho(pp)$, triangles - $\rho(sp)$. The dashed lines are guides to the eye.*

interfaces is significant.

These systems contain two Co/Cu interfaces, and one interface between vacuum and copper. They are therefore comparable to the Au/Co/Au multilayer (sample C) in chapter 5, as far as the number of magnetic interfaces is concerned. However, this does not imply that we must also observe an inversion of $\rho(pp)$ between Co/Cu(001) and Cu/Co/Cu(001). As discussed on page 80 the value of ρ cannot be predicted from simple arguments as it is determined by the amplitude and the phase of many unknown tensor elements, as well as by system parameters like layer dimensions and refractive indices.

The value of $\rho(sp)$ becomes already nearly constant after only 3 ML of cobalt: $\rho(sp, \geq 3 \text{ ML}) = -11$ %). The SH-intensities from the trilayers were typically of the order of a few tens of microVolts. We observed again the large variations of the SH-intensity with sample position due to sample inhomogeneities, and that both the $p_{in}p_{out}$ and $s_{in}p_{out}$ SH-signals were constant within roughly a factor of two for Co film thickness above 3 ML.[10]

[10]Comparison of the $p_{in}p_{out}$ and $s_{in}p_{out}$ SH-intensities shows that the latter is about two times higher.

6.5 MSHG spectroscopy of Co/Cu and Cu/Co/Cu

It is to be expected that the wavelength dependence (or spectroscopy) of MSHG will proof to be of vital importance in future experiments [27, 28]. Spectroscopy determines the photon-energies at which resonances in the system occur, and these resonances are directly related to the microscopic electronic structure of the interface. Furthermore, one might expect that adjusting the wavelength could increase the sensitivity to one of the interfaces. Whereas one of the tensor elements at an arbitrary interface A might be at resonance at a specific wavelength, this need not be the case at any other interface.

We have studied a Co/Cu(001) bilayer and a Cu/Co/Cu(001) trilayer in the $\lambda_0(2\omega) = 360 - 430$ nm ($\hbar 2\omega = 2.9 - 3.45$ eV) range. Unfortunately the absolute signals versus wavelength were not reliable, because of the sample inhomogeneity, and the uncontrolled variations of the pulse width of the incoming Ti:Sapphire beam. Since the SH-intensity is inversely proportional to the pulse width [26], this has a drastic influence. However, the relative magnetic effects were easily determined.

In the ideal case of a clear resonance of one of the tensor elements we would expect the relative magnetic effect to go to zero. Remember that the total SH-intensity from a magnetic system can be written as:

$$I(2\omega, \mathbf{M}^{\pm}) \propto |E_{even}(2\omega) \pm E_{odd}(2\omega)|^2 \tag{6.7}$$

where $E_{even}(2\omega)$ and $E_{odd}(2\omega)$ are the total SH-fields generated from the even and odd tensor elements respectively. These fields do not necessarily have the same phase. Resonance implies strong enhancement of one or several tensor elements at a certain energy. In the ideal case of a resonance of an even element exclusively: $E_{even}(2\omega) \gg E_{odd}(2\omega)$, so the difference between $I(2\omega, \mathbf{M}^{+})$ and $I(2\omega, \mathbf{M}^{-})$ becomes small and the relative magnetic effect goes to zero. The same result is obtained if one odd tensor element goes to resonance exclusively. In this case $E_{odd}(2\omega) \gg E_{even}(2\omega)$, but again ρ goes to zero.

Figure 6.11 shows the relative magnetic effect versus the energy of the second-harmonic photons for 10 ML Co/Cu(001). We observe that both $\rho(pp)$ and $\rho(sp)$ vary smoothly, but significantly with energy.

To the best of our knowledge, caculations of the wavelength dependence of MSHG are only available for nickel and iron surfaces [27, 28]. The results show that the odd element $\chi^{(D)}_{xzz}$ has a refined dependence on energy, with amplitude oscillations having a typical width of a few tenths of an electronVolt. Supposing that these results are also valid for cobalt, suggests the possibility of observing a minimum in $|\rho|$ within the energy-window of our spectroscopic

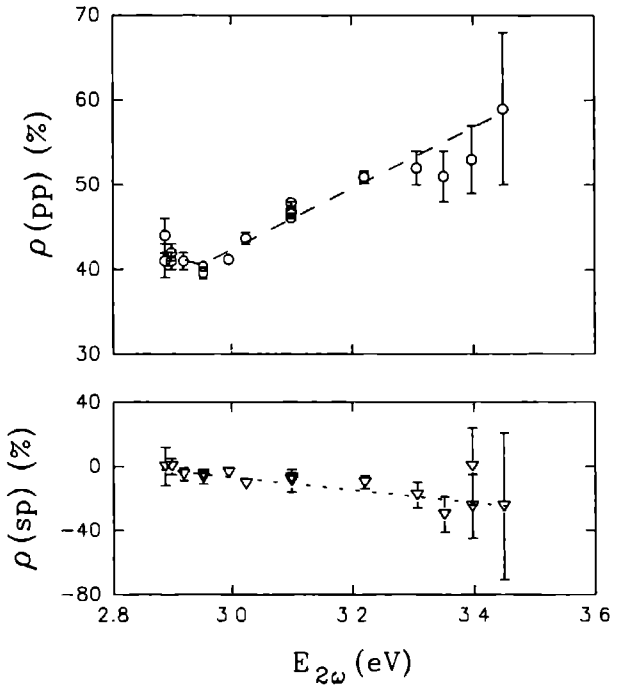

Figure 6.11: *The relative magnetic effect versus energy of the second-harmonic photons in transverse MSHG on 10 ML Co/Cu(001). The dashed lines are guides to the eye. Notice the difference in the vertical scales.*

experiments. The results in figure 6.11 show a shallow minimum of $\rho(pp)$ at $\hbar 2\omega = 2.95$ eV. At the same energy $\rho(sp)$ goes to zero. However, it is not clear that we are dealing with a resonance. Figure 6.12 shows the wavelength dependence of MSHG on 10 ML Cu/10 ML Co/Cu(001). Here we observe that both $\rho(pp)$ and $\rho(sp)$ go to zero at energies of about 3.5 eV.

It is remarkable that the dependence of the relative magnetic effect on wavelength is opposite in both systems, both for $p_{in}p_{out}$ and $s_{in}p_{out}$. We have considered the possibility that the energy dependence of the relative magnetic effect could be entirely determined by the dispersion of the media. Dispersion influences the electric fields at the interfaces, and thereby the total relative magnetic effect of the system, even if the tensor elements themselves remain unaltered. Simple calculations using the results of the theoretical analysis in section 6.6 show that dispersion causes variations of $\rho(pp)$ of only a few percent in 10 ML Co/Cu(001), and of no more than ten percent in the

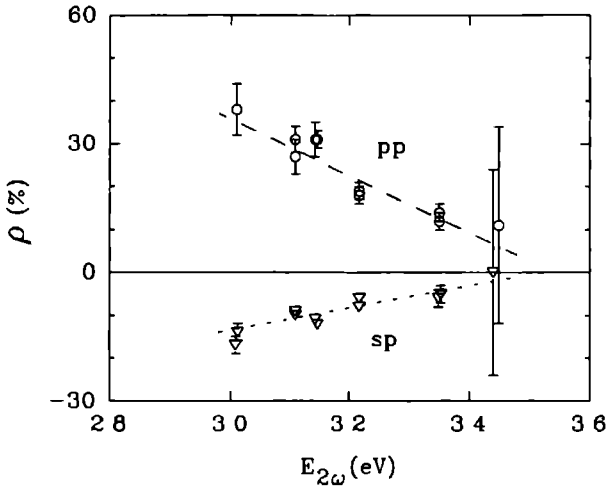

Figure 6.12: *The relative magnetic effect versus energy of the second-harmonic photons in transverse MSHG on 10 ML Cu/10 ML Co/Cu(001). The dashed lines are guides to the eye.*

10 ML Cu/10 ML Co /Cu(001). Therefore, the results cannot be explained by dispersion alone.

How to interpret the results remains as yet an open question, both due to the lack of experimental data, and the lack of theoretical calculations for the photon energy dependence of MSHG from Co/Cu(001). One might argue that the fact that we observe no minimum in $\rho(pp)$ at 3.1 eV (the energy that corresponds to a fundamental wavelength of 800 nm) suggests that this energy is off-resonance, thereby implying a phase difference of 90° between odd and even tensor elements (see section 2.2). However, the argument is rather weak, especially in view of the fact that the energy of the 400 nm photons of the SH-output in the Co/Cu experiments lays in the interband transition of copper. From the analysis of the Co/Au multilayers one might also argue that a value of about 40° would be a better guess (see section 5.3). The problem can only be solved by direct measurements of the phase of the tensor elements.

6.6 Preliminary theoretical analysis

In section 6.4 we have given explicit experimental proof of the interface sensitivity of MSHG. However, the main goal of the technique is to determine

the values of the tensor elements at the interfaces, and relate them to the local electronic and magnetic structure of the interface. As a first step, we have analysed the experimental results with the multiple reflection theory of chapter 3. We have to make some assumptions, because a full analysis is not yet possible, as the system contains (too) many free parameters (or unknown tensor elements). However, we shall see that this preliminary analysis tells us that the theory of chapters 2 and 3 leads in principle to a proper description of the results. Furthermore, the analysis indicates that thickness scans and adsorption experiments are very useful for determining the values of the tensor elements. The most reliable and most complete data are available for $p_{in}p_{out}$, therefore we shall limit ourselves to a discussion of this polarization combination. As in the previous chapter we try to relate the results on the Co/Cu(001) bilayers and the 10 ML Cu/Co/Cu(001) trilayers.

The growth of Co on Cu(001) and the growth of Cu on Co(001) is pseudomorphic [2, 7, 8], therefore the Co/Cu(001) bilayers and the 10 ML Cu/Co/Cu(001) trilayers contain exclusively fcc (001) interfaces. The Co/Cu(001) samples have two magnetic interfaces: **(1)** the interface between vacuum and cobalt, and **(2)** the interface between cobalt and copper substrate. The 10 ML Cu /Co/Cu(001) samples have one non-magnetic and two magnetic interfaces: **(1)** the interface between vacuum and non-magnetic copper overlayer, **(2)** the interface between copper overlayer and cobalt, and **(3)** the interface between cobalt and copper substrate. All magnetic interfaces have a similar set of nonzero tensor elements.

We define the **x**, **y** and **z** axes as in chapter 2 (see figure 2.1). The interface is parallel to the **x**,**y**-plane. The **x**-axis is lying in the plane of incidence, and the **z**-axis is normal to the interface. In transverse MSHG, the magnetization is parallel to the **y**-axis.[11] We can describe the nonlinear optical properties of the (001) magnetic interfaces by the the set of tensor elements of table 2.1 . In $p_{in}p_{out}$ transverse MSHG at an angle of incidence of 35° we detect the even elements:

$$\chi_{xxz}(M\mathbf{y}), \chi_{zxx}(M\mathbf{y}), \chi_{zzz}(M\mathbf{y}),$$

and the odd elements:

$$\chi_{xxx}(M\mathbf{y}), \chi_{xzz}(M\mathbf{y}), \chi_{zxz}(M\mathbf{y})$$

The experiments on the clean Cu(001) substrate gave a $p_{in}p_{out}$ SH-intensity of about 10 μV. Assuming that the second-harmonic light is generated exclusively

[11] At the beginning of this chapter we defined $\mathbf{M}^+$ as parallel to the positive **y**-axis.

by the vacuum/Cu(001) interface implies that contributions by this interface are certainly not negligible in the analysis of the Cu/Co/Cu(001) systems, where the total SH-signals were typically a few tens of microVolts. In the present configuration the vacuum/Cu interface contributions stem from (see table 2.2):

$$\chi_{xxz}, \chi_{zxx}, \chi_{zzz}$$

This implies that the Co /Cu(001) and Cu/Co/Cu(001) systems have, respectively, 6+6=12 and 6+3=9 independent complex tensor elements, that might contribute to the $p_{in}p_{out}$ SH-signal. To solve the complete set requires at least extensive study of the angle of incidence dependence and the phase of the SH-signal. These data are not available at present, therefore we make the following assumptions:

1. The essential nonlinear optical character of the magnetic interfaces is described by one even and one odd tensor element. The non-magnetic vacuum/Cu interface is described by one (even) tensor element. As we do not alter the angle of incidence, this can be interpreted as a representation in effective tensor elements.

2. Carbonmonoxyde adsorption reduces all contributions from the top interface to zero. The issue has been discussed in section 6.4.2 .

3. The even elements at all interfaces have identical phase. The phase difference between the odd and even elements is always 90°. This assumption cannot be defended from our results. It is quite likely that the real value will deviate significantly. However, the general conclusions of the following analysis remain unaltered.

We shall analyse the results in terms of the even element $\chi^{(D)}_{zxx}$ and the odd element $\chi^{(D)}_{xxx}$, i.e. the same combination that was used in the analysis of the Co/Au multilayers. However, we have verified that any combination of one odd and one even elements leads to similar results. The Co/Cu(001) bilayers have four variables:

$$\chi^{(D)}_{xxx,vac/Co} \quad \text{and} \quad \chi^{(D)}_{zxx,vac/Co}$$

$$\chi^{(D)}_{xxx,Co/Cu} \quad \text{and} \quad \chi^{(D)}_{zxx,Co/Cu}$$

We start with the results of figure 6.8 after CO adsorption, where the 7 ML Co/Cu(001) system has only contributions from the buried Co/Cu interface:

material	wavelength	refractive index
Cu	800 nm	$0.26 + i5.10$
	400 nm	$1.32 + i2.13$
Co	800 nm	$2.49 + i4.81$
	400 nm	$1.58 + i2.95$

Table 6.2: *Refractive indices of copper and cobalt at fundamental and second-harmonic wavelengths, data from Johnson and Christy [17].*

$I(2\omega, pp, \mathbf{M}^+) = 198$ μV and $I(2\omega, pp, \mathbf{M}^-) = 28$ μV. Using a computer program that contains the theory of chapter 3, the refractive indices of Johnson and Christy [17] for Co and Cu (see table 6.2), interface refractive indices $\hat{n}^i(\omega) = \hat{n}^i(2\omega) = 1$, and a thickness of 1.8 Å per monolayer of cobalt [14], we find two solutions for $\chi^{(D)}_{xxx,Co/Cu}$ and $\chi^{(D)}_{zxx,Co/Cu}$.[12] For each of these two solutions we may now solve the 7 ML Co/Cu(001) system before CO adsorption, where both the vacuum/Co and the Co/Cu interface are contributing. Since the buried Co/Cu interface is not altered by carbonmonoxyde adsorption, we may calculate $\chi^{(D)}_{xxx,vac/Co}$ and $\chi^{(D)}_{zxx,vac/Co}$, from the SH-intensities: $I(2\omega, pp, \mathbf{M}^+) = 196$ μV and $I(2\omega, pp, \mathbf{M}^-) = 69$ μV. The results are enlisted in table 6.3 .

From the model and the solutions at 7 ML Co we may now calculate the Co film thickness dependence of $\rho(pp)$. The results for solutions *A*-*D* are visualized in figure 6.13 . We observe that there is a clear distinction between the solutions. The present analysis would prefer solution *B*. However, the most important conclusion is that studying the film thickness dependence helps to determine the proper solution.

The ratio $\chi^{(D)}_{xxx,vac/Co}/\chi^{(D)}_{zxx,vac/Co}$ in solution *B* equals 0.67 which is not too

[12] Actually there are two more solutions. However, they differ only by an overall minussign from the first two and have no additional physical meaning.

Solution	Co/Cu interface		vacuum/Co interface	
	$\chi^{(D)}_{xxx}$ (10^{-7}a.u.)	$\chi^{(D)}_{zxx}$ (10^{-7}a.u.)	$\chi^{(D)}_{xxx}$ (10^{-7}a.u.)	$\chi^{(D)}_{zxx}$ (10^{-7}a.u.)
A	6.36 *i*	7.15	5.28*i*	-3.83
B	,,	,,	-8.82*i*	-13.2
C	,,	,,	-2.06*i*	1.30
D	,,	,,	-16.2*i*	-8.41
E	10.2 *i*	4.46	1.93*i*	-1.49
F	,,	,,	-5.25*i*	3.51
G	,,	,,	-19.5*i*	-6.07
H	,,	,,	-12.0*i*	-11.0

Table 6.3: *Solutions of the tensor elements in Co/Cu(001), starting from the assumptions on page 122, and using the multiple reflection theory of chapter 3. The amplitudes have been expressed in* 10^{-7}*a.u. because this order of magnitude leads directly to the input SH-intensities in microVolts.*

far from the theoretical estimate of 0.22 in equation B.38, taking into account the approximations that led to both numbers.[13] For the Co/Cu interface we find a ratio $\chi^{(D)}_{xxx,Co/Cu}/\chi^{(D)}_{zxx,Co/Cu} = 0.89$. Comparing the even and odd elements at the vacuum/Co and Co/Cu interfaces gives:

$$\chi^{(D)}_{xxx,vac/Co}/\chi^{(D)}_{xxx,Co/Cu} = -1.4$$

[13]Notice that the estimates of the ratios are directly comparable, due to the similarity in the number of x and z indices in the tensor elements. The theoretical estimates in appendix B give the ratio of $\chi^{(D)}_{zzz}$ and $\chi^{(D)}_{zzz}$. Besides, we have also analysed the Co/Cu(001) system, with the latter combination. The solution with the proper Co film thickness dependence, i.e. identical to solution *B*, has the same ratio (0.69) of odd and even elements at the vacuum/Co interface.

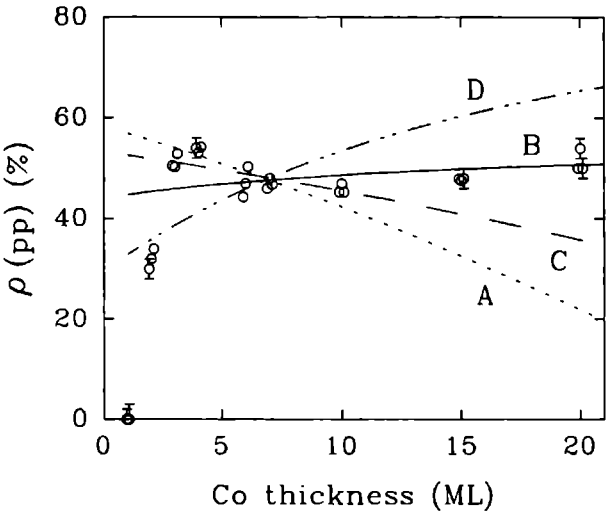

Figure 6.13: *Calculated Co film thickness dependence of $\rho(pp)$ in Co/Cu(001); circles - experimental data, the labels A-D correspond to the solutions in table 6.3 .*

and

$$\chi^{(D)}_{zxx,vac/Co}/\chi^{(D)}_{zxx,Co/Cu} = -1.9$$

This indicates that at the vacuum/Co and Co/Cu interfaces the amplitudes of both even and odd tensor elements are comparable. These ratios are found for any combination of one even and one odd tensor element.

The solutions for the Co/Cu interface ($\chi^{(D)}_{xxx,Co/Cu}$ and $\chi^{(D)}_{zxx,Co/Cu}$) can be used directly in the Cu/Co/Cu(001) trilayers to calculate $\rho(pp)$ of these systems.[14] Scanning the Co film thickness in 10 ML Cu/Co/Cu(001) with $\chi^{(D)}_{xxx,Co/Cu}$ and $\chi^{(D)}_{zxx,Co/Cu}$ from solutions *A-D*, and no SH-contributions from the vacuum/Cu interface gives a relative magnetic effect $\rho(pp) = 66$ %, virtually independent of Co thickness (solution *I* in table 6.4 and figure 6.14). So, the calculated value is higher than in the experiment, but has the proper sign. The absolute SH-signals are two orders of magnitude lower than in the experiment. However, as discussed at the beginning of this section, the vacuum/Cu contribution is not negligible. We have introduced an even contribution by the

[14]One monolayer of copper has a thickness of 1.8 Å [14].

Solution	vac./Cu	Cu/Co #1		Co/Cu #2	
	$\chi^{(D)}_{zxx}$ (10^{-7}a.u.)	$\chi^{(D)}_{zxx}$ (10^{-7}a.u.)	$\chi^{(D)}_{zxx}$ (10^{-7}a.u.)	$\chi^{(D)}_{zxx}$ (10^{-7}a.u.)	$\chi^{(D)}_{zxx}$ (10^{-7}a.u.)
I	0	-6.36i	-7.15	6.36i	7.15
J	-2.85	-6.36i	-7.15	6.36i	7.15

Table 6.4: *Solutions of the tensor elements in Cu/Co/Cu(001), starting from the analysis of the Co/Cu(001) bilayers. In solution I SHG by the vacuum/Cu interface is neglected. Solution J is obtained after fitting* $\chi^{(D)}_{zxx,vac/Cu}$. *The amplitudes have been expressed in* 10^{-7}*a.u. because this order of magnitude led directly to the input SH-intensities in microVolts.*

vacuum/Cu interface, $\chi^{(D)}_{zxx,vac/Cu}$ and fitted it to obtain a relative magnetic effect $\rho(pp, 7 \text{ ML}) = 22$ % (solution J in table 6.4 and figure 6.14). The calculated Co film thickness dependence of the latter solution corresponds rather well with experiment, as the relative magnetic effect is rather constant for film thicknesses above 5 ML, and the absolute SH-intensities are of the right order of magnitude, i.e. a few tens of microVolts. Furthermore, the SH-signal from the pure copper substrate, that can be calculated from $\chi^{(D)}_{zxx,vac/Cu}$ has the a value of 18 μV, which agrees rather well with the experimental value of about 10 μV. So, solution B (see table 6.3) in combination with $\chi^{(D)}_{zxx,vac/Cu} = -2.85 \cdot 10^{-7}$a.u. gives a proper description of thickness dependence in Co/Cu(001) and 10 ML Cu/Co/Cu(001) for Co films above about 5 ML.

The $\chi^{(D)}_{zxx,Co/Cu}$ and $\chi^{(D)}_{zxx,Co/Cu}$ of solutions E-H do not lead to a satisfying description of the trilayer and the copper substrate, because the calculated SH-intensities are too high in both cases. Therefore, solutions E-H will not be discussed in detail.

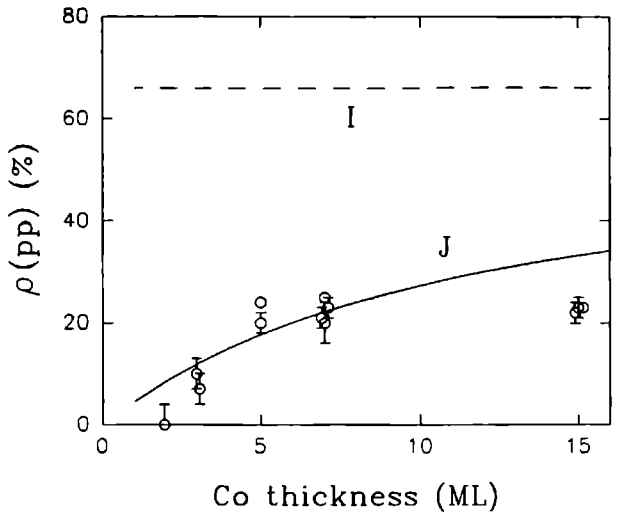

Figure 6.14: *Calculated Co film thickness dependence of $\rho(pp)$ in Cu/Co/Cu(001) trilayers; circles - experimental data, the labels I and J correspond to the solutions in table 6.4 .*

Returning to the Co/Cu(001) bilayers we have noticed that the calculated Co film thickness dependence of the absolute SH-intensities is quite different for solutions B and C. B shows an increasing SH-intensity, with increasing cobalt thickness. For a 20 ML Co film we calculate: $I(2\omega, pp, \mathbf{M}^+) = 318$ μV and $I(2\omega, pp, \mathbf{M}^-) = 104$ μV, i.e. an increase of about 50 % in comparison with the SH-intensities at 7 ML. With solution C we calculate for a 20 ML Co film : $I(2\omega, pp, \mathbf{M}^+) = 106$ μV and $I(2\omega, pp, \mathbf{M}^-) = 50$ μV, i.e. the SH-intensity decreases with increasing Co film thickness. So, from the point of view of the behavior of the calculated SH-signals one might prefer solution C (see figure 6.7).[15] However, we must realize that the absolute SH-intensities were not accurately measured. Furthermore, the intensities for the 7 ML Co film, that were used as a starting point in the calculation, are higher than the average SH-intensity in the 4-20 ML range (see figure 6.7). This leads to high SH-intensities in the calculations for all layer thicknesses. Therefore, at this stage the absolute SH-intensities do not help discriminating the proper solution.

An interesting point follows from an analysis of the detailed shape of the

[15]Solution D gives an increasing SH-intensity with increasing Co film thickness, i.e. similar to solution B.

carbonmonoxyde adsorption experiment in section 6.4.2 . In a first order approximation we suppose that the reduction of the amplitude of the tensor elements $\chi^{(D)}_{xxx,vac/Co}$ and $\chi^{(D)}_{zxx,vac/Co}$ is proportional to the CO dosage. Calculating the values of $\chi^{(D)}_{xxx,vac/Co}$ and $\chi^{(D)}_{zxx,vac/Co}$ from the SH-intensities at a CO dosage of 0.5L (where $I(2\omega, pp, \mathbf{M}^+)$ has a minimum, see figure 6.8) gives the rate at which the initial values of $\chi^{(D)}_{xxx,vac/Co}$ and $\chi^{(D)}_{zxx,vac/Co}$ (for the clean vacuum/Co interface) reduce with increasing carbonmonoxyde contamination. Without going into detail we have found that solution C can give the behavior that is observed in figure 6.8, i.e. a gradually decreasing $I(2\omega, pp, \mathbf{M}^-)$ and a minimum in $I(2\omega, pp, \mathbf{M}^+)$, whereas solution B cannot. Due to a phase shift of roughly 180° between the electric fields with and without CO contamination, in solution B, $I(2\omega, pp, \mathbf{M}^+)$ and $I(2\omega, pp, \mathbf{M}^-)$ always go through zero. The absence of a zero in $I(2\omega, pp, \mathbf{M}^+)$ in the CO adsorption experiment is quite clear. So, from the point of view of the adsorption experiments, solution C would be preferable to B, although one must realize that the above considerations are partly the result of the assumptions on page 122. The most important conclusion is therefore, that the detailed shape of the adsorption dependence of the SH-intensities seems helpful for determining the proper solution of the tensor elements.

6.7 Possible relation to quantum well states

The results of the MSHG experiments in the range of 1-6 ML can of course not be explained by simple multiple reflection arguments. We observe drastic changes for $s_{in}p_{out}$, and for $p_{in}p_{out}$ we measure an oscillatory-like structure (see figure 6.6). Although these effects might be caused by strain induced changes of $\chi^{(D)}$, one could speculate on a different origin, namely the appearance of electronic oscillations in the thin Co film. The connection between oscillations in the exchange coupling and oscillations of the Kerr rotation was first demonstrated by Bennett *et al.* [29].

The Cu/Co(001) system is well known for the appearance of quantum well states [6,30-33]. These oscillations are understood within a modified RKKY model, that takes the topology of the Fermi surface of the spacer into account [34-36].

Very recently, it has been shown that quantum well states in the non-magnetic spacer may act as the mediator for the coupling between magnetic films [6, 30, 31, 37]. The observed period of these states: 5.9 ± 0.5 ML in Cu/Co(001) [30] agrees very well with the long period exchange coupling of

about 6 ML in Co/Cu/Co/Cu(001) sandwiches [2, 30, 31, 38]. Johnson *et al.* have reported the observation of a superposition of two oscillatory terms in Co/Cu/Co(001), having periods of 2.6 ML and 8 ML, respectively [1]. The short period is in accordance with theoretical predictions [34, 35].

Bloemen *et al.* have reported an oscillatory period of 3.5 ML in the exchange coupling in Co/Cu/Co(001) upon varying the Co film thickness [41]. Furthermore, the possible existence of quantum well-like oscillations in the thin Co film in Co/Cu(001) was shown by Ortega *et al.* [31]. If one plots their measured photoemission intensity at the Fermi level as a function of Co film thickness (figure 2 in Ref. [31]), one finds one maximum around 3 to 4 ML, in remarkable agreement with the position of the anomalies we observed in our MSHG results. This suggests that the anomalous behavior in $\rho(pp)$ and $\rho(sp)$ between 1 and 6 ML might be connected with these electronic oscillations in the Co film.

To further investigate this hypothesis, we have also studied the Cu/Co(001) system, where quantum well states have been clearly identified, with energies shifting between 1 and 2 eV as a function of Cu thickness [6, 30, 31]. Probing with the incident fundamental wavelength of 800 nm, that corresponds to an energy of about 1.55 eV, we would expect enhancements of the nonlinear contributions by the vacuum/Cu and the top Cu/Co interfaces each time ω is near an electronic resonance. Because ρ is the result of interference between magnetic and non-magnetic terms, this will result in an oscillatory behavior of ρ as a function of Cu thickness. For the experiments we have used 10 ML Co/Cu(001) as a substrate. Figure 6.15 shows the MSHG results for this Cu/Co/Cu system, as a function of Cu coverage. We observe strong oscillations with amplitudes up to 70 %. Neglecting quantum well effects the Cu thickness dependence can be calculated from the multiple reflection model of chapter 3, and solution J of table 6.4. The dashed line in figure 6.15(a) shows the result of the calculations, clearly indicating that classical interference explains by no means the observed oscillations.

In view of the results by Kuzik *et al.* as discussed on page 108 one might argue that the oscillations are a simple consequence of variations of the dielectric constant. However, MOKE on the same samples did not show any oscillations, thereby eliminating this explanation.

A clear period of the oscillation is not easily distinguished. There is some indication of a period of about 5 ML, and substructures with length scales of typically 2-3 ML. At present a detailed analysis of the results is not possible. Much information is to be expected from accurate measurements of the Cu film thickness dependence of individual tensor elements (using longitudinal MSHG, see section 5.2.3). For now the amplitude of the oscillations in MSHG

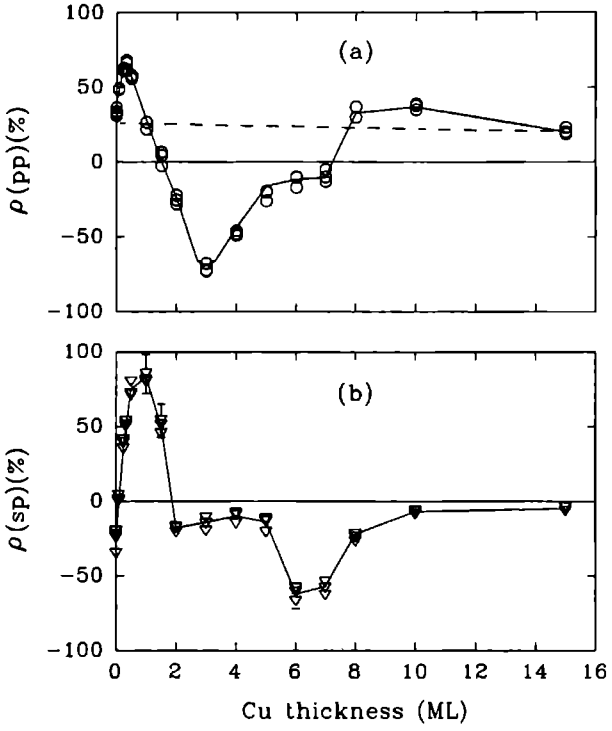

Figure 6.15: *The relative magnetic effects $\rho(pp)$ and $\rho(sp)$ as a function of Cu coverage on a 10 ML Co film on Cu(001); (a) circles - $\rho(pp)$, dashed line - result of model calculation including optical interference but neglecting quantum well oscillations; (b) triangles - $\rho(sp)$. The solid lines are guides to the eye.*

is astonishing, and it is quite satisfying that the 'period' is at least of the right order of magnitude.

6.8 Conclusion

Epitaxially grown fcc Co/Cu(001) multilayers were studied by the Magneto-Optical Kerr Effect (MOKE) and Magnetization induced Second-Harmonic Generation (MSHG).

The results of the longitudinal MOKE experiments could be described by a simple model, that uses the well-established thin-film additivity law for the

Kerr effect, while accounting for absorption and multiple reflections of the light in the multilayer. The model uses bulk refractive indices for the materials, and indicates that these indices accurately describe the optical properties of films above about 5 ML.

For the transverse MSHG experiments we used the 800 nm output of a Ti:Sapphire laser. In contrast to MOKE the relative magnetic effect in MSHG is nearly constant for Co films thicker than 6 ML ($\rho(pp) \approx 50$ % and $\rho(sp) \approx -10$ %). Furthermore, the absolute SH-signals were constant within roughly a factor of two. Similar behavior is observed in experiments on Cu/Co/Cu trilayers. The results clearly proof the interface sensitivity of MSHG.

We have observed large changes in the relative magnetic effect on adsorbing as little as one Langmuir of carbonmonoxyde on 7 ML Co/Cu(001) ($\rho(pp)$ increases from about 45 % to 75 %). Similar results have been obtained on adsorbing oxygen, on sputtering, and for different Co film thicknesses. It is well known that gas adsorption usually strongly reduces SHG from metal surfaces. Therefore, this is not only a second and independent proof of the interface sensitivity of MSHG, but also indicates that both the vacuum/Co and the Co/Cu(001) interface contribute significantly to the total SH-intensity.

The multiple reflection theory of chapter 3 gives a satisfying description of the Co film thickness dependence in the MSHG experiments on Co/Cu(001) and Cu/Co/Cu(001), for Co film thicknesses above about 5 ML. However, the present analysis requires some assumptions that over-simplify the system, and may not be entirely correct. Therefore, the most important conclusions of the present analysis are: (1) The multiple reflection theory leads in principle to a proper description of these ultrathin multilayers, and (2) the film thickness and adsorption dependence of MSHG seem useful tools for determining the values of the tensor elements.

The spectroscopy (or wavelength dependence) of MSHG determines the photon-energies at which resonances in the system occur, thereby revealing the electronic structure of the interface. It is probably an important tool in future experiments. We have observed that both $\rho(pp)$ and $\rho(sp)$ vary smoothly, but significantly within the $E_{2\omega} = 2.9 - 3.45$ eV window. The results cannot be explained from simple dispersion alone, and must be related to the electronic structure.

The oscillation-like behavior of the relative magnetic effect that has been found for Co thicknesses in the 1-6 ML range are not only a third proof of the interface sensitivity of MSHG, but also possibly related to quantum well states in the Co film. To support this hypothesis, we have also studied the Cu/Co(001) system, as it is well known for the appearance of quantum well states. When growing up to 15 ML Cu on top of 10 ML Co/Cu(001), huge

oscillations in the relative MSHG signals are observed, that are most certainly not explained by multiple reflections. The period of the oscillations cannot be determined at present. Though the oscillations need a more detailed study, the results are very exciting as they clearly show the great potential of MSHG for studying magnetic interface properties.

Now that the interface sensitivity of MSHG has been extensively discussed, this chapter is ended with some suggestions for further research.

Of course there is the obvious need to improve the signal to noise ratios. In order to be able to relate the microscopic structure of the interfaces to the macroscopic tensor elements, the latter must be accurately determined. The longitudinal configuration seems preferable for such experiments (see section 5.2.3), and improved sample homogeneity in combination with direct phase measurements of the SH-fields will be of vital importance. Enhanced sensitivity to one interface, i.e. interface selection, might be feasible by adjusting the wavelength and/or the film thicknesses, both due to resonances of tensor elements at this particular interface and due to destructive interference of the fields at others. Sensitivity to buried interfaces is enhanced by gas adsorption, as it reduces SHG by the top interface.

In appendix B we have shown that $\chi^{(D),odd}$ can be interpreted as a first order perturbation due to the magnetization. Perturbations of $\chi^{(D),even}$ are only of second order. This suggests that $\chi^{(D),odd}(M) \propto M$, while $\chi^{(D),even}M) \propto const. + M^2$. Verification of this rule is possible by studying MSHG from a paramagnetic material (where $M \propto H$), and would support the microscopic theory. Furthermore, and even more important, this consideration indicates that $\chi^{(D),odd}$ could be proportional to the local magnetization, i.e. MSHG would be easily applicable as a probe for the magnetic moment at the interface.

MSHG probably measures some sort of projection of for example quantum well states on the interfaces. The energy of these states must depend on the shape of the wall. Therefore, modification of the wall by e.g. gas adsorption or overlayer growth should have an influence. In future measurements of the oscillations in Cu/Co(001) it would be better to increase the thickness of the Co substrate, as it will reduce SHG by the deepest Co/Cu interface, thereby reducing the complexity of the system.

It would be of utmost interest when the interface sensitivity of MSHG could be exploited to improve understanding of the role of the interfaces in the exchange coupling. Bansmann *et al.* have reported adsorbate-induced reductions of the coercive force of the surface hysteresis curves [42]. Similar

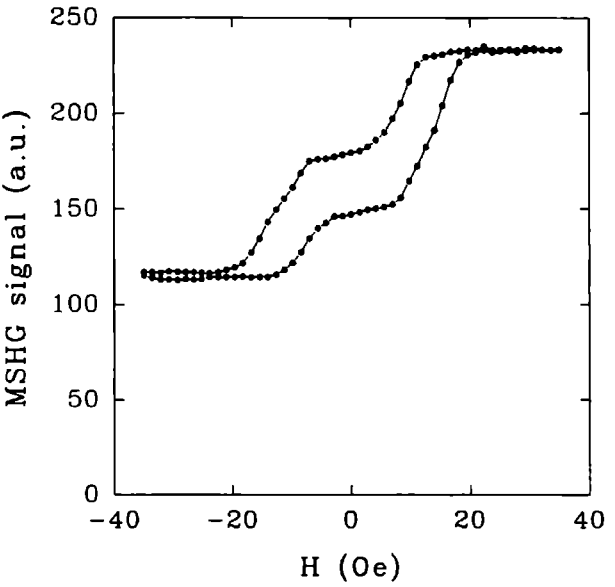

Figure 6.16: $p_{in}p_{out}$ *MSHG hysteresis on anti-ferromagnetically coupled cobalt layers in 3 ML Co/7 ML Cu/3 ML Co/Cu(001).*

experiments on buried interfaces could give valuable information about the relative strength of the coupling between magnetic atoms within one layer, and the interlayer coupling at the interface (between magnetic and non-magnetic atoms). This might improve understanding of the influence of the interfaces in the exchange coupling in multilayers. As a preliminary result figure 6.16 shows the $p_{in}p_{out}$ MSHG hysteresis on 3 ML Co/7 ML Cu/3 ML Co/Cu(001). The cobalt layers in the system are anti-ferromagnetically coupled [2]. The three important regions, i.e. both magnetizations parallel and negative, anti-parallel coupling at $H = 0$, and both magnetizations parallel and positive, are clearly distinguishable.

The technique has great potential of solving questions about the presence of magnetically dead or life layers at surface and interface (let us not forget that MSHG is also applicable to clean crystal surfaces), e.g. the enhanced magnetic moment at the chromium surface [43] could be verified, and its dependence on the presence of other materials may be measured.

Curie temperatures at surfaces may be very different from the bulk, as has been shown for e.g. gadolinium [44]. Similar effects are to be expected for buried interfaces. Also preliminary results indicate that MSHG is sensitive

to intermixing at the interface (due to elevated temperatures), which opens up the possibility to check the relation between the magnetic moments and interdiffusion.

References

[1] M.T. Johnson, S.T. Purcell, N.W.E. McGee, R. Coehoorn, J. aan de Stegge, and W. Hoving, Phys. Rev. Lett. **68**, 2688 (1992).

[2] A. Cebollada, R. Miranda, C.M. Schneider, P. Schuster, and J. Kirschner, J. Magn. Magn. Mat. **102**, 25 (1991).

[3] S.S.P. Parkin, N. More and K.P. Roche, Phys. Rev. Lett. **64**, 2304 (1990)

[4] R. Schad, C.D. Potter, P. Beliën, G. Verbanck, V.V. Moshchalkov, and Y. Bruynseraede, Appl. Phys. Lett. **64**, 3500 (1994).

[5] Y. Wang, P.M. Levy, and J.L. Fry, Phys. Rev. Lett. **65**, 2732 (1990).

[6] N.B. Brookes, Y. Chang and P.D. Johnson, Phys. Rev. Lett. **67**, 354 (1991).

[7] C.M. Schneider, J.J. de Miguel, P. Bressler, P. Schuster, R. Miranda, and J. Kirschner, J. Electron Spec. Rel. Phen. **51**, 263 (1990).

[8] L. González, R. Miranda, M. Salmerón, J.A. Vergés, and F. Ynduráin, Phys. Rev. B **24**, 3245 (1981).

[9] E.R. Moog, C. Liu, S.D. Bader, and J. Zak, Phys. Rev. B **39**, 6949 (1989).

[10] J. Zak, E.R. Moog, C. Liu, and S.D. Bader, J. Magn. Magn. Mat. **88**, L261 (1990).

[11] R. Atkinson, and P.H. Lissberger, J. Magn. Magn. Mat. **118**, 271 (1993).

[12] R. Gamble, and P.H. Lissberger, J. Opt. Soc. Am. A **5**, 1533 (1988).

[13] A.J. Kolk, and M. Orlovic, J. Appl. Phys. **34**, 1060 (1963).

[14] L.M. Falicov *et al.*, J. Mater. Res **5**, 1299 (1990).

[15] F.A. Jenkins, and H.E. White, *Fundamentals of optics*, 4^{th} edition (McGraw-Hill International Book Company, Tokyo, 1983).

[16] W.G. Driscoll, and W. Vaughan, *Handbook of optics*, (McGraw-Hill Book Company, New York, 1978).

[17] P.B. Johnson and R.W.Christy, Phys. Rev. B **9**, 5056 (1974); Phys. Rev. B **6**, 4370 (1972).

[18] R. Gamble, and P.H. Lissberger, J. Opt. Soc. Am. A **5**, 1533 (1988).

[19] T. Yoshino, and S. Tanaka, Jpn. J. Appl. Phys. **5**, 989 (1966).

[20] W.A. McGahan, and J.A. Woollam, Appl. Phys. Comm. **9**, 1 (1989).

[21] D. Keay, and P.H. Lissberger, Opt. Act. **15**, 373 (1968).

[22] J. Inglesfield, *private communication.*

[23] L.A. Kuzik, Yu.E. Petrov, F.A. Pudonin, and V.A. Yakovlev, JETP **78**, 114 (1994).

[24] G.L. Richmond, J.M. Robinson, and V.L. Shannon, Prog. Surf. Sci. **28**, 1 (1988).

[25] J. Reif, J.C. Zink, C.M. Schneider, and J. Kirschner, Phys. Rev. Lett. **67**, 2878 (1991).

[26] Y.R. Shen, Ann. Rev. Mater. Sci. **16**, 69 (1986).

[27] W. Hübner, Phys. Rev. B **42**, 11553 (1990).

[28] U. Pustogowa, W. Hübner, and K.-H. Bennemann, Phys. Rev. B **48**, 8607 (1993).

[29] W.R. Bennett, W. Schwarzacher, and W.F. Egelhoff Jr, Phys. Rev. Lett. **65**, 3169 (1990).

[30] J.E. Ortega, and F.J. Himpsel, Phys. Rev. Lett. **69**, 844 (1992).

[31] J.E. Ortega, F.J. Himpsel, G.J. Mankey, and R.F. Willis, Phys. Rev. B **47**, 1540 (1993).

[32] C. Carbone, E. Vescovo, O. Rader, W. Gudat, and W. Eberhardt, Phys. Rev. Lett. **71**, 2805 (1993).

[33] K. Garrison, Y. Chang, and P.D. Johnson, Phys. Rev. Lett. **71**, 2801 (1993).

[34] P. Bruno and C. Chappert, Phys. Rev. Lett. **67**, 1602 (1991);

[35] P. Bruno and C. Chappert, Phys. Rev. B. **46**, 261 (1992).

[36] R. Coehoorn, Phys. Rev. B. **44**, 9331 (1991).

[37] T. Katayama, Y. Suzuki, M. Hayashi, and A. Thiaville, J. Magn. Magn. Mat. **126**, 527 (1993).

[38] J.J. de Miguel, A. Cebollada, J.M. Gallego, R. Miranda, C.M. Schneider, P. Schuster, and J. Kirschner, J. Magn. Magn. Mat. **93**, 1 (1991).

[39] C.M. Schneider, P. Bressler, P. Schuster, J. Kirschner, J.J. de Miguel, and R. Miranda, Phys. Rev. Lett. **64**, 1059 (1990).

[40] J.J. de Miguel, A, Cebollada, J.M. Gallego, S. Ferrer, R. Miranda, C.M. Schneider, P. Bressler, J. Garbe, K. Bethke, and J. Kirschner, Surf. Sci. **211/212**, 732 (1989).

[41] P.J.H. Bloemen, M.T. Johnson, M.T.H. van de Vorst, R. Coehoorn, J.J. de Vries, R. Jungblut, J. aan de Stegge, A. Reinders, and W.J.M. de Jonge, Phys. Rev. Lett. **72**, 764 (1994).

[42] J. Bansmann, M. Getzlaff, C. Westphal, and G. Schönhense, J. Magn. Magn .Mat. **117**, 38 (1992).

[43] A.J. Freeman, and C.L. Fu, J. Appl. Phys. **61**, 3356 (1987).

[44] D. Weller, S.F. Alvarado, and M. Campagna, Physica B&C **130**, 72 (1985).

Chapter 7

(M)SHG on crystal surfaces

Better understanding of the mechanism of Magnetization induced Second-Harmonic Generation from magnetic interfaces, inevitably requires reliable measurements of the absolute SH-intensities from simple and well-defined systems. Ferromagnetic crystal surfaces are probably the best candidates. Spectroscopic MSHG on nickel and iron is of particular interest, because of the possibility of direct comparison of experiment and theory [1, 2]. We have studied Ni(110) and Fe(110). Up to now we have made no reliable observations of Magnetization induced SHG in these systems. Although lack of surface quality cannot be entirely excluded, there are several indications that the explanation may be more involved.

7.1 (M)SHG on Ni(110)

Figure 7.1 shows the transverse MOKE hysteresis of the nickel crystal. It was measured ex-situ, while using the UHV compatible electromagnet of figure 4.3 .[1] Although the hysteresis has not been measured extremely accurate, as we have used the simple experimental configuration of figure 4.7 , it is clear that the applied magnetic field is sufficient to magnetize the crystal.

The surface of the Ni(110) single crystal was mechanically polished with diamond power, with a final grain size of $\frac{1}{4}\mu$m. The crystal was placed in UHV#1 (see section 4.1.2). Surface preparation consisted of repeated cycles (several tens of times) of 15 minutes Ar^+-sputtering at 500 eV (target currents up to a few $\mu A/cm^2$), followed by annealing at 500 °C for a few minutes. Although this is one of many 'standard' preparation methods for Ni(110) [3],

[1]The magnetic field was applied along one of the (111) easy-axes that are lying in the Ni(110) surface [8].

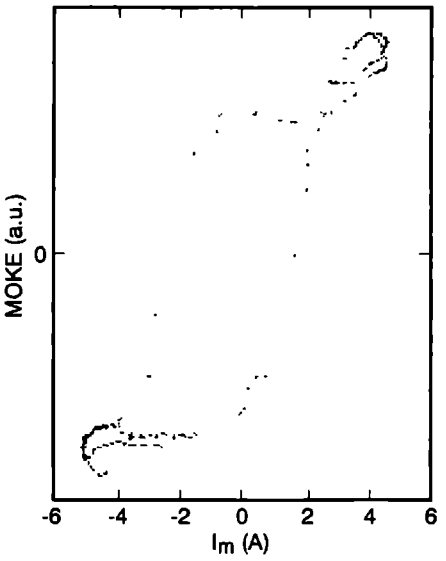

Figure 7.1: *Transverse Magneto-Optical Kerr Effect of the Ni(110) crystal, while using the UHV compatible magnet of figure 4.3; I_m - current through coil.*

AES spectra showed significant residues of carbon, oxygen, and sulfur at the surface up to a total amount of 10-15 atomic %.

For the LH-transverse MSHG experiments (see figure 5.3) we have used the Nd:YAG-laser set up of figure 4.1. Excitation at 532 nm, with a pulse intensity of about $140\mu J/mm^2$, at an angle of incidence of 55°, gave an easily detectable $p_{in}p_{out}$ SH-intensity.[2] No laser induced damage was observed. However, a few Langmuirs of oxygen reduced the SH-intensity by typically a factor of three, indicating that we are fairly interface sensitive [4]. In all experiments $\rho(pp)$ was zero within the experimental error of about 5 %.

An obvious explanation would be that the contaminations (C,O and/or S) destroy the magnetic order of the surface, and thereby the magnetic effect in MSHG, as was suggested by Reif *et al.* [5]. However, recently Böhmer *et al.* have observed MSHG from polycrystalline nickel, under ambient conditions, using a fundamental wavelength of 600 nm. Although the surface was of course completely oxidized, the effect was still there: $\rho(pp) = 19$ % [6]. It is interest-

[2]We have used a long-focus lens (f=$\frac{4}{3}$m) to reduce the beam area, thus giving a semi-parallel laser beam.

ing to realize that the theoretical analysis for MSHG from the nickel surface by Hübner *et al.* gave a minimum for the odd tensor element $\chi^{(D)}_{xzz}$ at 532 nm (2.33 eV), while there is a maximum at 600 nm (2.07 eV) [1]. Although their tight-binding calculations have an accuracy of a few tenths of electronVolts [7], and the influence of oxidation on the MSHG spectroscopy is as yet unknown, the coincidence is nevertheless striking. So, the zero magnetization induced effects in our experiments on the Ni(110) surface might also have a (partly) spectroscopic origin.

A hydrogen treatment[3] of the nickel reduced the sulfur contamination to below the AES detection-limit of about half a percent. However oxygen and especially carbon contaminations were very persistent (total amount: $\sim$ 8 atomic %). Flash heating until temperatures of 800-1000 °C using 600 eV electrons, or oxygen titration ($\sim$ 1Langmuir) at several temperatures and with varying dosage, followed by short annealing, gave no improvement of the surface quality.

As we were essentially interested in studying MSHG from a perfectly clean ferromagnetic surface, and had the opportunity to study the exact Fe(110) crystal Reif *et al.* had been using in their first MSHG experiments [5], we ceased experiments on the Ni(110) for the time being.[4]

7.2 (M)SHG on Fe(110)

The sample configuration is shown in figure 4.4, and is the exact configuration that was used by Reif *et al.* in their experiments [5], i.e. sample, sample holder, magnet, and even the sample manipulator are identical. Therefore, we did not measure a MOKE hysteresis, as it has been verified that the sample is a single domain, and that the available magnetic field is enough to invert the direction of the remanent magnetization [5, 9].[5] Sample preparation consisted of repeated cycles of Ar^+-sputtering at 500 eV for about half an hour a rate of a few $\mu A/cm^2$, followed by rapid sample heating until 500 °C.[6] AES at room temperature showed a total amount of carbon and oxygen of about 10 atomic %. Usually there was much more C than O, indicating that carbonmonoxyde adsorption is not the main cause of the lack of surface quality. Sulfur and nitrogen contaminations were well below 1 atomic %. O_2 titration at room

[3] 18 hours at 650 °C in $4\text{-}5\cdot10^{-4}$ mbar H_2 flow [8].

[4] The Fe(110) crystal was kindly lend to us by J. Kirschner.

[5] We did observe, that a thin alumel wire was attracted by the sample if current was running through the magnet coil, indicating magnetization of the iron crystal.

[6] At 480 °C all carbonmonoxyde is desorbed, as was verified by mass spectrometry.

temperature (~1Langmuir) followed by rapid sample heating to 500 °C did not improve the surface quality.[7]

For the LH-transverse MSHG experiments on the Fe(110) we also used the Nd:YAG-laser set up of figure 4.1, operating at 532 nm. At a pulse intensity of about 100 $\mu J/cm^2$, an angle of incidence of 55°, and sample temperatures $t_s \lesssim 100$ °C, $\rho(pp)$ was zero within the experimental error of about 3 %, quite different from the value $\rho(pp) = -17$ % that has been observed by Reif *et al.* [5]. Again one might argue that our observation is caused by a lack of surface quality. However, we have observed $p_{in}p_{out}$ SH-intensity reductions up to a factor of 15 on adsorbing a few Langmuirs of O_2 at temperatures well below 100 °C. These results clearly show the surface sensitivity of our SHG experiments.

In contradiction to the results reported by Reif *et al.* [5], we do observe that the *total* SH-intensity is reduced on carbonmonoxyde adsorption. A 35 % reduction of the *total* $p_{in}p_{out}$ SH-intensity is observed after leaving the sample undisturbed in the UHV chamber ($p = 3 \cdot 10^{-10}$ torr) for three quarters of an hour, which corresponds to a CO dosage less than half a Langmuir. Reif *et al.* claim that the total $p_{in}p_{out}$ SH-intensity did not reduce, even after a CO dosage of more than 2.5 Langmuir.[8] Furthermore, we have observed that leaving the sample in the UHV chamber for two days led to a low $p_{in}p_{out}$ SH-intensity. However, rapid sample heating until the CO desorption temperature of 480 °C gave an increase of the SH-intensity with a factor of six. The results of Reif *et al.* are therefore somewhat strange, and make their quantitative analysis rather doubtful.

Musket *et al.* have mentioned the observation that carbon, oxygen and nitrogen dissolve into the bulk of a Fe(111) crystal at 450 °C [3]. AES spectra of our Fe(110) surface at 400 °C showed no contaminations above 1 atomic %, except carbon which was about 3 %. The sample surface remains clean for long periods of time as can be seen in figure 7.2 , that shows the AES spectrum after several hours at 400 °C. Surface sensitivity of SHG at this temperature was verified after observing that adsorbing a few Langmuirs of O_2 reduced the SH-intensity by again a factor of 15.

[7] Significant reductions of the carbon contamination were obtained, but always accompanied by an increase of the amount of oxygen at the surface. Acethylene titration [3] (~1Langmuir) followed by rapid sample heating to 500 °C reduced the oxygen contamination but gave an increased amount of carbon.

[8] Their experiments were done at a base pressure of $7 \cdot 10^{-10}$. Assuming that one third of the rest gasses is carbonmonoxyde leads to an estimated dosage of 2.5L CO after 180 minutes.

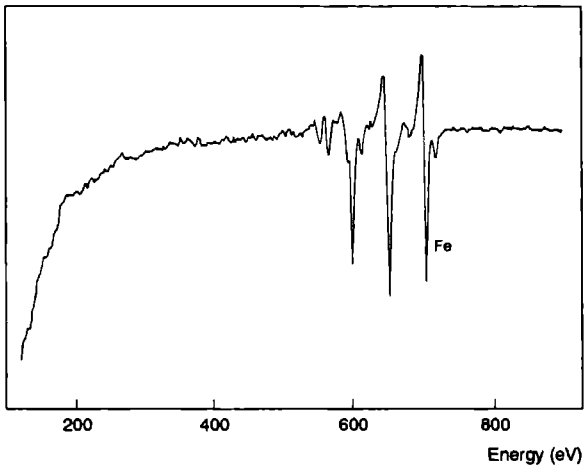

Figure 7.2: *Auger spectrum of Fe(110) at 400 °C, taken after several hours. Initially are all contaminations below 1 atomic %, except C that reaches 3 %. The contaminations do not increase much with time.*

Even at this elevated temperature, significant surface magnetization is expected. This can be seen from an estimate using the theoretical curve for surface magnetization versus temperature [10], and the bulk Curie temperature of iron $T_C = 1043$ K [11]. We estimate a surface magnetization that is about one half of the low temperature value. As discussed in section 6.8 one would expect that: $\chi^{(D),odd}(M) \propto M$, while $\chi^{(D),even}(M)$ is independent of M in a first order approximation. So, due to the elevated temperature $\chi^{(D),odd}(M)$ is reduced by a factor of two, while $\chi^{(D),even}(M)$ remains approximately constant. Reif *et al.* have estimated for the clean Fe(110) surface at room temperature:

$$R \equiv \left| \frac{\chi^{(D),odd}(M)}{\chi^{(D),even}(M)} \right| = 0.25 \tag{7.1}$$

while using the simple formula:

$$\rho = \frac{2R}{1+R^2} \tag{7.2}$$

At 400 °C R would reduce to about 0.12 . Substituting this value into equation 7.2 gives an estimated value of $\rho(pp) = 24$ % at 400 °C. However, our experiments gave $\rho(pp) = 0$ % within the experimental error of about 4 %.

At this point it might be interesting to mention that as a part of the series of experiments on Co/Cu(001) we did two preliminary experiments on Fe/Cu(001). MSHG was clearly observed from a 20 ML bcc Fe film on Cu(001), using a fundamental wavelength of 800 nm: $\rho(pp) = 10 \pm 1$ %, $\rho(sp) = (-3 \pm 1) \times 10$ % (for details about the experimental set up see chapter 6). Furthermore, we evaporated a 2 ML fcc Fe film on Cu(001) at room temperature. The remanent magnetization was perpendicular to the plane of the film, as verified by MOKE. No magnetization induced SHG from the 800 nm beam was observed within the experimental error of a few percent, for both $p_{in}p_{out}$ and $s_{in}p_{out}$. This is in agreement with the phenomenological theory of chapter 2 (see table 2.3). The $p_{in}s_{out}$ polarization combination detects the odd element $\chi^{(D)}_{yzx}(M\mathbf{z})$ exclusively. The SH-signal in this polarization combination was virtually zero. As all odd tensor elements in a system with a magnetization perpendicular to the plane of the film, have an equal amplitude, the result indicates that it migh be difficult to study perpendicularly magnetized films with MSHG.

The results of the SHG experiments on the Fe(110) crystal are very unsatisfying. Although we have shown that the SHG experiments are surface sensitive, the relative magnetic effect was zero, quite opposite to the observations by Reif *et al.* [5]. Furthermore, we observe significant dependence of the absolute $p_{in}p_{out}$ SH-intensity on adsorbing less than half a Langmuir of carbonmonoxyde, whereas Reif *et al.* claim that this is most certainly not the case.

An explanation could follow from the assumption that the contributions from the Fe(110) surface are exclusively odd in the magnetization. This implies that under normal conditions magnetization induced effects cannot be observed (see chapter 1). However, if these odd Fe(110) contributions interfere with an external even SH-source (for example at a window of the UHV chamber), magnetic effects could be observed. This might have been the case in the experiments by Reif *et al.* Carbonmonoxyde adsorption reduces the amplitude of the odd tensor elements at the Fe(110) surface, thus reducing the entire SH-signal. However, in case of an external source, these (even) contributions remain unaltered, thereby explaining the disappearance of the magnetization induced effect, while the non-magnetric contributions remain.

The problem definitely needs attention. In future MSHG experiments on ferromagnetic crystal surfaces, the above hypothesis should be verified. In these experiments an improved UHV quality (base pressure below $1 \cdot 10^{-10}$ torr) is desirable. One might consider an initial cleaning stage of the crystal surface, while the magnet is left out of the UHV-chamber. This allows high tem-

perature sputtering and heavy hydrogen and oxygen treatments at elevated temperatures to remove the sulfur and carbon contaminations [3]. Hopefully improved surface quality remains even after restoring the magnet followed by standard preparation methods. Improved surface quality may also be obtained from homo-epitaxy.[9] In view of the results on Ni(110) it might be useful to try MSHG at several fundamental wavelengths. If no magnetic effect is observed, an artificial 'even' external source of SHG (e.g. a quartz crystal) might be helpful.

References

[1] W. Hübner, Phys. Rev. B **42**, 11553 (1990).

[2] U. Pustogowa, W. Hübner, and K.-H. Bennemann, Phys. Rev. B **48**, 8607 (1993).

[3] R.G. Musket, W. McLean, C.A. Colmenares, D.M. Makowiecki, and W.J. Siekhaus, Appl. Surf. Sci. **10**, 143 (1982).

[4] X.D. Zhu, W. Daum, X.D. Xiao, R. Chin, and Y.R. Shen, Phys. Rev. B **43**, 11571 (1991).

[5] J. Reif, J.C. Zink, C.M. Schneider, and J. Kirschner, Phys. Rev. Lett. **67**, 2878 (1991).

[6] K. Böhmer, J. Hohlfeld, and E. Matthias, to be published.

[7] W. Hübner, *private communication.*

[8] R.J.H. Kappert, *Spectroscopic studies of local magnetic properties in metals* (Thesis, Katholieke Universiteit Nijmegen, Nijmegen, The Netherlands, 1992).

[9] C.M. Schneider, and J. Kirschner, *private communication.*

[10] T. Kaneyoshi, J. Phys.: Condens. Matter **3** ,4497 (1991), see page 4505.

[11] *Solid State Physics*, N.W. Ashcroft, N.D. Mermin (Saunders College, Philadelphia, 1978).

[9]For example: An epitaxially grown Fe film on top of an Fe substrate.

Appendix A

Boundary conditions at a polarized sheet

The boundary conditions for the infinitesimal nonlinear sheet in figure 3.4 were derived by Heinz [1]. For the readers convenience I shall give an extended version of his analysis, that is directly related to the specific situation in this thesis.

A.1 Boundary condition for D_z

Figure A.1 shows a schematic representation of a nonlinear layer of thickness 2δ and refractive index $\hat{n}^t(2\omega)$ at $z = 0$ in a vacuum environment.[1]

We derive the boundary condition for the perpendicular component of the displacement field starting from the consideration that there is no net charge in the layer:

$$\int_{\Delta V} \nabla \cdot \mathbf{D} d^3r = 4\pi \int_{\Delta V} \rho(2\omega) d^3r = 0 \qquad \text{(A.1)}$$

where ΔV is the volume of a cylindrical excision of the nonlinear sheet (see figure A.1), and $\mathbf{D}$ is the displacement field at frequency 2ω. For all the fields and polarizations in this appendix we presume: $\mathbf{F} = \mathbf{F}_{2\omega}(\mathbf{r})e^{-\imath 2\omega t}$.

In CGS units the displacement field is related to the electric field and the polarization through the relation: $\mathbf{D} = \mathbf{E} + 4\pi\mathbf{P}$, where $\mathbf{P}$ is the total polarization of the sheet and can be written as: $\mathbf{P} = \mathbf{P}_{ind} + \mathbf{P}_{nl}$, where $\mathbf{P}_{ind}$ represents the induced polarization, and $\mathbf{P}_{nl}$ the nonlinear polarization generated by the fundamental field. So we may write:

[1] This is exactly the situation we created in section 3.3.

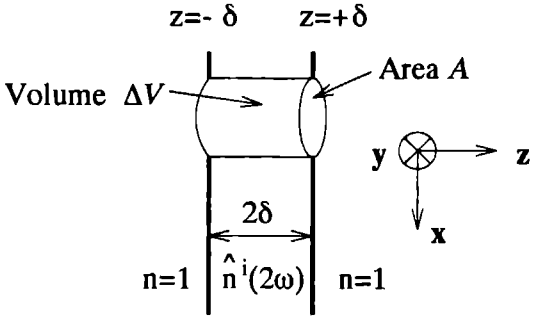

Figure A.1: *Infinitesimal nonlinear sheet inside vacuum. The boundaries are at $z = -\delta$ and $z = +\delta$ and the sheet has a refractive index $\hat{n}^i(2\omega)$. The cylinder with volume $\Delta V = A2\delta$ is used in the analysis and has faces lying in the boundaries.*

$$\mathbf{D} = \hat{\epsilon}^i(2\omega)\mathbf{E} + 4\pi\mathbf{P}_{nl} \tag{A.2}$$

Before we continue with the derivation of the boundary conditions it is useful to look explicitly at the position dependence of this equation. Using the general expression for the total field of eq. 3.3 in a slightly different form, and the expression for $\mathbf{P}_{nl}$ of eq. 3.35 with $k_y(\omega) \neq 0$, we may write:

$$\begin{aligned}\mathbf{D}(z)e^{i(\hat{k}_x^i(2\omega)x+\hat{k}_y^i(2\omega))} &= \hat{\epsilon}^i(2\omega)\mathbf{E}(z)e^{i(\hat{k}_x^i(2\omega)x+\hat{k}_y^i(2\omega))} \\ &\quad + 4\pi\mathbf{P}_{nl}(z)e^{i(2k_x(\omega)x+2k_y(\omega))}\end{aligned} \tag{A.3}$$

Since the equation must hold at all points on the interface, we obtain:

$$\hat{k}_x^i(2\omega) = 2k_x(\omega) \in \Re \quad \text{and} \quad \hat{k}_y^i(2\omega) = 2k_y(\omega) \in \Re \tag{A.4}$$

This is the nonlinear equivalent of Snell's law [2]. Since standard Snell's law applies of course to the second-harmonic fields once they are generated, we find that throughout the system:

$$\mathbf{k}_{\|}(2\omega) = 2\mathbf{k}_{\|}(\omega) \tag{A.5}$$

Using the divergence theorem and eq. A.2, eq. A.1 can be written as:

$$\hat{\epsilon}^i(2\omega)\int_O \mathbf{E}\cdot\mathbf{n}d^2r = -4\pi\int_{\Delta V}\nabla\cdot\mathbf{P}_{nl}d^3r \tag{A.6}$$

where O is the surface area of the cylinder. We 'create' a nonlinear interface by studying this equation in the limit for $\delta \to 0$, such that the total polarization in the sheet remains constant:

$$\lim_{\delta \to 0} \int_{-\delta}^{+\delta} \mathbf{P}_{nl} dz = \mathbf{P}^{sh} \tag{A.7}$$

where $\mathbf{P}^{sh}$ is the net dipole moment per unit area in the interface generated by the fundamental field. Since $E_{\parallel}$ is continuous across an interface, the field inside the nonlinear sheet has to be finite, so:

$$\lim_{\delta \to 0} \int_{-\delta}^{+\delta} E_{\parallel} dz = 0 \tag{A.8}$$

We may now develop the left hand side of eq. A.6 (notice that O refers to the entire surface of the cylinder in figure A.1, whereas A refers only to the cylindrical faces lying in the boundaries):

$$\hat{\epsilon}^i(2\omega) \lim_{\delta \to 0} \int_O \mathbf{E}(\mathbf{r}) \cdot \mathbf{n} d^2 r =$$

$$\hat{\epsilon}^i(2\omega) \lim_{\delta \to 0} \int_A [E_z(x, y, z = +\delta) - E_z(x, y, z = -\delta)] dx dy \tag{A.9}$$

with (see eq. 3.3):

$$E_z(x, y, \pm\delta) = \; [E_z^+(0, 0, \pm\delta) + E_z^-(0, 0, \pm\delta)] \; e^{i(k_x(2\omega)x + k_y(2\omega)y)} \tag{A.10}$$

So,

$$\hat{\epsilon}^i(2\omega) \lim_{\delta \to 0} \int_O \mathbf{E}(\mathbf{r}) \cdot \mathbf{n} d^2 r = \hat{\epsilon}^i(2\omega) I_A \lim_{\delta \to 0} \; [E_z(0, 0, +\delta) - E_z(0, 0, -\delta)] \tag{A.11}$$

with

$$I_A = \int_A e^{i(k_x(2\omega)x + k_y(2\omega)y)} dx dy \tag{A.12}$$

Developing the right hand side of eq. A.6 along similar lines leads to:

$$-4\pi \lim_{\delta \to 0} \int_{\Delta V} \nabla \cdot \mathbf{P}_{nl} d^3 r =$$

$$- 4\pi I_A \lim_{\delta \to 0} \int_{-\delta}^{+\delta} [\frac{\partial P_{nl,x}}{\partial x}(0, 0, z) + \frac{\partial P_{nl,y}}{\partial y}(0, 0, z)] dz \tag{A.13}$$

where we have used eq. A.5. Because of the translation symmetry parallel to the interface, the relations hold for any position at the interface. Using eq. A.7 and realizing that D_z is continuous across the interfaces at $z = -\delta$ and $z = +\delta$ we end up with:

$$\Delta D_z = \hat{\epsilon}^i(2\omega)\left[E_z(0,0,+\delta) - E_z(0,0,-\delta)\right]$$

$$= -4\pi\left(\frac{\partial P_x^{sh}}{\partial x} + \frac{\partial P_y^{sh}}{\partial y}\right) = -4\pi i(k_x(2\omega)P_x^s + k_y(2\omega)P_y^s) \qquad \text{(A.14)}$$

where ΔD_z represents the jump of the perpendicular component of the displacement field while moving from the vacuum on the left, across the sheet, to the vacuum on the right.

A.2 Boundary condition for E_x and E_y

We can also derive the boundary conditions for $E_{\|}$. Let us first consider that (in CGS units):

$$\oint_R \mathbf{E}\cdot\mathbf{dl} = \int_S (\nabla\times\mathbf{E})\cdot\mathbf{n}d^2r = -\frac{1}{c}\int_S \frac{\partial\mathbf{B}}{\partial t}\cdot\mathbf{n}d^2r = \frac{i2\omega}{c}\int_S B_y dxdz \qquad \text{(A.15)}$$

where R is a rectangular path through the interface, situated in the **x**,**z**-plane. The part of the path that is directed into the positive z-direction is located at $x = 0$ (see figure A.2). S is the area whose perimeter is the path R, and **n** is parallel to the **y**-axis. We have used subsequently Stokes's theorem, Faraday's law and $\mathbf{B}(\mathbf{r},t) = \mathbf{B}(\mathbf{r})e^{-i2\omega t}$.

Since $\nabla\cdot\mathbf{B} = 0$, **B** is continuous everywhere and finite inside the nonlinear sheet, so we have:

$$\lim_{\delta\to 0}\int_{-\delta}^{+\delta}\mathbf{B}dz = \mathbf{0} \qquad \text{(A.16)}$$

This immediately leads to:

$$\lim_{\delta\to 0}\oint_R \mathbf{E}\cdot\mathbf{dl} = 0 \qquad \text{(A.17)}$$

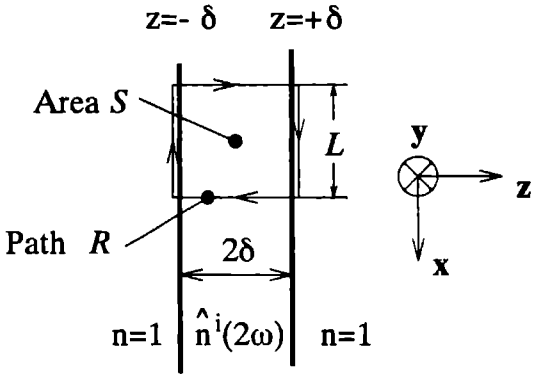

Figure A.2: *Infinitesimal nonlinear sheet inside vacuum. The boundaries are at $z = -\delta$ and $z = +\delta$ and the sheet has a refractive index $\hat{n}^i(2\omega)$. The rectangular path R is lying in the* **x**,**z**-*plane and is used in the analysis. It has two sides of length L in the boundaries.*

Rewriting the line integral in this equation gives:

$$\int_0^L e^{ik_x(2\omega)x}dx \cdot \lim_{\delta\to 0} \left[E_x(0,0,+\delta) - E_x(0,0,-\delta)\right]$$

$$+ (1 - e^{ik_x(2\omega)L}) \cdot \lim_{\delta\to 0} \int_{-\delta}^{+\delta} E_z(0,0,z)dz = 0 \qquad \text{(A.18)}$$

where we have used the equation:

$$E_z(L,0,z) = E_z(0,0,z)e^{ik_x(2\omega)L} \qquad \text{(A.19)}$$

Realizing that E_x is continuous across the interfaces at $z = -\delta$ and $z = +\delta$, and working out the integral in the left hand side of eq. A.18 gives:

$$\Delta E_x = ik_x(2\omega) \lim_{\delta\to 0} \int_{-\delta}^{+\delta} E_z(0,0,z)dz \qquad \text{(A.20)}$$

We can work out this last integral after realizing that the continuity of D_z leads to a finite value for D_z inside the nonlinear sheet, so:

$$\lim_{\delta\to 0} \int_{-\delta}^{+\delta} D_z dz = 0 \qquad \text{(A.21)}$$

using eq. A.2 and A.7 we get:

$$\hat{\epsilon}^i(2\omega) \lim_{\delta \to 0} \int_{-\delta}^{+\delta} E_z dz = -4\pi P_z^{sh} \tag{A.22}$$

We now use equation A.22 to solve the integral in eq. A.20 and obtain:

$$\Delta E_x = -\frac{4\pi i}{\hat{\epsilon}^i(2\omega)} k_x(2\omega) P_z^{sh} \tag{A.23}$$

Along similar lines we derive:

$$\Delta E_y = -\frac{4\pi i}{\hat{\epsilon}^i(2\omega)} k_y(2\omega) P_z^{sh} \tag{A.24}$$

Similar to ΔD_z, the expressions for ΔE_x and ΔE_y represent the jumps of the parallel components of the electric field while moving from the vacuum on the left, across the sheet, to the vacuum on the right.

A.3 Boundary condition for H_x and H_y

Finally we also deduce the boundary condition for H_x (and H_y). We may write (in CGS units):

$$\oint_R \mathbf{H} \cdot \mathbf{dl} = \int_S (\nabla \times \mathbf{H}) \cdot \mathbf{n} d^2 r = \frac{1}{c} \int_S \frac{\partial \mathbf{D}}{\partial t} \cdot \mathbf{n} dx dz = -\frac{i2\omega}{c} \int_S D_y d^2 r \tag{A.25}$$

where R is a rectangular path through the interface, lying in the **x**,**z**-plane. The part of the path that is directed into the positive z-direction is situated at $x = 0$ (see figure A.2). S is the area whose perimeter is the path R, and **n** is parallel to the **y**-axis. We have used subsequently Stokes's theorem, the generalized Ampère's law with **J**=**0** and $\mathbf{D}(\mathbf{r}, t) = \mathbf{D}(\mathbf{r}) e^{-i2\omega t}$. Using eq. A.2 and A.8, we derive:

$$\lim_{\delta \to 0} \oint_R \mathbf{H} \cdot \mathbf{dl} = -\frac{i2\omega}{c} 4\pi \lim_{\delta \to 0} \int_S P_{nl,y} d^2 r \tag{A.26}$$

Working out the integrals on both sides gives:

$$(1 - e^{ik_x(2\omega)L}) \cdot \lim_{\delta \to 0} \int_{-\delta}^{\delta} H_z(0,0,z) dz + I_L \cdot \lim_{\delta \to 0} \left[H_x(0,0,\delta) - H_x(0,0,-\delta) \right]$$

$$= -\frac{i2\omega}{c} 4\pi I_L \lim_{\delta \to 0} \int_{-\delta}^{\delta} P_{nl,y}(0,0,z) dz \tag{A.27}$$

with

$$I_L = \int_0^L e^{ik_x(2\omega)x} dx \tag{A.28}$$

Using eq. A.16 and $\mathbf{H} \approx \mathbf{B}$, because $\mu \approx 1$ for optical frequencies (even in magnetic materials), in combination with eq. A.7 and the continuity of H_x across the boundaries at $z = -\delta$ and $z = +\delta$, we end with:

$$\Delta H_x = -\frac{i2\omega}{c} 4\pi P_y^{sh} \tag{A.29}$$

Along similar line we derive:

$$\Delta H_y = \frac{i2\omega}{c} 4\pi P_x^{sh} \tag{A.30}$$

The whole analysis applies equally well to forward and backward fields and the detailed spatial dependence of the polarization is not important. Notice that all boundary conditions reduce to the ones already used in section 3.2 if there is no nonlinear source at the interface ($\mathbf{P}^{sh} = \mathbf{0}$).

References

[1] T.F. Heinz, *Nonlinear optics of surfaces and adsorbates* (Thesis, Lawrence Berkeley Laboratory, Berkeley, USA, 1982).

[2] Y.R. Shen, *The principles of nonlinear optics* (Wiley, New York, 1984).

Appendix B

Quantum mechanical approach to MSHG

The phenomenological theory of Ru-Pin Pan *et al.*, as described in chapter 2, provides a convenient description of Magnetization induced optical Second-Harmonic Generation. However, the ultimate goal of MSHG is to determine the microscopic electronic and magnetic properties of magnetic interfaces and analyse their role in multilayered structures. This requires better understanding of the microscopic origin of MSHG and its dependency on e.g. structural and local magnetic properties. The macroscopic tensor elements (i.e. the experimental values) must be related to the microscopic electronic structure through quantum mechanics and band structure theory. For iron and nickel Hübner, Pustogowa and Bennemann have given a thorough quantum mechanical analysis of nonlinear magneto-optical Kerr effects (or MSHG) based on the complete band structure of the materials [1-7].

As an introduction to such an approach, this appendix gives the elementary microscopic theory of MSHG. Section B.1 briefly discusses the derivation of quantum mechanical expressions for the nonlinear susceptibility tensor, as described by Shen and Bloembergen [8, 9]. Section B.2 gives a simple microscopic description of the magnetization induced nonlinear susceptibilty tensor $\chi^{(D)}(\mathbf{M})$, and summarizes the results of theoretical estimates of its amplitude.[1]

[1] I would like to thank G. Spierings for allowing me to use parts of his 'doctoraalscriptie' as a starting point for this appendix.

B.1 Nonlinear optical susceptibilities

Nonlinear optical susceptibilities describe the characteristic properties of the medium and depend on its detailed electronic and atomic structure. The density matrix formalism is probably most convenient for calculating these susceptiblities. The wave vector of a system under the influence of an electromagnetic field must be considered as a statistical mixture of states, and the density matrix operator is defined as [10]: $\rho = |\psi\rangle\langle\psi|$, where $|\psi\rangle$ is the wave vector describing the system. The expectation value of the polarization $\mathbf{P}$ is now given by:

$$\langle \mathbf{P} \rangle = Tr(\rho \mathbf{P}) \tag{B.1}$$

The time dependence of the density operator follows from Liouville's equation:

$$\frac{\partial \rho}{\partial t} = \frac{1}{i\hbar}[\mathcal{H}, \rho] \tag{B.2}$$

$\mathcal{H}$ is the Hamiltonian of the system: $\mathcal{H} = \mathcal{H}_0 + \mathcal{H}_{int} + \mathcal{H}_{random}$, where $\mathcal{H}_0$ is the Hamiltonian of the unperturbed system, with eigen states $|n\rangle$, so $\mathcal{H}_0|n\rangle = E_n|n\rangle$. $\mathcal{H}_{int}$ is the Hamiltonian describing the interaction of light with matter (the coherent perturbations):

$$\mathcal{H}_{int} = e\mathbf{r} \cdot \mathbf{E} \tag{B.3}$$

and $\mathcal{H}_{random}$ describes all incoherent perturbations that are responsible for the relaxation of material excitations. It is useful to make a perturbation expansion of the density operator and the polarization:

$$\rho = \rho^{(0)} + \rho^{(1)} + \rho^{(2)} + \dots \tag{B.4}$$

and

$$\langle \mathbf{P} \rangle = \langle \mathbf{P}^{(1)} \rangle + \langle \mathbf{P}^{(2)} \rangle + \dots \tag{B.5}$$

$\langle \mathbf{P}^{(0)} \rangle = 0$ because we assume that there is no permanent dipole moment. When we treat $\mathcal{H}_{int}$ as a first order perturbation and collect terms of the same order, we find:

$$\frac{\partial \rho^{(1)}}{\partial t} = \frac{1}{i\hbar}\left(\left[\mathcal{H}_0, \rho^{(1)}\right] + \left[\mathcal{H}_{int}, \rho^{(0)}\right]\right) + \left(\frac{\partial \rho^{(1)}}{\partial t}\right)_{relax} \tag{B.6}$$

$$\frac{\partial \rho^{(2)}}{\partial t} = \frac{1}{i\hbar}\left(\left[\mathcal{H}_0, \rho^{(2)}\right] + \left[\mathcal{H}_{int}, \rho^{(1)}\right]\right) + \left(\frac{\partial \rho^{(2)}}{\partial t}\right)_{relax} \tag{B.7}$$

We introduce a Fourier expansion:

$$\mathcal{H}_{int} = \sum_i \mathcal{H}_{int}(\omega_i) \quad \text{and} \quad \rho^{(n)} = \sum_j \rho^{(n)}(\omega_j) \tag{B.8}$$

so,

$$\frac{\partial \rho^{(n)}(\omega_j)}{\partial t} = -i\omega_j \rho^{(n)}(\omega_j) \tag{B.9}$$

In thermal equilibrium the matrix elements of the unperturbed density operator are given by [11]:

$$\rho^{(0)}_{nn'} = f(E_n)\delta_{nn'} \tag{B.10}$$

where $\rho^{(m)}_{nn'} = \langle n|\rho^{(m)}|n'\rangle$ and $f(E_n)$ is the normalized distribution function of the energy eigen states that is applicable. Collecting terms with the same frequency in eq. B.6 and sandwiching the result between states $|n\rangle$ and $|n'\rangle$ gives:

$$\rho^{(1)}_{nn'}(\omega_j) = \frac{[\mathcal{H}_{int}(\omega_j)]_{nn'}}{\hbar(\omega_j - \omega_{nn'} + i\Gamma_{nn'})}\left(\rho^{(0)}_{n'n'}(\omega_j) - \rho^{(0)}_{nn}(\omega_j)\right) \tag{B.11}$$

where we have applied eq. B.10, and where $\hbar\omega_{nn'} = E_n - E_{n'}$. $\Gamma_{nn'}$ is a characteristic relaxation time between states $|n\rangle$ and $|n'\rangle$:

$$\left(\frac{\partial \rho^{(m)}_{nn'}}{\partial t}\right)_{relax} = -\Gamma_{nn'}\rho^{(m)}_{nn'} \tag{B.12}$$

The same procedure can be followed for the second order perturbation of the density operator. If the system is driven by electromagnetic fields of frequencies ω_j and ω_k we find:

$$\begin{aligned}
&\rho^{(2)}_{nn'}(\omega_j + \omega_k) = \tfrac{1}{\hbar(\omega_j+\omega_k-\omega_{nn'}+i\Gamma_{gn})} \times \\
&\textstyle\sum_{n''}\Big\{[\mathcal{H}_{int}(\omega_j)]_{nn''}\,\rho^{(1)}_{n''n'}(\omega_k) - \rho^{(1)}_{nn''}(\omega_k)\,[\mathcal{H}_{int}(\omega_j)]_{n''n'} \\
&\qquad + [\mathcal{H}(\omega_k)]_{nn''}\,\rho^{(1)}_{n''n'}(\omega_j) - \rho^{(1)}_{nn''}(\omega_j)\,[\mathcal{H}_{int}(\omega_k)]_{n''n'}\Big\}
\end{aligned} \tag{B.13}$$

From the results we can calculate the second order induced polarization:

$$\langle \mathbf{P}^{(2)}\rangle = Tr(\rho^{(2)}\mathbf{P}) = \sum_{gn}(\rho^{(2)}_{gn}\mathbf{P}_{ng}) = -Ne\sum_{gn}\rho^{(2)}_{gn}\mathbf{r}_{ng} \tag{B.14}$$

Substituting eq. B.13 into eq. B.14, and using eq. B.3 and B.11 gives:

$$\begin{aligned}
&\langle P^{(2)}_i(\omega_1+\omega_2)\rangle = -\textstyle\sum_{gnn'} Ne^3 \tfrac{1}{\hbar(\omega_1+\omega_2-\omega_{gn}+i\Gamma_{gn})} \times \\
&\left\{\tfrac{(\mathbf{E}(\omega_1)\cdot\mathbf{r})_{gn'}(\mathbf{E}(\omega_2)\cdot\mathbf{r})_{nn'}}{\hbar(\omega_2-\omega_{n'n}+i\Gamma_{n'n})}\left(\rho^{(0)}_{nn}(\omega_2) - \rho^{(0)}_{n'n'}(\omega_2)\right) + 3 \text{ similar terms}\right\}\cdot(r_i)_{ng}
\end{aligned} \tag{B.15}$$

From the equation

$$\mathbf{P}_i^{(2)}(\omega) = \chi_{jkl}^{(2)}(\omega = \omega_1 + \omega_2) E_j(\omega_1) E_k(\omega_2) \tag{B.16}$$

we can calculate the tensor elements. After some rearranging of terms and some renaming of indices we find:

$$\chi_{jkl}^{(2)}(\omega = \omega_1 + \omega_2) = \\ -N\frac{e^3}{\hbar^2}\sum_{gnn'}\left\{\frac{(r_i)_{gn}(r_j)_{nn'}(r_k)_{n'g}}{(\omega-\omega_{ng}+i\Gamma_{ng})(\omega_2-\omega_{n'g}+i\Gamma_{n'g})} + 5 \text{ similar terms}\right\} f(E_g) \tag{B.17}$$

In the case of a metal, $|n\rangle$ is a Blochstate:

$$|n, \mathbf{q}\rangle = \frac{1}{\sqrt{\Omega}} u_{\mathbf{q}n}(\mathbf{r}) e^{i\mathbf{q}\cdot\mathbf{r}} \tag{B.18}$$

where Ω is the volume of a direct lattice primitive cell and $u_{\mathbf{q}n}(\mathbf{r})$ is a function with the periodicity of the direct lattice, $\mathbf{q}$ is the electron wavevector and n is the band index. These Blochstates obey the relation:

$$\int d\mathbf{q}\langle n, \mathbf{q}|\mathbf{r}|n', \mathbf{q}\rangle = -\int d\mathbf{q}\langle n', \mathbf{q}|\mathbf{r}|n, \mathbf{q}\rangle \tag{B.19}$$

For the off resonance case, Γ can be neglected, and we obtain:

$$\chi_{jkl}^{(2)}(\omega = \omega_1 + \omega_2) = -\frac{e^3}{\hbar^2}\sum_{\mathbf{q},g,n,n'}\left\{\frac{\langle g,\mathbf{q}|r_i|n,\mathbf{q}\rangle\langle n,\mathbf{q}|r_j|n',\mathbf{q}\rangle\langle n',\mathbf{q}|r_k|g,\mathbf{q}\rangle}{(\omega-\omega_{ng}(\mathbf{q}))(\omega_2-\omega_{n'g}(\mathbf{q}))}\right. \\ + \frac{\langle g,\mathbf{q}|r_i|n,\mathbf{q}\rangle\langle n,\mathbf{q}|r_k|n',\mathbf{q}\rangle\langle n',\mathbf{q}|r_j|g,\mathbf{q}\rangle}{(\omega-\omega_{ng}(\mathbf{q}))(\omega_1-\omega_{n'g}(\mathbf{q}))} + \frac{\langle g,\mathbf{q}|r_k|n,\mathbf{q}\rangle\langle n,\mathbf{q}|r_j|n',\mathbf{q}\rangle\langle n',\mathbf{q}|r_i|g,\mathbf{q}\rangle}{(\omega+\omega_{n'g}(\mathbf{q}))(\omega_2+\omega_{ng}(\mathbf{q}))} \\ + \frac{\langle g,\mathbf{q}|r_j|n,\mathbf{q}\rangle\langle n,\mathbf{q}|r_k|n',\mathbf{q}\rangle\langle n',\mathbf{q}|r_i|g,\mathbf{q}\rangle}{(\omega+\omega_{n'g}(\mathbf{q}))(\omega_1+\omega_{ng}(\mathbf{q}))} + \frac{\langle g,\mathbf{q}|r_j|n,\mathbf{q}\rangle\langle n,\mathbf{q}|r_i|n',\mathbf{q}\rangle\langle n',\mathbf{q}|r_k|g,\mathbf{q}\rangle}{(\omega_1-\omega_{ng}(\mathbf{q}))(\omega_2+\omega_{n'g}(\mathbf{q}))} \\ \left. + \frac{\langle g,\mathbf{q}|r_k|n,\mathbf{q}\rangle\langle n,\mathbf{q}|r_i|n',\mathbf{q}\rangle\langle n',\mathbf{q}|r_j|g,\mathbf{q}\rangle}{(\omega_1+\omega_{n'g}(\mathbf{q}))(\omega_2-\omega_{ng}(\mathbf{q}))}\right\} f_g(\mathbf{q}) \tag{B.20}$$

where $f_g(\mathbf{q})$ is the Fermi distribution function for the state $|g, \mathbf{q}\rangle$.

B.2 Quantum mechanical expression for χ(M)

In the previous section we considered a system that is driven by two electric fields $\mathbf{E}(\omega_j)$ and $\mathbf{E}(\omega_k)$. By taking $\omega_j = \omega_k = \omega$, and assuming that ω is off

resonance we get the following second-harmonic dipole tensor elements:

$$\chi^{(D)}_{jkl}(2\omega) = -\frac{e^3}{\hbar^2}\sum_{\mathbf{q}}\sum_{g,n,n'}\left(\frac{(r_i)_{gn}(r_j)_{nn'}(r_k)_{n'g}}{(2\omega-\omega_{ng})(\omega-\omega_{n'g})} + \text{5 similar terms}\right) f_g(\mathbf{q}) \quad \text{(B.21)}$$

There exist two ways in which the magnetization could influence the susceptibility: (1) The energy eigenvalues shift, which would result in different values of ω_{ng} for different spin states, (2) The electronic eigenfunctions change, because they are perturbed, which would lead to differences in the transition matrix elements $(r_i)_{gn}$ for the different spin states. Both are a result of the combination of spin-orbit coupling and exchange interaction. Kittel has shown that the second effect has the largest influence on the optical susceptibility [12].

We shall treat the spin-orbit interaction energy as being the perturbing Hamiltonian [1, 13]:

$$H = H_0 + H_{s.o.} \quad \text{(B.22)}$$

with [14]:

$$H_{s.o.} = \frac{1}{2m^2c^2}\left[\nabla V(\mathbf{r}) \times \mathbf{p}\right]\cdot\mathbf{S} = h(\mathbf{r})\mathbf{L}\cdot\mathbf{S} \quad \text{(B.23)}$$

Spin-orbit coupling changes the orbital momentum $\mathbf{p}$ of the electrons, and thus the polarization of the generated light, much the same way as an external magnetic field would do [1], so

$$-i\hbar\dot{\mathbf{p}} = [H_{s.o.}, \mathbf{p}] = [h(\mathbf{r})\mathbf{L}\cdot\mathbf{S}, \mathbf{p}] = -h(\mathbf{r})\mathbf{p}\times\mathbf{S} \quad \text{(B.24)}$$

In non-ferromagnetic materials both spin states are equally occupied so no net effect occurs. However, in ferromagnetic materials, exchange interaction splits the band structure and spin states are not equally occupied, causing a net rotation of the polarization [1].

Let $\psi_n(\mathbf{k},\mathbf{r})\alpha(s)$ be the unperturbed eigenfunctions of H_0, where $\alpha(s)$ are the eigenfunctions of the spin operator. In the mean field approximation for the exchange forces the quantities $E_n(\mathbf{k})\pm\delta$ are taken as the energy eigenvalues of the eigenfunctions $\psi_n(\mathbf{k},\mathbf{r})\alpha(\pm1)$ [12, 15]. Time independent perturbation theory gives the eigenfunctions of the Hamiltonian in eq. B.22 [12]:

$$\phi_{\lambda,\pm1}(\mathbf{r}) = \left[\psi_n(\mathbf{k},\mathbf{r}) \pm \xi_n(\mathbf{k},\mathbf{r})\right]\alpha(\pm1) \quad \text{(B.25)}$$

Here λ denotes all the necessary quantum numbers, and

$$\xi_n(\mathbf{k},\mathbf{r}) = \sum_{m\neq n} b_{nm}(\mathbf{k})\psi_m(\mathbf{k},\mathbf{r}) \quad \text{(B.26)}$$

with

$$b_{nm}(\mathbf{k}) = \frac{-i\hbar^2/4m^2c^2}{E_n(\mathbf{k}) - E_m(\mathbf{k})} \int \psi_m^*(\mathbf{k})(\nabla V \times \nabla)_{z_0}\psi_n(\mathbf{k})d\tau \qquad \text{(B.27)}$$

where z_0 is the quantization direction of the spin. Within a first order approximation the energies stay the same, so:

$$(H_0 + H_{s.o.})\phi_{\lambda,\pm 1} = (E_n(\mathbf{k}) \pm \delta)\phi_{\lambda,\pm 1} \qquad \text{(B.28)}$$

We now obtain the tensor elements describing SHG from the magnetized system by using the wave functions $\phi_{\lambda,\pm 1}$ of eq. B.25 in eq. B.21. Considering only terms up to first order in b_{nm}, one may rewrite the susceptibility as:

$$\chi_{jkl}^{(D)} = \chi_{jkl}^{(D),even} + \chi_{jkl}^{(D),odd} \qquad \text{(B.29)}$$

where $\chi_{jkl}^{(D),even}$ is the part of the nonlinear susceptibility tensor that is independent of the spin orientation. The elements of $\chi_{jkl}^{(D),even}$ are of zeroth order in b_{nm}:

$$\chi_{jkl}^{(D),even} = -\frac{e^3}{\hbar^2} \sum_{\mathbf{k}} \sum_{g,n,n',\sigma} \left(\frac{\langle r_i \rangle_{gn} \langle r_j \rangle_{nn'} \langle r_k \rangle_{n'g}}{(2\omega - \omega_{ng})(\omega - \omega_{n'g})} + 5 \text{ similar terms} \right) f_g(\mathbf{k}) \qquad \text{(B.30)}$$

The result is of course the same as for the non-magnetic system (eq. B.21). $\chi^{(D),odd}$ is the tensor that does depend on the spin orientation of the electron. The elements of $\chi^{(D),odd}$ are of first order in b_{nm}:

$$\chi_{jkl}^{(D),odd} =$$

$$-\frac{e^3}{\hbar^2} \sum_{\mathbf{k}} \sum_{g,n,n',\sigma} \left(\sum_m \pm b_{gm}^* \frac{\langle r_i \rangle_{gn} \langle r_j \rangle_{nn'} \langle r_k \rangle_{n'm}}{(2\omega - \omega_{ng})(\omega - \omega_{n'g})} + 35 \text{ similar terms} \right) f_g(\mathbf{k}, \sigma) \qquad \text{(B.31)}$$

where σ is a spin index. Whether there is a plus or a minus sign in eq B.31 depends on the spin of the electron. If both spin states are filled, all contributions to $\chi_{jkl}^{(D),odd}$ will cancel, because of the summation over σ. If however a magnetization is present, both spin states are not equally occupied, and eq. B.31 will give a contribution to the susceptibility.

It is interesting to realize that eq. B.30 implies that there are no contributions of first order in b_{nm} to $\chi^{(D),even}$, i.e. the lowest order effects of the magnetization on the even elements is of second order. This suggests that the even elements are probably less dependent on the size of the magnetization than the odd elements (that are of first order in b_{nm}).

B.3 Theoretical estimates of χ(M)

The value of $\chi^{(D),odd}$ has been estimated for nickel and iron. Ru-Pin Pan *et al.* made a rather crude approximation for Ni(001) by assuming that both all odd and all even tensor elements are equal, and obtained [4, 13]:

$$\left| \omega^2 \chi^{(D),odd} \right|_{Ni} \sim 10^{12} \text{ V}^{-1}\text{s}^{-2}\text{m} \sim 10^{-16} \text{ esu} \tag{B.32}$$

The same surface has been thoroughly analysed by Hübner *et al.* After including the complete band structure and dipole transition matrix elements they obtained [2, 3]:

$$\left| \omega^2 \chi^{(D)}_{xzz} \right|_{Ni} \sim 10^{17} \text{ V}^{-1}\text{s}^{-2}\text{m} \tag{B.33}$$

Pustogowa *et al.* used a similar approach to the surface of iron and found [5, 6]:

$$\left| \omega^2 \chi^{(D)}_{xzz} \right|_{Fe} \sim 10^{16} \text{ V}^{-1}\text{s}^{-2}\text{m} \tag{B.34}$$

All these values are well above the detection limit of SHG, that is $10^9 - 10^{10}$ mV^{-1}s^{-2} or $10^{-19} - 10^{-18}$ esu [4, 16] implying that magnetization induced tensor elements should be observable.

Furthermore, the estimated ratios of odd and even elements are high enough to induce observable changes of the SH-intensity on inverting the magnetization. For nickel both Ru-Pin Pan *et al.* and Hübner *et al.* estimated [3, 13]:

$$\left| \chi^{(D),odd}/\chi^{(D),even} \right|_{Ni} = 0.07 \tag{B.35}$$

and for iron Pustogowa *et al.* deduced [5, 6]:

$$\left| \chi^{(D),odd}/\chi^{(D),even} \right|_{Fe} = 0.18 \tag{B.36}$$

Reif *et al.* deduced the latter ratio by simply scaling the nickel ratio of eq. B.35 by the ratio of the bulk magnetic moments for iron an nickel, $\mu_{Fe}/\mu_{Ni} = 3.8$, and obtained [17]:

$$\left| \chi^{(D),odd}/\chi^{(D),even} \right|_{Fe} = 0.27 \tag{B.37}$$

The value is in close agreement with the result of a simple analysis of their experiments on the Fe(110) surface, and also close to the value given by Pustogowa *et al.* (see eq. B.36). Scaling by the surface magnetic moments in

stead of the bulk magnetic moments does not significantly alter the estimate [18]. Using a similar approach for cobalt gives with $\mu_{Co}/\mu_{Ni} = 3.1$ [18]:

$$\left| \chi^{(D),odd}/\chi^{(D),even} \right|_{Co} = 0.22 \tag{B.38}$$

References

[1] W. Hübner, and K.-H. Bennemann, Phys. Rev. B **40**, 5973 (1989).

[2] W. Hübner, and K.-H. Bennemann, Surf. Sci. **242**, 299 (1991).

[3] W. Hübner, Phys. Rev. B **42**, 11553 (1990).

[4] W. Hübner, and K.-H. Bennemann, Vacuum **41**, 514 (1990).

[5] U. Pustogowa, W. Hübner, and K.-H. Bennemann, Phys. Rev. B **48**, 8607 (1993).

[6] U. Pustogowa, W. Hübner, and K.-H. Bennemann, Surf. Sci. **307-309**, 1129 (1994).

[7] U. Pustogowa, W. Hübner, and K.-H. Bennemann, Phys. Rev. B **49**, 10031 (1994).

[8] Y.R. Shen, *The principles of nonlinear optics* (Wiley, New York, 1984).

[9] N. Bloembergen, *Nonlinear optics* (Benjamin, Amsterdam, 1965).

[10] C. Cohen-Tannoudji, B. Diu, and F. Laloë, *Quantum mechanics* (Wiley, New York, 1977).

[11] U. Fano, Rev. Mod. Phys. **29**, 74 (1957).

[12] P.N. Argyres, Phys. Rev. **97**, 334 (1955).

[13] Ru-Pin Pan, H.D. Wei, and Y.R. Shen, Phys. Rev. B **39**, 1229 (1989).

[14] *Quantum Physics*, S. Gasiorowicz (Wiley, New York, 1974).

[15] *Solid State Physics*, N.W. Ashcroft, N.D. Mermin (Saunders College, Philadelphia, 1978).

[16] Y.R. Shen, Ann. Rev. Mater. Sci. **16**, 69 (1986).

[17] J. Reif, J.C. Zink, C.M. Schneider, and J. Kirschner, Phys. Rev. Lett. **67**, 2878 (1991).

[18] A.J. Freeman, and C.L. Fu, J. Appl. Phys. **61**, 3356 (1987).

Summary

Stimulated by the ever-increasing demand for high speed storage equipment, with long memory lifetimes and small volumes, artificial materials like thin films and multilayers have become of utmost importance. Besides their technological significance, a number of extraordinary phenomena are observed in these systems, the oscillatory exchange coupling through non-magnetic layers being one of the current highlights. Since interfaces have a major influence on the magnetic characteristics of multilayers, and spin behavior at interfaces is quite different from the bulk, a study of buried interfaces in magnetic multilayers is both desirable and interesting.

Spin polarized electronic techniques are difficult to use in studies of buried interfaces due to the very short mean free path of electrons. An optical technique does not have this disadvantage. Second-Harmonic Generation (SHG) is a well established optical probe, that derives its sensitivity to (buried) interfaces from symmetry breaking at boundaries between centrosymmetric media. It has been shown, from a theoretical point of view, that magnetization induced effects from interfaces should be detectable with SHG. Spin-orbit coupling in combination with exchange interaction alters both the energy eigenvalues and the electronic wave functions of the system, and causes detectable effects. Magnetization induced Second-Harmonic Generation (MSHG) could become a valuable alternative to Mössbauer Spectroscopy, with the advantage of ex-situ applicability, and high lateral resolution, while not requiring isotopes.

Phenomenologically, the origin of MSHG can be understood after introducing a magnetization dependent nonlinear susceptibility tensor. Symmetry analysis shows that the inversion symmetry of the bulk is not broken by the magnetization, so the basic argument for potential interface sensitivity of MSHG remains valid. However, the magnetization does introduce new tensor elements, and in fact two sets of elements may be distinguished: odd and even in the magnetization, respectively. Inversion of the magnetization causes a phase change of 180° between the even and odd contributions and leads to a

different SH-intensity.

In this thesis the influence of the magnetization on the second-harmonic signal from magnetic multilayers is discussed. The main goal is to demonstrate that MSHG is sensitive to the magnetic properties of buried interfaces. We have studied polycrystalline Co/Au multilayers with slab thicknesses of about 50Å at a wavelength of 532 nm, and epitaxially grown ultrathin Co films on Cu(001), with slabs of only a few monolayers (ML), at 800 nm. The reflected second-harmonic signal from the Co/Au and Co/Cu multilayers depended strongly on the magnetization, with relative intensity changes that were more than one order of magnitude higher than in comparable measurements of the Magneto-Optical Kerr Effect (MOKE). The phenomenological theory for interface MSHG accurately describes the experimental results.

A quantitative analysis of SHG from multilayers requires a model that accounts for the multiple reflections of the light. We have introduced a flexible model after extending standard transfer-matrix theory for light propagation in multilayers. Electric dipole sources of second-harmonic radiation are included in infinitesimal nonlinear sheets at every interface.

Interface sensitivity of MSHG on the Co/Au multilayers, was shown after observing that incrementing the number of Au/Co interfaces, inverts the relative magnetic effect.[1] The results could be explained in terms of pure interface contributions, after applying the multiple reflection model, which we consider as indirect proof of interface sensitivity.

The Co film thickness dependence of MOKE on Co/Cu(001) in the 1-20 ML Co range could be described by the well-known thin-film additivity law, while accounting for absorption and multiple reflections of the light. The results proof that the Co films are properly magnetized. In contrast to MOKE the relative magnetic effect in MSHG is nearly constant for Co films thicker than 6 ML. The absolute SH-signals were constant within roughly a factor of two for Co film thicknesses above 3 ML. Similar behavior was observed in experiments on Cu/Co/Cu trilayers. The results clearly proof the interface sensitivity of MSHG.

We have observed that the relative magnetic effect in MSHG from Co /Cu(001), changes dramatically on adsorbing a few Langmuirs of gas. This is second and independent proof of the interface sensitivity of MSHG. Furthermore, these results indicate that both the vacuum/Co and the Co/Cu(001) interface contribute significantly to the total SH-intensity.

The present theoretical analysis requires some assumptions that over-sim-

[1]Relative magnetic effect in MSHG: $\rho = [I_{sh}(+M) - I_{sh}(-M)] \,/\, [I_{sh}(+M) + I_{sh}(-M)]$.

plify the system, and may not be entirely correct. Therefore, the most important conclusions of the analysis are: (1) The multiple reflection theory leads in principle to a proper description of these ultrathin multilayers (for films above about 5 ML), and (2) the film thickness and adsorption dependence of MSHG seem useful tools for determining the values of the tensor elements.

Preliminary spectroscopic experiments verified the expected sensitivity of MSHG to the interface electronic structure.

The Co film thickness dependence of the relative magnetic effect in MSHG shows oscillatory-like behavior in the 1-6 ML range. This is not only a third proof of the interface sensitivity of MSHG, but the effect is also possibly related to quantum well states in the Co film. Studies of the Cu/Co(001) system, that is well known for the appearance of quantum well states, support this hypothesis, as huge oscillations in the relative magnetic effects are observed for Cu overlayers of 1-10 ML. A period is not clearly distinguishable, but the width of the substructures is of the proper order of magnitude. Though the oscillations need a more detailed study, the results are very exciting, as they reveal an opportunity to study the coupling mechanism in multilayers.

Now that we have shown the interface sensitivity of Magnetization induced Second-Harmonic Generation in two very different systems, the technique may be used to study intermixing, to verify the presence of magnetically dead or magnetically life layers, and possibly even as a quantitative probe of local magnetic moments at buried interfaces. In fact MSHG seems to have great potential of becoming a powerful external macroscopic probe for the microscopic magnetic properties of buried interfaces.

Samenvatting

Gestimuleerd door de toenemende vraag naar data-opslagapparatuur met een grote snelheid, een hoge geheugen-leeftijd en een klein volume, zijn kunstmatige materialen, zoals dunne films en multilagen van onmisbaar belang geworden. Daarnaast worden in deze systemen een groot aantal zeer interessante verschijnselen waargenomen, waarbij vooral de oscillerende exchange-koppeling door niet-magnetische lagen momenteel een grote aandacht geniet. Omdat grenslagen een grote invloed hebben op de magnetische eigenschappen van multilagen en het spin-gedrag aan grenslagen nogal kan verschillen van het gedrag in de bulk, is een studie van begraven grenslagen in magnetische multilagen zowel gewenst als ook interessant.

Door de korte vrije-weglengte van elektronen zijn spin-gepolariseerde elektronische technieken moeilijk te gebruiken voor het bestuderen van begraven grenslagen. Een optische techniek heeft dit nadeel niet. Tweede-Harmonische Generatie (THG) is een bekende optische techniek die zijn gevoeligheid voor (begraven) grenslagen dankt aan de symmetrie-breking aan de grenzen tussen centrosymmetrische media. Theoretisch is reeds aangetoond dat de magnetisatie een duidelijke invloed heeft op THG door grenslagen. Spin-baan koppeling in combinatie met exchange wisselwerking verandert zowel de eigenenergieën als ook de elektronische golf-functies van het systeem en veroorzaakt meetbare effecten. Magnetisatie geïnduceerde Tweede-Harmonische Generatie (MTHG) zou een waardevol alternatief kunnen worden voor Mössbauer Spectroscopie met als voordelen: ex-situ toepasbaarheid, een hoge laterale resolutie en het ontbreken van de noodzaak van het gebruik van isotopen.

Fenomenologisch kan de oorsprong van MTHG verklaard worden na het introduceren van een magnetisatie afhankelijke niet-lineaire susceptibiliteits-tensor. Een symmetrie-analyse toont aan dat de inversie-symmetrie van de bulk behouden blijft ondanks de magnetisatie. Het basis-argument voor de potentiële grenslaag-gevoeligheid van MTHG blijft dus geldig. Desalniettemin kunnen twee sets van tensor-elementen onderscheiden worden, even respectievelijk oneven in de magnetisatie. Inverteren van de magnetisatie veroor-

zaakt een fase-draaiing van 180 graden tussen de even en oneven bijdragen en leidt tot een andere tweede-harmonische intensiteit.

In dit proefschrift wordt de invloed van de magnetisatie op het tweede-harmonische signaal van multilagen bediscussieerd. Het hoofddoel is aan te tonen dat MTHG gevoelig is voor de magnetische eigenschappen van begraven grenslagen. Hiertoe zijn twee systemen bestudeerd: (1) polykristallijne Co/Au multilagen met laagdiktes van ongeveer 50Å bij een golflengte van 532 nm, en (2) epitaxiaal gegroeide ultradunne Co films op Cu(001) met laagdiktes van een paar monolagen (ML) bij 800 nm. Het gereflecteerde tweede-harmonische signaal van zowel de Co/Au als de Co/Cu multilagen hangt sterk af van de magnetisatie, waarbij de relatieve intensiteits-veranderingen meer dan een orde van grootte hoger zijn dan in vergelijkbare metingen van het Magneto-Optische Kerr Effect (MOKE). De fenomenologische theorie voor MTHG aan grenslagen geeft een goede beschrijving van de experimentele resultaten.

Een kwantitatieve analyse van THG in multilagen vereist een model dat rekening houdt met de meervoudige reflecties van het licht. We hebben een flexibel model ontwikkeld na het uitbreiden van de standaard matrix-theorie voor de propagatie van licht in multilagen. Electrische dipool-bronnen van tweede-harmonische straling worden meegenomen in infinitesimale niet-lineaire laagjes aan elk interface.

De grenslaag-gevoeligheid van MTHG aan Co/Au multilagen werd aangetoond met de observatie dat één extra Co/Au grenslaag het relatieve magnetische effect inverteert.[1] Bovendien konden de resulaten beschreven worden in termen van pure grenslaag-bijdragen, na toepassing van het meervoudige reflectie model. Dit beschouwen we als een indirect bewijs van grenslaag-gevoeligheid.

De Co film dikte-afhandelijkheid van de MOKE-amplitude in metingen aan Co/Cu(001), met 1-20 ML Co, kon worden beschreven met de bekende dunne film optelbaarheidswet, terwijl rekening werd gehouden met de absorptie en de meervoudige reflecties van het licht. De resultaten tonen aan dat de Co films goed gemagnetiseerd zijn. In tegenstelling tot MOKE is het relatieve magnetische effect in MTHG vrijwel constant voor Co films dikker dan 6 ML. Verder zijn ook de absolute tweede-harmonische signalen constant binnen ongeveer een factor twee voor Co films dikker dan 3 ML. Vergelijkbare resultaten zijn verkregen in metingen aan Cu/Co/Cu drielaagssystemen. De resultaten tonen duidelijk aan dat MTHG grenslaag-gevoelig is.

Daarnaast hebben we waargenomen dat het relatieve magnetische effect

[1] Relatieve magnetische effect: $\rho = [I_{sh}(+M) - I_{sh}(-M)] \,/\, [I_{sh}(+M) + I_{sh}(-M)]$.

in MTHG van Co/Cu(001) dramatisch verandert na adsorptie van een paar Langmuir gas. Dit is een tweede en onafhankelijk bewijs van de grenslaag-gevoeligheid van MTHG. Bovendien geven de resulaten aan dat zowel de vacuum/Co als ook de Co/Cu(001) grenslaag significant bijdragen aan de totale tweede-harmonische intensiteit.

De huidige theoretische analyse is gebaseerd op een aantal vereenvoudigingen en aannames, die mogelijk niet helemaal correct zijn. Daarom zijn de belangrijkste conclusies van de analyse als volgt: (1) de meervoudige reflectie theorie leidt in principe tot een goede beschrijving van deze ultradunne multilagen (voor films met een dikte boven 5 ML), en (2) de film dikte- en de adsorptie-afhankelijkheid van MTHG lijken bruikbaar bij het bepalen van de waarden van de tensor elementen.

De voorlopige resulaten van spectroscopische experimenten laten de verwachte gevoeligheid van MTHG voor de elektronische structuur zien.

The Co film dikte-afhankelijkheid van het relatieve magnetische effect vertoont een oscillatie-achtig gedrag in het 1-6 ML gebied. Dit is niet alleen een derde bewijs van de grenslaag-gevoeligheid van MTHG, maar het effect is mogelijk gerelateerd aan quantum-put toestanden in de Co film. Experimenten op Cu/Co(001), dat bekend staat om de aanwezigheid van quantum-put toestanden, ondersteunen deze hypothese, omdat sterke oscillaties in het relatieve MTHG signaal zijn waargenomen voor Cu toplagen met diktes van 1-10 ML. Een periode is niet duidelijk onderscheidbaar, maar de breedte van de substructuren is van de goede orde van grootte. Alhoewel een nauwkeuriger studie van deze oscillaties noodzakelijk is, zijn de resultaten zeer interresant, omdat ze duidelijk aangeven dat MTHG een grote potentie bezit voor het bestuderen van het koppelings-mechanisme in multilagen.

Nu de grenslaag-gevoeligheid van Magnetisatie geïnduceerde Tweede-Harmonische Generatie in twee zeer verschillende systemen is aangetoond, zou de techniek gebruikt kunnen gaan worden voor het bestuderen van intermixing, of voor het bepalen van de aanwezigheid van magnetisch 'dode' of juist 'levende' lagen, en misschien zelfs voor het meten van locale magnetische momenten in begraven grenslagen. In ieder geval is MTHG een veelbelovende macroscopische probe voor de microscopsche magnetische eigenschappen van begraven grenslagen.

Voor niet-natuurkundigen

In de komende pagina's wil ik proberen om een voor iedereen begrijpelijk overzicht van de inhoud van dit proefschrift te geven. Ik zal ingaan op de achtergronden en de motivatie van het onderzoek, maar ook in het kort beschrijven wat de belangrijkste resultaten zijn.

Vaste stoffen, oppervlakken en grenslagen

Een zeer groot deel van alle natuurkundigen in de wereld verricht onderzoek aan vaste stoffen. Dat is niet zonder reden want onze gebruiksvoorwerpen en machines bestaan grotendeels uit vaste stoffen: van de scheepswand van de mammoettanker en de aktieve elementen in de auto-katalysator tot de harddisc en de microprocessor in de personal computer. Veel technologisch hoogwaardige produkten, zoals microprocessors, zijn opgebouwd uit dunne laagjes van verschillende vaste stoffen, de zogenaamde multilagen (in het Engels: 'multilayers'). Er ontstaan op deze manier systemen met zeer bruikbare eigenschappen. Figuur 1 toont een drielaagssysteem. Een dunne laag magnetisch materiaal is geplaatst op een stevige ondergrond (ook wel substraat genaamd). Over de magnetische laag is een dun laagje goud aangebracht. Goud is een edelmetaal en het beschermt de onderliggende laag tegen de invloed van de atmosfeer. Het totale syteem is nu én stevig én magnetisch én goed beschermd. Hierdoor is het zeer bruikbaar voor de opslag van gegevens en een typisch voorbeeld van wat te vinden is op harddiscs en videotapes.

Een bekend voorbeeld van een vaste stof is staal, een belangrijk bestanddeel van bijvoorbeeld de auto en veel huishoudelijke apparaten. Iedereen die wel eens een oude(re) auto heeft gehad, kent het probleem van de roestvorming. Roesten is in feite niets anders dan een chemische reaktie tussen het staal en de zuurstof in de lucht. Indien men op tijd aktie onderneemt is het eenvoudig om de roest te verwijderen. Na wat krabben en schuren komt weer schoon metaal te voorschijn, met andere woorden *alleen het oppervlak van het metaal*

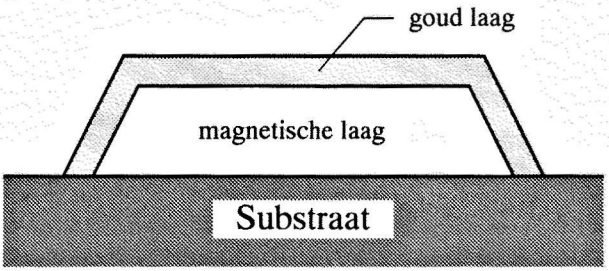

Figuur 1: *Een typisch voorbeeld van een systeem dat geschikt is voor de magnetische opslag van gegevens in computers. Het substraat zorgt voor stevigheid en de goudlaag beschermt de magnetische laag tegen de invloeden van de atmosfeer. De zwarte lijnen geven grenslagen aan.*

was aangetast. Dit is slechts één voorbeeld van de vele chemische reakties die mogelijk zijn aan het oppervlak van een materiaal. In dit geval is er sprake van een ongewenst proces, maar in de katalysator van moderne auto's maakt men nuttig gebruik van het oppervlak van de vaste stof als initiator van gewenste chemische reakties.

Tot nu toe hebben we alleen gesproken over het oppervlak als de plek waar chemische reakties plaats kunnen vinden. Het oppervlak is echter ook te interpreteren als *een grensgebied tussen materiaal en atmosfeer.* Zo'n grensgebied vinden we overal waar twee verschillende stoffen met elkaar in kontakt komen, dus ook in het drielaagssysteem van figuur 1. In de natuurkunde spreekt men in verband met de zeer geringe afmetingen van het grensgebied liever over een grenslaag (in het Engels: 'interface'). De grenslaag kan geheel nieuwe eigenschappen bezitten, die niet in het binnenste van de omringende materialen voorkomen. Verder heeft de aanwezigheid van een grenslaag vaak een sterke invloed op het systeem als geheel. De eigenschappen van grenslagen zijn van groot belang in bijvoorbeeld de halfgeleider-technologie en bij de magnetische opslag van gegevens.

Binnen de Vaste Stoffysica probeert men meestal kennis te krijgen over één bepaalde eigenschap van de materie. Het is van het grootste belang omstandigheden te creëren waarbij juist deze eigenschap sterk naar voren komt. Om enig idee te geven van de begrippen 'vaste stof' en 'oppervlak' heb ik in het voorgaande het materiaal staal als voorbeeld genomen. Staal is een complexe legering van ijzer, koolstof en andere spore-elementen. Het is moeilijk

om de eigenschappen van zo'n legering goed te beschrijven. Men geeft daarom meestal de voorkeur aan systemen die een eenvoudige samenstelling hebben, bijvoorbeeld puur ijzer.

Het is niet gemakkelijk om een systeem met een goed gedefiniërde samenstelling te prepareren. Het wordt echter nog moeilijker wanneer we perfecte oppervlakken of grenslagen willen bestuderen. Stel: we hebben een stuk ijzer roestvrij gemaakt. Het duurt dan maar ruwweg 10 nanosekonden (0,00000001 sekonde) voordat het oppervlak weer volledig is aangetast door de zuurstof in de atmosfeer, ook al is het dan nog niet te zien met het blote oog. Het is bijna onmogelijk om in deze extreem korte tijd een experiment te doen.

Het probleem is op te lossen door het ijzer in een omgeving te plaatsen waar zich geen zuurstof bevindt. Dit kan bereikt worden in een Ultra Hoog Vacuum (UHV) kamer. Dit is een kleine ruimte, met een middellijn van enkele tientallen centimeters, waaruit alle gassen die normaal in onze atmosfeer aanwezig zijn, worden verwijderd. Figuur 2 toont een typische UHV-kamer. Wanneer we onder deze omstandigheden het ijzer een schoon oppervlak geven, zal het vervolgens 'nooit' meer roesten: er is immers geen zuurstof aanwezig. Het woord 'nooit' is tussen aanhalingstekens geplaatst, omdat we deze ideale situatie niet kunnen bereiken. Met de vacuumkamers die in dit proefschrift zijn beschreven, kan een oppervlak gedurende enkele uren schoon worden gehouden, hetgeen voldoende is voor het uitvoeren van experimenten.

Aan het begin van dit hoofdstuk is aangegeven dat multilagen van technologisch belang zijn. UHV is een ideale omgeving voor het maken van deze multilagen.

Tweede-Harmonische Generatie aan grenslagen

In het voorafgaande deel heb ik geprobeerd toe te lichten dat oppervlakken en grenslagen een belangrijk deel van de materie zijn en dat hun eigenschappen niet alleen interessant zijn vanuit wetenschappelijk oogpunt, maar ook van groot technologisch belang. Verder heb ik uitgelegd dat UHV kamers noodzakelijk zijn bij oppervlakte-onderzoek. Maar stel nu, dat we een mooi oppervlak gemaakt hebben, hoe kunnen we dan wat leren over zijn eigenschappen?

Het grote probleem bij oppervlakte-onderzoek is dat maar een heel klein deel van het materiaal als oppervlak gezien kan worden. Stel dat we een bolletje ijzer met een diameter van één centimeter vergroten tot het net zo groot is als de aarde, dan nog zou het oppervlak maar enkele tientallen centimeters dik zijn. Het probleem is misschien het best te omschrijven door te stellen dat we zittend op de maan informatie trachten te krijgen over de humuslaag op

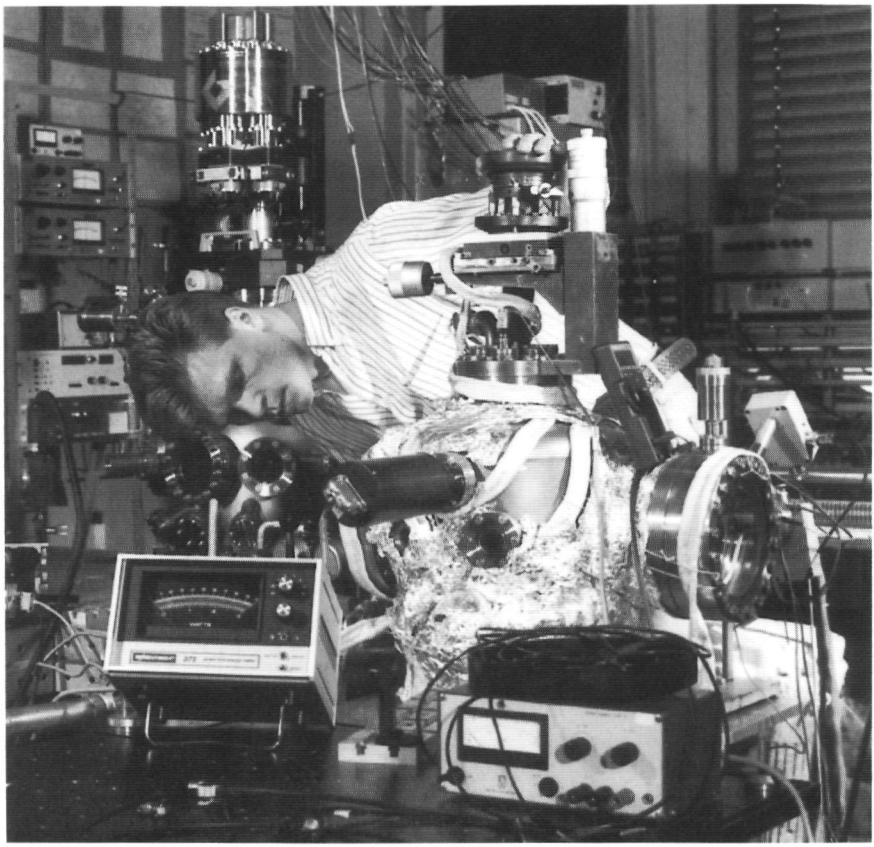

Figuur 2: *Eén van de Nijmeegse laboratoria voor oppervlakte-onderzoek. De zilverkleurige constructie op de voorgrond is een UHV-kamer.*

aarde. We moeten dan een methode ontwikkelen die wel kijkt naar de samenstelling van deze humuslaag, maar niet naar de lucht erboven, noch naar de grond eronder en dat is geen eenvoudige opgave.

Terugkomend op de vaste stoffen moet de methode gevoelig zijn voor de fysische eigenschappen van de bovenste 2 à 3 atoomlagen van het materiaal. In de loop van de jaren zijn er vele technieken ontwikkeld die in staat zijn de eigenschappen van het oppervlak te scheiden van de eigenschappen van het binnenste van het materiaal. We zeggen dan dat deze technieken oppervlaktegevoelig zijn. Een voorbeeld van zo'n techniek is de Scanning Tunneling Microscoop (STM), die wel tot een miljard maal kan vergroten en in staat is de atomen af te beelden. Er bestaan veel technieken die op de één of andere

manier gebruik maken van elektronen (elektronen zijn kleine geladen deeltjes die in alle stoffen voorkomen). Al deze technieken hebben over het algemeen een behoorlijke oppervlakte-gevoeligheid en veel interessante eigenschappen. Het is echter nogal nadelig dat ze eigenlijk alleen onder ideale omstandigheden zijn te gebruiken.

Een techniek die dit nadeel niet heeft en die in de laatste tien jaar in toenemende mate wordt gebruikt, is optische Tweede-Harmonische Generatie (THG). Wanneer licht met een bepaalde kleur op een stuk materiaal valt, wordt het deels gereflecteerd. Het gereflecteerde licht heeft natuurlijk dezelfde kleur als het inkomende licht. Dit is echter niet het enige wat er gebeurt. In het materiaal kunnen allerlei processen plaats vinden die het inkomende licht omzetten in licht met een andere kleur. In de natuurkunde spreekt men niet zo vaak over 'de kleur' van het licht, men heeft het liever over 'de frequentie', omdat dit een preciezere aanduiding is. Er is echter een duidelijk verband tussen 'kleur' en 'frequentie'.

Eén van deze processen is optische Tweede-Harmonische Generatie. Hierbij wordt het inkomende licht omgezet in licht met een frequentie die *precies twee maal zo groot* is als de frequentie van het inkomende licht (in het Engels wordt deze techniek 'optical Second-Harmonic Generation' genoemd). Het speciale van dit proces is dat het in het ideale geval alleen plaats vindt in grenslagen. THG is dus een grenslaag-gevoelige techniek. THG is een zeer inefficiënt proces, d.w.z. dat maar een zeer klein deel van het inkomende licht wordt omgezet in tweede-harmonische licht (typisch maar 1 miljoen-miljardste deel). Bij de experimenten moet daarom altijd gebruik worden gemaakt van een krachtige laser.

Figuur 3 toont een schematische voorstelling van een laserbundel die op het drielaagssysteem van figuur 1 valt. Een deel van de laserbundel wordt gereflecteerd door het oppervlak van het goud, een ander deel dringt het materiaal binnen en loopt door het goud naar de grenslaag tussen het goud en het magnetische materiaal. Ook hier wordt een deel van het licht gereflecteerd en een ander deel gaat door naar de laatste grenslaag, die tussen het magnetische materiaal en het substraat. Het inkomende laserlicht bereikt dus uiteindelijk alle grenslagen in het systeem. Aan al deze grenslagen wordt tweede-harmonische licht gegenereerd, dus én aan de grenslaag tussen lucht en goud én aan de grenslaag tussen goud en magnetisch materiaal én aan de grenslaag tussen magnetisch materiaal en het substraat. Een deel van dit licht komt naar buiten en kan gemeten worden met de detector (zie figuur 3). *THG is dus gevoelig voor de eigenschappen van diep liggende grenslagen en dat is vrijwel uniek!*

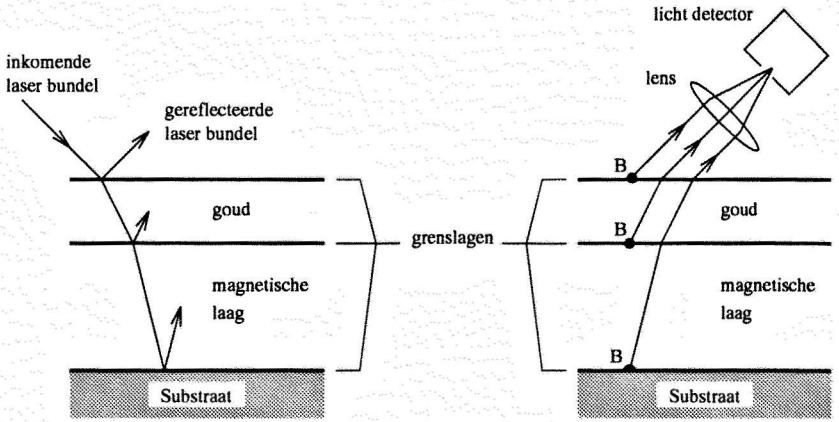

Figuur 3: *Reflectie en Tweede-Harmonische Generatie; de linker figuur geeft schematisch weer hoe een inkomende bundel het materiaal binnen dringt. De rechter figuur geeft aan dat zich aan de grenslagen bronnen (B) bevinden waar tweede-harmonische licht gegenereerd wordt. Dit nieuwe licht komt naar buiten en wordt gemeten met de licht-gevoelige detector.*

THG aan magnetische multilagen

De titel van dit proefschrift luidt: 'Magnetization induced optical Second-Harmonic Generation on magnetic multilayers: A new probe for interface magnetism'. Vrij vertaald in het Nederlands wordt dit:

> *'Door de magnetisatie van het materiaal veroorzaakte optische Tweede-Harmonische Generatie in magnetische multilagen: Een nieuwe manier om de magnetische eigenschappen van grenslagen te bestuderen.'*

Behalve de term 'magnetisatie' zijn alle begrippen in deze titel al toegelicht in de voorafgaande tekst.

De term 'magnetisatie' is direct verbonden met 'magnetisme' en 'magneet'. Velen van u hebben misschien wel eens gespeeld met een magneet en weten dat magnetisme overgedragen kan worden van een magneet naar bijvoorbeeld een spijker die er bij in de buurt komt. De spijker is daarna ook magnetisch geworden en kan op zijn beurt weer andere spijkers aantrekken. We zeggen

dat de spijker nu gemagnetiseerd is, of ook wel dat er in de spijker een magnetisatie aanwezig is. Het is niet nodig om de spijker constant in de buurt van de magneet te houden. Als de magnetisatie eenmaal is overgedragen van de magneet naar de spijker blijft deze permanent in de spijker aanwezig. Alleen bepaalde materialen kunnen gemagnetiseerd worden. Een kompasnaald is een gemagnetiseerd stukje metaal. De naald wijst altijd naar het noorden. De magnetisatie blijft dus niet alleen permanent in het materiaal aanwezig, maar heeft ook een richting. Wanneer we het systeem uit figuur 1 in de buurt van een magneet brengen zal de magnetische laag gemagnetiseerd worden én blijven, ook nadat de magneet verwijderd is. We hebben dus in feite informatie opgeslagen in een geheugen.

In figuur 3 is de middelste laag aangeduid als magnetisch materiaal, d.w.z. dat deze laag gemagnetiseerd kan worden. Het is al heel lang bekend dat het feit dat een materiaal gemagnetiseerd is een duidelijke invloed heeft op het gereflecteerde licht.[1] Dit wordt het Magneto-Optische Kerr Effect (MOKE) genoemd. MOKE is een optische techniek die gevoelig is voor de magnetisatie van het binnenste van het materiaal. THG is gevoelig voor de eigenschappen van grenslagen én THG is ook een optische techniek, dus

Het idee:
Optische Tweede-Harmonische Generatie zou wel eens gevoelig kunnen zijn voor de magnetische eigenschappen van diep liggende grenslagen. Zo'n techniek kan zeer bruikbaar zijn bij het vergroten van de kennis over deze grenslagen, en dus bij de ontwikkeling van nieuwe magnetische multilagen die nodig zijn voor het verbeteren van bijvoorbeeld de bestaande computers.

In dit proefschrift wordt met experimenten bewezen dat THG inderdaad gevoelig is voor de magnetische eigenschappen van grenslagen. In één van de experimenten hebben we metingen gedaan aan dunne laagjes gemagnetiseerd cobalt op een substraat van koper (zie figuur 3). Er hoefde geen beschermende laag goud aangebracht te worden omdat de experimenten zijn gedaan in een UHV-kamer, waar geen gevaar is dat het magnetische materiaal reageert met bijvoorbeeld zuurstof. We hebben laagjes cobalt van verschillende dikte gemaakt en ze met behulp van een electromagneet gemagnetiseerd. Vervolgens hebben we gemeten hoeveel de signalen veranderen met het omdraaien van de richting van de magnetisatie.

[1] John Kerr, The London, Edinburgh, and Dublin Philosophical Magazine and Journal of Science **3**, pagina 321-343, 1877.

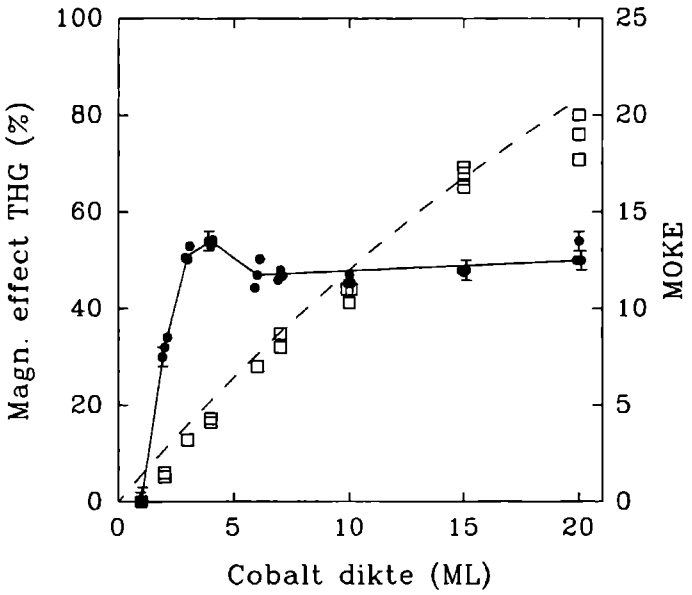

Figuur 4: *Metingen aan gemagnetiseerd cobalt; de vierkantjes en de gestippelde lijn tonen het MOKE-signaal. De rondjes en de doorgetrokken lijn geven de resulaten van de THG experimenten. MOKE en THG hangen heel verschillend af van de dikte van het cobalt, waaruit we concluderen dat THG grenslaag-gevoelig is.*

De resultaten van één van deze experimenten staan weergegeven in figuur 4. In het proefschrift zijn onderdelen van deze figuur te vinden op pagina's 103 en 110. Op de horizontale as van figuur 4 staat de dikte van het cobalt uitgezet in monolagen (ML). Eén monolaag heeft de dikte van één laagje atomen. Het experiment is dus gedaan aan zeer dunne laagjes cobalt (20 ML=0,0000036 mm). MOKE is gevoelig voor het binnenste van het materiaal en je zou dus verwachten dat het MOKE signaal groter wordt met het toenemen van de dikte van het cobalt. De experimenten laten zien dat deze veronderstelling klopt (zie de vierkantjes en de gestippelde lijn in figuur 4).

De THG-experimenten aan deze systemen geven heel andere resultaten (zie de rondjes en de doorgetrokken lijn in figuur 4). Met 'Magnetisch effect THG (%)' bedoelen we de relatieve verandering van het THG-signaal met het omdraaien van de magnetisatie. We zien dat voor cobalt diktes boven 6ML het magnetische effect THG nauwelijks verandert met het toenemen van de

dikte van het cobalt.

De conclusie:
Uit de resultaten volgt dat het binnenste van het materiaal geen invloed heeft op het tweede-harmonische signaal en dat THG grenslaaggevoelig is.

Deze conclusie wordt gesteund door een groot aantal andere resultaten, die ik hier niet verder zal bespreken. Ik hoop dat deze pagina's enig idee hebben gegeven van de motivatie van het onderzoek en de uitvoering van de experimenten. Misschien is niet alles helemaal duidelijk, maar ik hoop dat u heeft begrepen dat we het toepassingsgebied van de techniek optische Tweede-Harmonische Generatie (THG) hebben uitgebreid naar magnetische systemen. Uit alle op dit moment beschikbare gegevens menen we te kunnen concluderen dat THG gevoelig is voor de magnetische eigenschappen van diep liggende grenslagen. We hopen dat de techniek in de toekomst de kennis over deze grenslagen zal vergroten, wat misschien zou kunnen leiden tot een verbetering van de op dit moment bestaande systemen voor de magnetische opslag van gegevens.

Harald Wierenga
Nijmegen, 30 augustus 1994

Publicaties

1. H.A. Wierenga, L.L. Soethout, J.W Gerritsen, L.E.C. van de Leemput, H. van Kempen, and G. Schmid. *Direct imaging of* $Pd_{561}(phen)_{38\pm2}O_n$ *and* $Au_{55}(PPh_3)_{12}Cl_6$ *clusters using Scanning Tunneling Microscopy*, Adv. Mater. **2**, 183 (1990).

2. L.E.C. van de Leemput, J.W. Gerritsen, P H.H. Rongen, R.T.M. Smokers, H.A. Wierenga, and H. van Kempen: *Scanning Tunneling Microscopy observations of metallic clusters* Pd_{561} *and* Au_{55} *and the implications of their use as a well defined tip*, J. Vac. Sci. Technol B **9**, 814 (1991).

3. C W van Hasselt, M A. Verheijen, H A, Wierenga, and Th. Rasing: *Optical Second Harmonic Generation study of vicinal Si(111) surfaces*, Proceedings 2^{nd} EPIOPTIC Workshop, Berlin, 41 (1991).

4. I. Muševič, B. Žekš, R. Blinc, H.A. Wierenga, and Th. Rasing: *Phason dispersion and magnetic field induced band gap in a ferroelectric liquid crystal*, Phys. Rev. Lett. **68**, 1850 (1992).

5. I. Muševič, B. Žekš, R Blinc, H A. Wierenga, and Th. Rasing: *Observation of magnetically induced changes in the phason band structure in a ferroelectric liquid crystal*, Physica B **177**, 511 (1992).

6 G G. Malliaras, H.A. Wierenga, and Th. Rasing: *Optical Second Harmonic Generation study of vicinal Si(110) surfaces*, Proceedings 12^{th} Greek-Bulgarian Symposium on Semiconductor Physics, Thessaloniki, 131 (1992).

7. G.G. Malliaras, H.A. Wierenga, and Th. Rasing *Study of the step structure of vicinal Si(110) surfaces using Optical Second Harmonic Generation*, Surf. Sci. (IV-12, ICSS-8, The Hague, 1992) **287-288**, 703 (1993)

8 G Spierings, V Koutsos, H A. Wierenga, M.W J Prins, D Abraham, and Th. Rasing: *Optical Second Harmonic Generation study of interface magnetism*, Surf. Sci (IV-12, ICSS-8, The Hague, 1992) **287-288**, 747 (1993).

9. G. Spierings, V. Koutsos, H.A. Wierenga, M W J. Prins, D Abraham, and Th. Rasing: *Interface magnetism studied by Optical Second Harmonic Generation*, J Magn. Magn. Mat (Symposium Magnetic Thin Films, Lyon, 1992) **121**, 109 (1993).

10. D. Johannsmann, H. Zhou, P. Sonderkaer, H. Wierenga, B.O. Myrvold, and Y.R. Shen: *Odd-even effects in tilt angles and orientational orders of liquid crystals on rubbed polymer surfaces*, Phys. Rev. E **48**, 1889 (1993).

11. H.A. Wierenga, M.W.J. Prins, D. Abraham, and Th. Rasing: *Magnetization induced optical second-harmonic generation: A probe for interface magnetism*, Phys. Rev. B **50**, 1282 (1994).

12. Th. Rasing and H.A. Wierenga: *Magnetic field induced second harmonic generation*, accepted for publication in Ferroelectrics.

13. H.A. Wierenga, M.W.J. Prins, and Th. Rasing: *Magnetization induced optical second-harmonic generation from magnetic multilayers*, accepted for publication in Physica B.

14. M. Barmentlo, R.W.J. Hollering, H.A. Wierenga, C.W. van Hasselt, and Th. Rasing, *Liquid-crystal monolayers in high magnetic fields: A second-harmonic generation study*, accepted for publication in Physica B.

15. R. Vollmer, A. Kirilyuk, H. Schwabe, J. Kirschner, H.A. Wierenga, W. de Jong, and Th. Rasing, *Direct comparison of nonlinear and linear Kerr-effect measurements on thin Co-films on Cu(001)*, accepted for publication in J. Magn. Magn. Mat.

16. B. Koopmans, A.M. Janner, H.A. Wierenga, Th. Rasing, G.A. Sawatzky, and F. van der Woude, *Separation of interface and bulk contributions in second-harmonic generation from magnetic and nonmagnetic multilayers*, submitted.

17. H.A. Wierenga, W. de Jong, M.W.J. Prins, Th. Rasing, R. Vollmer, A. Kirilyuk, H. Schwabe, and J. Kirschner: *Interface magnetism and quantum well oscillations in Co-Cu(001) multilayers observed by magnetization induced second-harmonic generation*, submitted.

18. H.A. Wierenga, W. de Jong, M.W.J. Prins, Th. Rasing, R. Vollmer, A. Kirilyuk, H. Schwabe, and J. Kirschner: *Nonlinear and linear Kerr studies of Co/Cu multilayers*, submitted.

Curriculum vitae

Harm Albert Wierenga
geboren: 31 mei 1966 te Coevorden

1978-1984	Ongedeeld VWO aan het Stedelijk Lyceum te Zutphen.
1984-1989	Studie natuurkunde aan de Katholieke Universiteit Nijmegen.
1989	Doctoraalexamen natuurkunde met als specialisatie Experimentele Vaste Stoffysica. Afstudeer onderwerp: Scanning Tunneling Microscopy aan 'magische' metaalclusters.
1989	Pilot project voor AKZO Research Laboratories Arnhem (drie maanden). Onderwerp: Scanning Tunneling Microscopy aan koolstofgarens.
1989-1994	Als Onderzoeker in Opleiding werkzaam aan de Katholieke Universiteit Nijmegen op de afdeling Experimentele Vaste Stoffysica 2 onder leiding van Prof.Dr. H. van Kempen en Dr. Th. Rasing. Onderwerp: Opbouw laboratorium voor optical Second-Harmonic Generation. Onderzoek met behulp van deze techniek aan Silicium-Siliciumoxyde en magnetische systemen.
1992	Werkbezoek aan de groep van Prof.Dr. Y.R. Shen, University of California te Berkeley, USA (drie maanden). Onderwerp: Onderzoek invloed polymeercoating op oriëntatie vloeibaar kristal met behulp van optical Second-Harmonic Generation.
1994	Wetenschappelijk medewerker in de groep 'Magnetisme' van het Philips Natuurkundig Laboratorium te Eindhoven.

Stellingen

behorende bij het proefschrift:

Magnetization induced optical Second-Harmonic Generation on magnetic multilayers:

A new probe for interface magnetism

door: **Harald Wierenga**

I

Gezien de grote invloed van Radio 3 op jongeren enerzijds en het belang van een goede scholing anderzijds, zouden diskjockeys zich moeten onthouden van negatieve uitlatingen aangaande schoolzaken.

II

Belangrijker dan kennis is het besef van wat men niet weet.

III

Het feit dat wetenschappers in televisiereklames nog steeds worden afgebeeld in een witte jas, wordt niet veroorzaakt door de reklame-technische behoefte aan een eenvoudig stereotype, maar door de wijdverbreide maatschappelijke onbekendheid met de wetenschap.

IV

De veel gebruikte uitspraak: 'Ik heb helaas geen tijd' dient vervangen te worden door: 'Het spijt me, maar ik heb andere prioriteiten'.

V

Daar concurrerende groepen vaak lange tijd met vergelijkbaar onderzoek bezig zijn, wordt het hebben van de eerste publikatie nogal eens overgewaardeerd.

VI

Het feit dat de media meer aandacht besteden aan promoties op het gebied van de sociologie en de psychologie dan aan die op het gebied van de natuurkunde, wordt veroorzaakt door een verschil in toegankelijkheid en niet door een verschil in maatschappelijke relevantie.

VII

Binnen geloofsgemeenschappen dient het gebruik van uitdrukkingen die duiden op absolute kennis van 'de waarheid' en 'de zin van het leven' vermeden te worden. Afgezien van het feit dat het absolute karakter van deze kennis uiteindelijk niet essentieel is in het persoonlijke leven van de geloofsgenoten, wordt het geloof als geheel ondermijnd door een veelal mettertijd noodzakelijke correctie van het standpunt.

VIII

Gezien het ontbreken van een causaal verband tussen de begrippen 'uitstel' en 'afstel' duidt de uitdrukking: 'Van uitstel komt afstel' eerder op een pessimistische volksaard, dan op een diep inzicht.

IX

0830301 you 0172509 0360607 0280107 1180902 1003108 0160906 leads 1650702 1180902 0780904 sentence, you 1152801 1160802 0182405 know 0622604 0622605 0622606 1410103 0360512 0841302 1231508 0651012 0510404 1423502.